NASA CONTRACTOR REPORT 177463

Study of Helium Transfer Technology for STICCR - Fluid Management

D. J. Frank
S. W. K. Yuan
R. K. Grove
J. M. L'Heureux

Lockheed Missiles & Space Company, Inc.
Palo Alto, California

Prepared for
Ames Research Center
under Contract NAS2-12051

National Aeronautics and
Space Administration

Ames Research Center
Moffett Field, California 94035

CONTENTS

CONTENTS (Cont.)

Section 1
INTRODUCTION

The design and development of a system for collecting and delivering superfluid helium (He II) to a pump inlet in low gravity presents unique problems in hydrodynamics and thermodynamics. Solution of these problems requires perceptive interpretation of available technology and realistic appraisal of any need for new supporting technology. In general, the state of the art is sufficiently advanced at this time to design a device to control He II in a low-gravity environment. Three types of fluid control have been demonstrated successfully in flight. They are:

(1) Settling accelerations
(2) Passive expulsion (surface-tension devices)
(3) Positive expulsion

Each of these offers unique advantages and disadvantages when applied to a set of requirements. A preliminary review was discussed in Ref. 1-1. This report evaluates in detail three passive expulsion devices with emphasis on an enclosed capillary gallery channel device. An open capillary device was reviewed but did not satisfy the requirement of controlling the fluid against the required adverse acceleration. An integrated fountain-effect pump (FEP) and gallery device was evaluated and it was determined that it could meet all the requirements. This type of device would require development and verification tests that can be performed on the ground. The performance of the enclosed capillary device can be characterized with ground tests. The only aspect that needs orbital verification is the behavior of "trapped" vapor in the device. This is discussed further in Section 2.3. Presently an enclosed capillary device is baselined for the means of collecting He II in the orbital NASA/Goddard SHOOT experiment. If this experiment is successful, valuable data will be obtained.

1.1 REQUIREMENTS

The He-II transfer requirements used in this study are based primarily on the needs for orbital refilling of the Space Infrared Telescope Facility (SIRTF). Because the on-orbit vent of the tank is performed by the porous plug, there is no need to control the vapor ullage, which simplifies the design.

Preliminary requirements were established and were used in the study. These requirements are summarized in Table 1-1.

The actual tank geometry has not been established. The three candidates that have been suggested are shown in Fig. 1-1. Configuration a is spherical with an inner diameter of 292 cm. Configuration b is similar but utilizes elipsoidal ends with a cylindrical section. Configuration c has spherical segments as ends and utilizes a cylindrical section between them. The final configuration of the tanker has not been selected. A number of parameters should be used to evaluate each candidate. Some of these parameters are weight, volume-to-length ratio, thermal protection system, modularity, and liquid management. Configurations a and b would be structurally more sound

Table 1-1 FLUID MANAGEMENT REQUIREMENTS

Tank Volume: 13,000 L

Flow Rate: nominal 500 L/h, goal 1,000 L/h

Temperature: 1.8 ● 0.05 K

Maximum Orbital Accelerations: steady 10^{-4} g_0 (any direction)

Minimum Expulsion Efficiency: 95 percent

Structural Loads: cool-down from 300 K, 12 g_0 static load, random vibration at TBD, multiple flights

Maximum Thermal Load: 0.5 W parasitic, 50 W pump dissipation

Submerged Pump Envelope: 5 in. diameter, 6 in. high

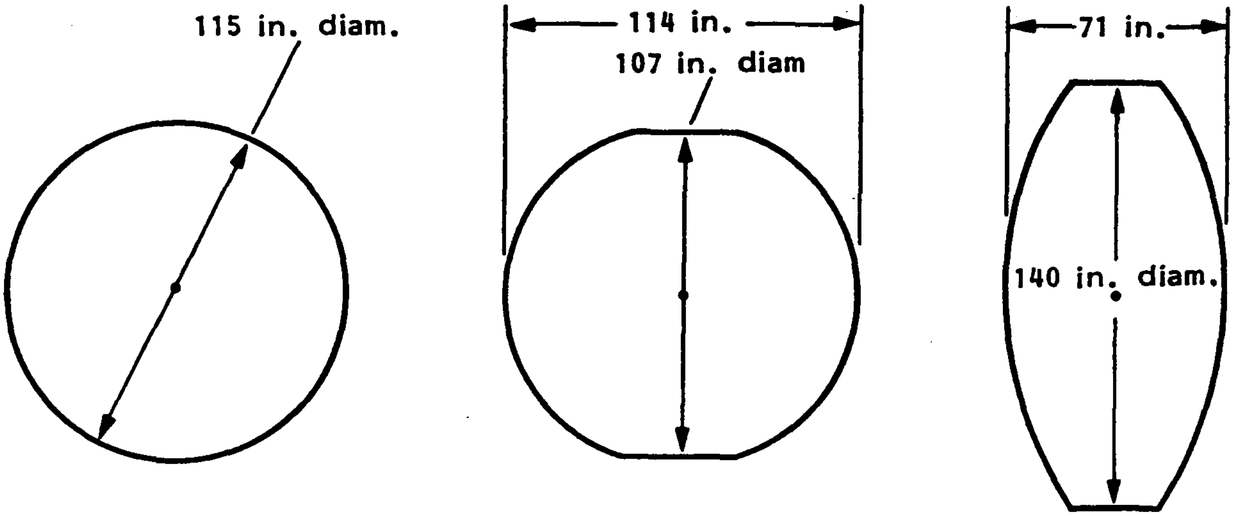

a. SPHERICAL

b. CYLINDRICAL WITH ELIPTICAL ENDS

c. CYLINDRICAL WITH SPHERICAL ENDS

Fig. 1-1 Tank Geometry Candidates (13,000 L)

and would lead to a lower weight. Configuration c has the smallest volume-to-length ratio. Configurations b and c would provide modularity by allowing the tank volume to be changed by changing the cylindrical section. Configuration c has a lot of sharp curvature sections which would trap some liquid under low gravity and would probably lead to higher residuals at depletion. The final selection of the tank should be based on all these considerations and on a detailed mission analysis, to determine if a low volume-to-length ratio is a driving parameter. The tank selection will be further addressed in the NASA/JSC Superfluid Helium Tanker (SFHT) study.

For this study, configuration b was selected; however, the general analysis and conclusions regarding the fluid management devices would apply to all configurations.

The design margins that will be used in this study represent a tradeoff between maximizing excess capability for system reliability versus obtaining a system design which can be manufactured by conventional methods at reasonable cost. Based on LMSC's previous experience with capillary devices, a factor of 3 conservatism in capillary capability performance will be used. This will allow relatively wide tolerances on manufacturing accuracy and/or raw material construction (i.e. screen hole sizes) as well as permitting variations in the requirements themselves. Since there is no data on the capillary retention capability of screens to He II, it will be assumed that the liquid only reaches one half its theoretical value when applied to screens.

In any tests that are identified, a test factor of conservatism of 2 should be adopted to allow for the variability imposed by test conditions while still overtesting relative to the requirement values.

1.2 BULK-LIQUID BEHAVIOR

The governing parameters used for determining the bulk liquid configuration in low gravity are the dimensionless Bond number (Bo), which is the ratio of body forces to surface force ($\rho g r^2/\sigma$), and the contact angle.

The configuration of the liquid-vapor interface has been studied analytically by many investigators. All these analyses indicate that the interface configuration is primarily dependent on the contact angle and that during zero gravity the interface tends to assume a constant-curvature surface that intersects the tank wall at the contact angle. In Section 2.2, it will be shown that He II has a zero contact angle. Therefore, in spheres, the interface takes the form of a spherical vapor bubble in the interior of the liquid for all percentages of filling. The interface in other geometric containers takes the form where it intercepts the tank wall at a contact angle of 0° for all percentages of filling until the vapor ullage is small enough to take a spherical configuration. This is shown in Fig. 1-2, where sketches of the interface for various containers are shown for liquid fillings of 10, 50, and 90 percent. These are based on results of drop-tower tests (Ref. 1-2)

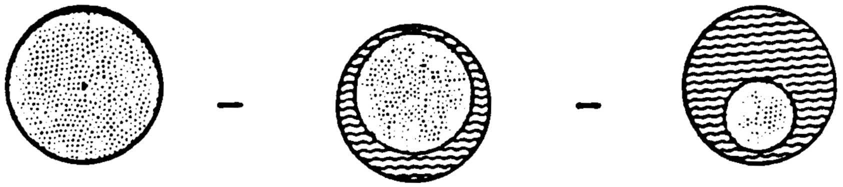

a. SPHERICAL CONTAINERS

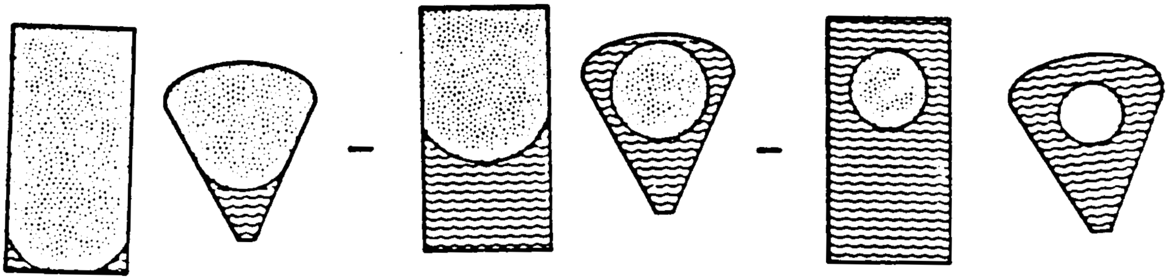

b. OTHER GEOMETRIC CONTAINERS

Fig. 1-2 Configuration of Liquid-Vapor Interface During Weightlessness

with ethyl alcohol (contact angle, 0°). During these tests, the drag acceleration on the small experimental packages was kept below 10^{-5} g_0, leading to an extremely small Bond number and assuring that the surface tension forces are dominant.

In the large tank that is being analyzed in this study, the Bond number is very large even at a low acceleration of 10^{-4} g_0. This is primarily due to the low kinematic surface tension (σ/ρ) of the He II and the large radius of the tank. The kinematic surface tension of helium, as shown in Fig. 1-3, is an order of magnitude lower than that of other cryogens and storable propellants.

This low value makes it more difficult to utilize surface tension forces to control the liquid behavior against adverse acceleration. The Bond number of the He II in tanks is shown in Fig. 1-4. For the tank being studied, with an average radius of 140 cm at an acceleration of 10^{-4} g_0, the Bond number is

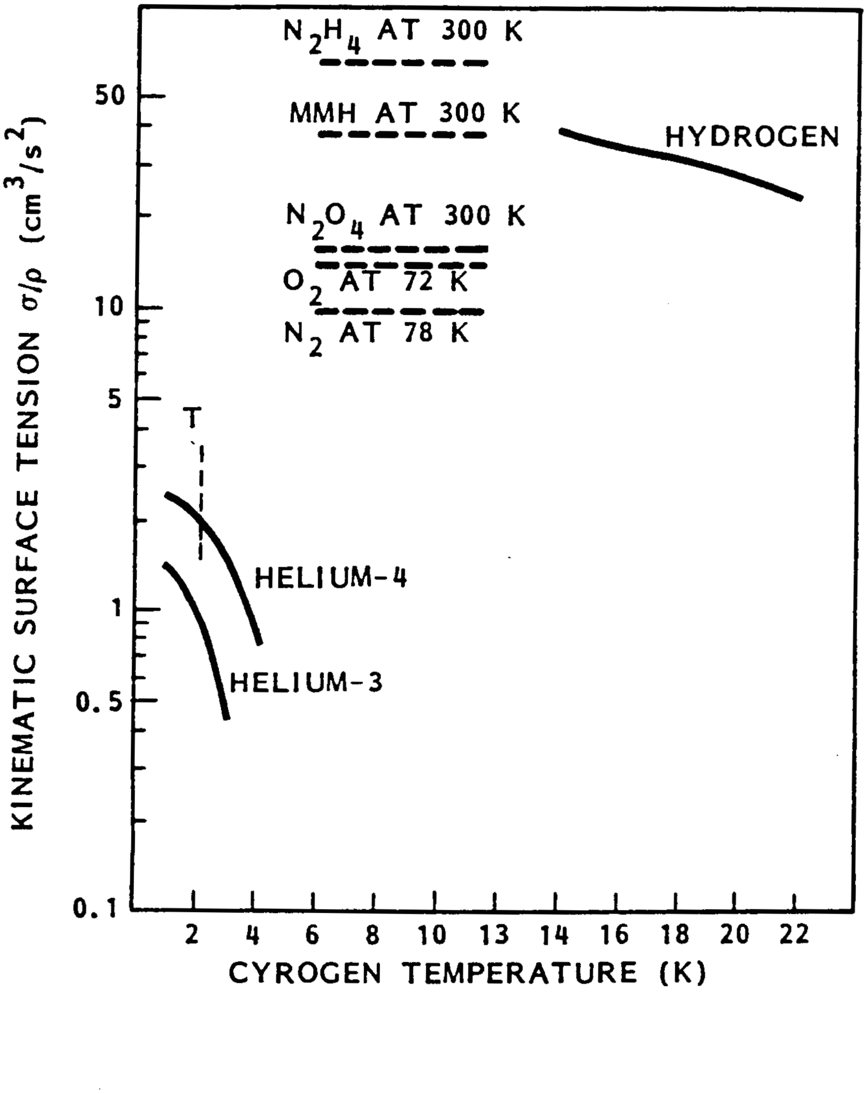

Fig. 1-3 Kinematic Surface Tension

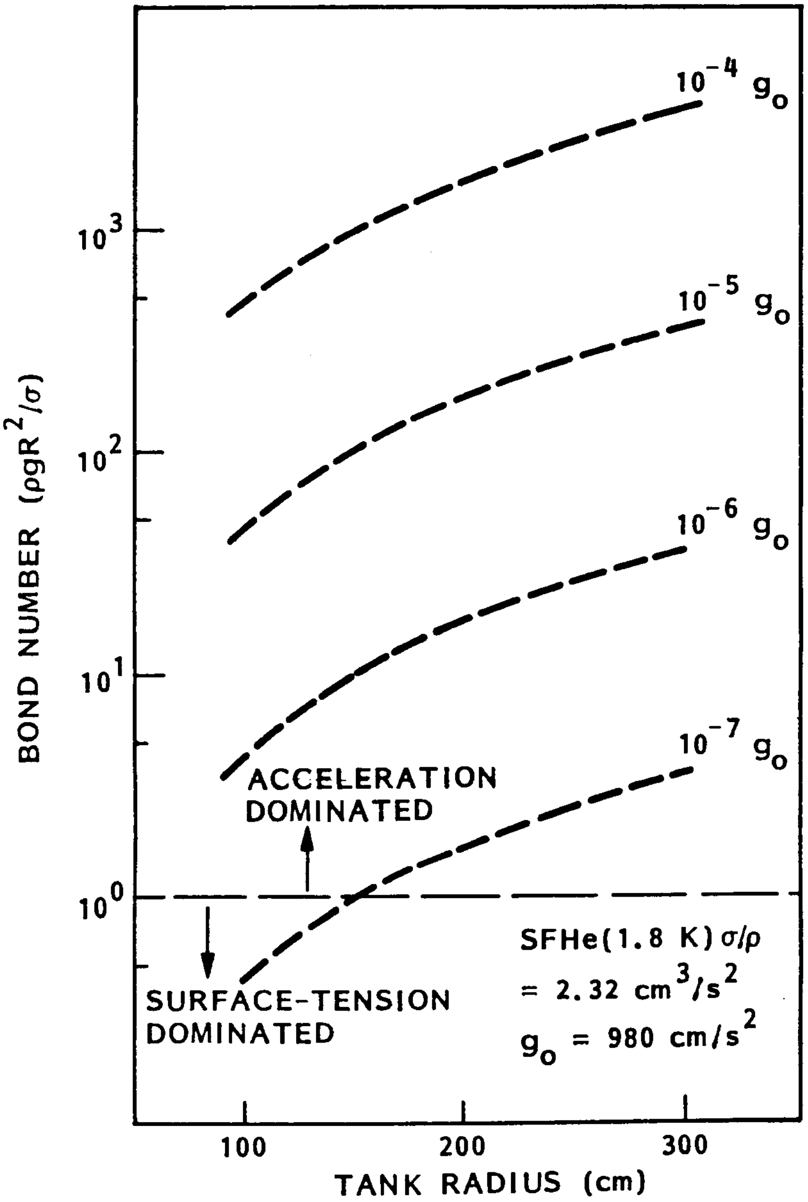

Fig. 1-4 He-II Tank Bond Numbers

887. This shows that the liquid-vapor interface shape is dominated by the acceleration forces and will be essentially flat. A small curvature will exist at the tank wall to preserve a zero contact angle.

No attempts were made to model the forces due to sloshing of the fluid. However, since the liquid will be settled in a 1-g_0 and a 10^{-4} g_0 acceleration field, it is worth noting that the natural frequencies of the fluid are readily available. Since the tank being studied is nearly spherical, data on spherical tanks can be used to predict natural frequencies. In modeling, the frequency parameter λ_n is used. This parameter is a function of the liquid-depth ratio (h/2R) for settled liquids, where h is the maximum depth of the liquid and R is the tank radius. The natural frequency can then be found by the following expression

$$W_n = \sqrt{\lambda_n} \sqrt{\frac{g}{R}}$$

where g is the settling acceleration. The values of the frequency parameter for various depth ratios are shown in Table 1-2 for the first three natural frequencies (Ref. 1-3).

For the tank in question (R = 140 cm), when it is 90 percent full (h/2R = 0.8) the first natural frequency is 0.69 Hz at 1 g_0 and 0.0069 Hz at the orbital acceleration of 10^{-4} g_0. These frequencies will decrease as the tank is drained. This information can be used to determine if sloshing will be a problem for the orbital attitude-control system of the tanker and to determine if any slosh control in the tank is required. The gallery devices described in Sections 4 and 5 will not damp the fluid sloshing in the tank.

Table 1-2 NATURAL FREQUENCY PARAMETER IN SPHERICAL TANKS

Liquid-Depth Ratio, h/2R	Natural Frequency Parameter		
	$\sqrt{\lambda_1}$	$\sqrt{\lambda_2}$	$\sqrt{\lambda_3}$
0.1	1.0573	2.7758	3.6775
0.2	1.0938	2.4947	3.2430
0.3	1.1370	2.3731	3.0592
0.4	1.1893	2.3232	2.9785
0.5	1.2540	2.3218	2.9639
0.6	1.3376	2.3655	3.0080
0.7	1.4528	2.4655	3.1236
0.8	1.6300	2.6608	3.3580
0.9	1.9770	3.1019	3.8969

Section 2

He-II PROPERTIES

In the design of low-gravity liquid-management devices, the properties of the liquid must be well established in order to properly model the performance of the device. In particular the surface tension and the wetting characteristics must be known. In this study, the properties of He-II at 1.8 K were used throughout and are summarized in Table 2-1.

Table 2-1 He-II PROPERTIES AT 1.8 K

Density (ρ)	0.1453 g/m^3
Vapor Pressure (P_v)	12.26 torr
Surface Tension (σ)	0.3377×10^{-5} N/cm
Bulk Viscosity (η_n)	12.799×10^{-6} g/cm-s

The experimental measurements of He II were reviewed in order to have confidence in the value used for the study. The wetting characteristics of the fluid were also studied and reviewed.

2.1 SURFACE TENSION

The surface tension of a liquid is a measure of the free energy associated with unit area of its surface. Surface tension is most often measured by the conventional capillary-rise method, in which the rise of He II in contact with its saturated vapor in capillaries is measured. A literature search was conducted and a summary of the results is shown in Fig. 2-1. The measurements by Onnes (Ref. 2-1) were performed in capillaries of 180-μm and 400-μm diameter. Atkins and Narahara (Ref. 2-2) made more than 300 measurements in the course of their investigation with small capillaries of diameters in the range between 70 μm and 140 μm and with larger capillaries between 240 μm and 460 μm. Their values are consistently higher than the Allen/Misener and

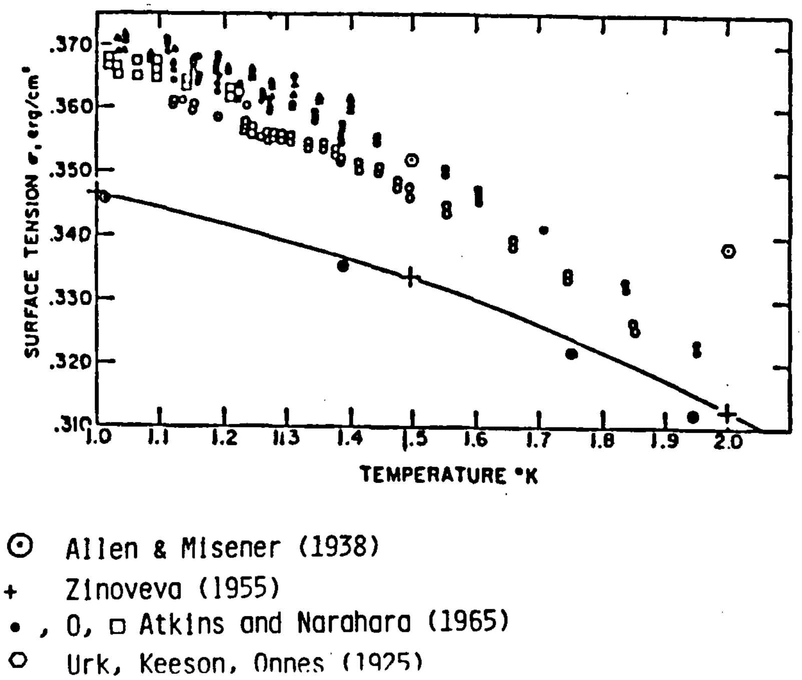

Fig. 2-1 Review of He-II Surface Tension Data

Zinoveva data (Refs. 2-3 and 2-4), with a difference as much as 7 percent at 1 K and much lower at 1.8 K. Atkins used the method of least squares to curve-fit his data and came up with the following equation for the surface tension (erg/cm^2) of He II at low temperatures:

$$\sigma = 0.3729-0.0081\ T^{2.5}$$

This empirical curve, evaluated at 1.8 K, gives the value shown in Table 2-1.

2.2 CONTACT ANGLE

The contact angle is defined as the angle at whicn the liquid-vapor interface meets the solid surface, measured through the liquid, as shown in the following illustration. The lower the contact angle, the more the fluid is considered a good wetter.

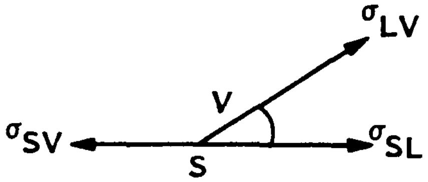

From the Young's equation the contact angle can be expressed as a function of various surface tension forces

$$\cos \theta = \frac{\sigma_{SV} - \sigma_{SL}}{\sigma_{LV}} \tag{2.1}$$

where θ is the contact angle and σ is the surface tension. Subscripts S, L and V stand for solid, liquid, and vapor, respectively, such that σ_{SV} represents the surface tension between the solid and vapor phase.

Most of the solids in nature can be categorized as being low- or high-surface-energy solids. For low-surface-energy solids (e.g., Teflon and graphite), Girifalco and Good (Ref. 2-5) proposed an analogy between the surface-tension forces and the attractive energy between like and unlike molecules. They show that the surface tension between the solid and liquid can be written as

$$\begin{aligned} \sigma_{SL} &= \sigma_{SV} + \sigma_{LV} - \frac{8(\sigma_{SV}\sigma_{LV})^{1/2}(V_S V_L)^{1/3}}{(V_S^{1/3} - V_L^{1/3})^2} \\ &= \sigma_{SV} + \sigma_{LV} - 2\Phi(\sigma_{SV}\sigma_{LV})^{1/2} \end{aligned} \tag{2.2}$$

where V_S and V_L are the molar volume of the solid and the liquid respectively. Combining the Young's equation (Eq. (2.1)) with Eq. (2.2) it can be shown that if

$$\Phi^2 \sigma_{SV} > \sigma_{LV}$$

then the contact angle has to be equal to zero. For the contact of He-II with most solids $\Phi \sim 1$, and since $\sigma_{SV} >> \sigma_{LV}$ (0.34 erg/cm) it can be concluded that $\theta = 0$.

As for the case of high-surface-energy solids (e.g., most metals) the interaction between the solid and fluid (vapor or liquid) is by adsorption.

Since He II is a saturated vapor, the number of adsorption layers approaches infinity. There is no distinction between a solid surface covered by a saturated vapor film or a surface covered by liquid. Therefore, the contact angle must be zero.

Various experimental observations made in one g_0 and in low g_0 environments (Refs. 2-6 and 2-7) show that He II will coat the inside of a tank with a saturated film of a few hundred angstroms. In the absence of gravity, the He II will tend to distribute itself to fill areas of sharp curvature and will distribute itself uniformly so that all surfaces will be covered with bulk liquid. These observations essentially show that He II is a very good wetter and therefore must have a zero contact angle.

2.3 VAPOR ULLAGE

The thermodynamic analysis in Ref. 2-8 indicated that the stable equilibrium state of a capillary system in an isothermal environment is the state where the potential energy

$$PE = \sigma A_c$$

has the least value. A_c is defined as the capillary area. There may be several states for which small perturbations in configuration result in an increase in PE; all of these states save the one of lowest PE are metastable, for with a sufficiently large disturbance, the system will pass to the stable state. This behavior is indicated in the sketch below.

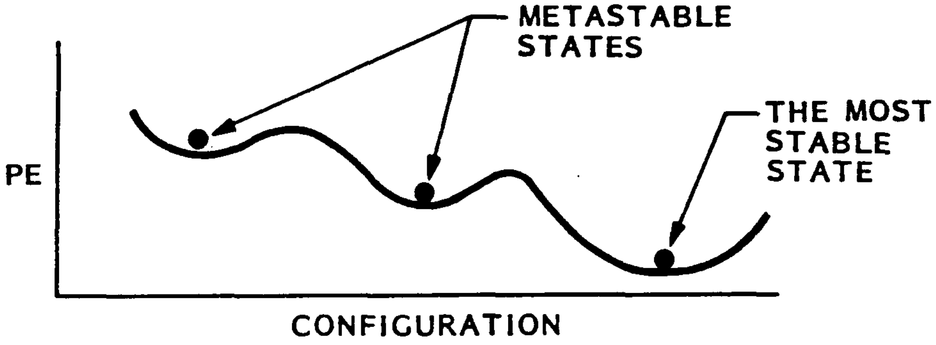

We can use this idea to determine where vapor is most likely to be found in a container. It is important to realize that one cannot be sure from these considerations that the system will indeed be in this stable state; it may be "trapped" in a metastable state. Since the surface tension is presumed to be dependent only on temperature, it is constant in an isothermal system; we need only to investigate the capillary area A_c. Thus, the calculation is entirely geometrical.

Consider first a collection of vapor bubbles away from interaction with walls. Suppose the bubbles are floating aimlessly about, and we seek to learn if there will be any tendency for them to merge upon contact with one another. Let us take the simple case where all N bubbles have the same diameter D. If V represents the total vapor volume, then

$$V = C_1 ND^3$$

The capillary area of each will be proportional to D^2, and the total capillary area is therefore

$$A_c = C_2 ND^2$$

Since V is fixed, we conclude that the capillary area is of the form

$$A_c = C_3 N^{1/3}$$

The capillary area will therefore be least when the bubbles are merged into one. The general proof of this is a classic problem in the calculus of variations, where one finds that the shape of smallest surface area for given volume is a single sphere. We conclude therefore that the vapor bubbles will tend to coalesce to form a single large sphere.

When a vapor bubble is imbedded in a liquid, the pressure difference between the inside and the outside of the bubble is given by

$$\Delta P = \sigma \left(\frac{1}{r_1} + \frac{1}{r_2}\right)$$

where r_1 and r_2 are the principal radiu of curvature. For a spherical bubble where r_1 is equal to r_2, this reduces to

$$\Delta P = \frac{2\sigma}{r}$$

Therefore, for a system which has more than one bubble, the pressure inside the smallest will be the largest.

For a saturated liquid-vapor system, there may be a "temperature" at the interface which corresponds to the pressure inside the bubble. If this is somewhat the case, then there may be a higher "temperature" in the bubble that has the highest pressure and smallest radius. This would set up a potential to drive energy from the smallest bubble to the larger one.

In the case of He II, where the thermal conductivity of the liquid is enormous, the potential to drive energy would be large. In this case, vapor in the smaller bubble would condense and, in order to conserve mass, the vapor would reappear in the larger ullage. This mechanism would drive energy from the smaller bubble to the larger one and allow the vapor to achieve a minimum capillary area. This phenomenon is probably what has been observed with helium boiling. Observations in 1-g_0 have shown that as the temperature of helium is reduced to below the lambda point, boiling ceases, all vaporization takes place at the liquid/vapor interface that has a large radius, and no smaller radii bubbles are seen.

In the case of He-II management devices, it would appear that any vapor bubbles trapped in the device would condense and reappear in the larger vapor ullage.

Section 3

OPEN-CAPILLARY DEVICES

One of the simplest types of devices used for liquid management in low gravity is an open capillary device as shown in Fig. 3-1 This device utilizes the surface tension of the liquid to form fillets betwen the baffles. The extension of the ends of the baffles provides the means of acquiring the liquid that may be settled on the side of the tank and bringing it to the core of the baffles. At the outlet a gas arrester is needed to suppress the surface dip of the liquid as it enters the outlet cavity which would house the pump.

Because the spacing between the baffles is large, and the surface tension forces are inversely proportional to the meniscus radius, the capability of such a device is generally very low. A top-level assessment of its performance was performed to determine its capability before any design or detailed analysis was performed, if warranted.

Under low accelerations, the liquid is assumed to be uniformly distributed among the baffles. With a zero contact angle, the liquid geometry in each channel is as shown below where tan $\delta/2 = r/R$.

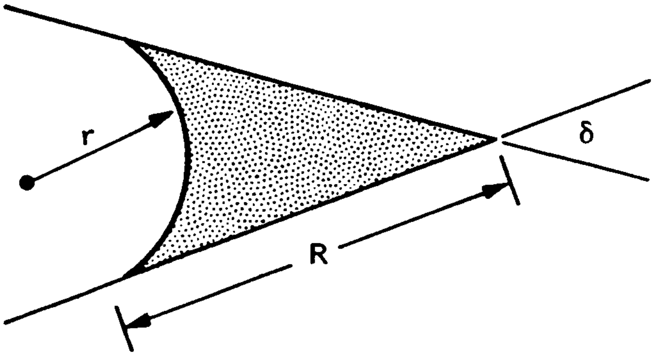

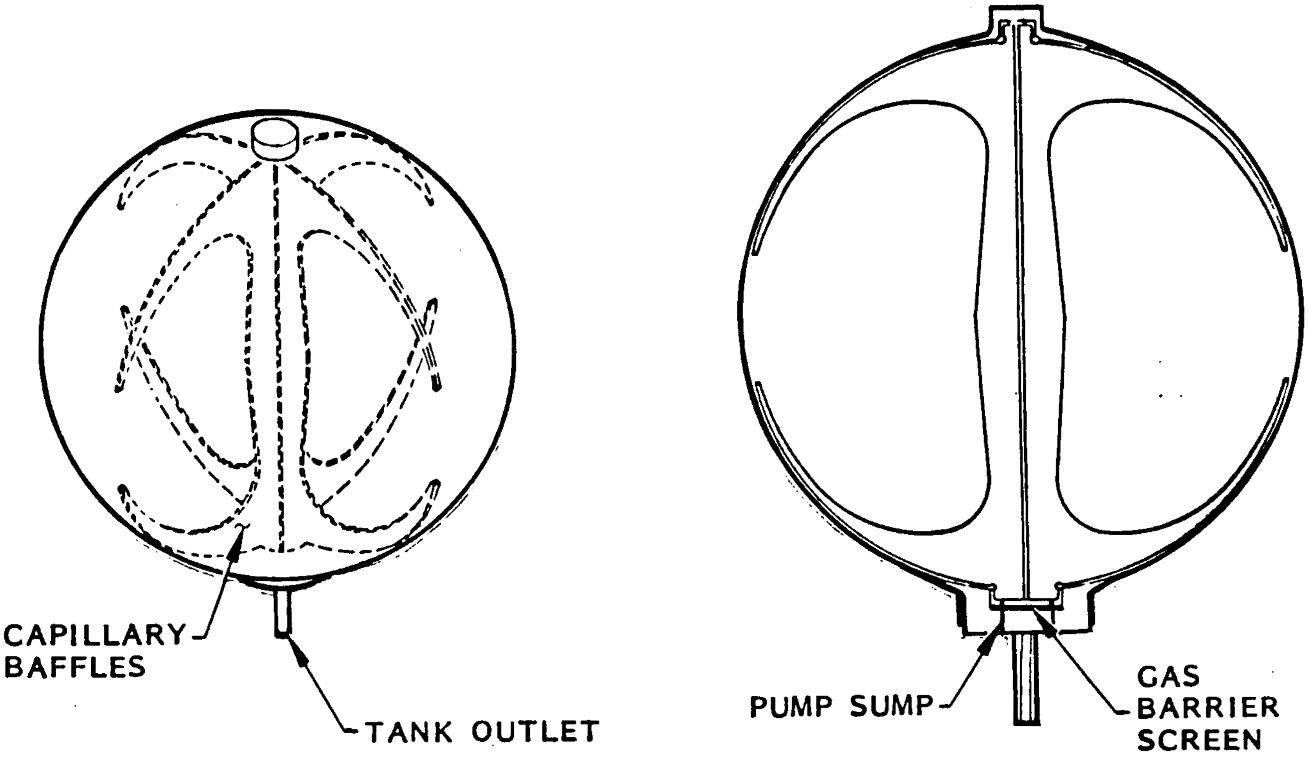

Fig. 3-1 Baffle Capillary Device

The cross-sectional area of the liquid mass in each channel is given by

$$A_C = r^2 \left(\frac{1}{\tan \delta/2} + \frac{\delta}{2} - \frac{\pi}{2} \right)$$

and assuming that the total flow is evenly distributed in each channel, the velocity is

$$V = \frac{Q_T}{nA_C} = \frac{Q_T}{nr^2} \left(\frac{1}{\tan \delta/2} + \frac{S}{2} - \frac{\pi}{2} \right)^{-1} \qquad (3.1)$$

where n is the number of baffles, and $\delta = 2\pi/n$.

Neglecting flow losses due to friction, the capillary capability of the vapor/liquid interface is reduced to:

$$\Delta P_{cap} = \Delta P_{hydro} + \Delta P_{dynamic}$$

Therefore, the maximum adverse acceleration that the capillary system can stand up to is:

$$\frac{g}{g_0} = \frac{1}{h}\left(\frac{\sigma}{\rho g_0 r} - \frac{V^2}{2g_0}\right) \tag{3.2}$$

substituting Eq. (3.1) for the velocity in Eq. (3.2), a fourth-order polynomial equation for determining the minimum meniscus radius can be written.

$$\frac{g}{g_0} r^4 - \frac{1}{h}\frac{\sigma}{\rho g_0} r^3 + \frac{1}{2hg_0}\left(\frac{Q_T}{n}\right)^2 \left(\frac{1}{\tan \delta/2} + \frac{\delta}{2} - \frac{\pi}{2}\right)^{-2} = 0 \tag{3.3}$$

To determine the maximum acceleration that the capillary forces could overcome, this equation was solved for various accelerations until only a single real root could be found. These results are shown in Fig. 3-2. It can be seen that for the nominal flow rate of 500 L/h, an open capillary system for He II can only manage the liquid against adverse accelerations in the range of 10^{-7} g_0 to 10^{-6} g_0. These results are based on a factor-of-three conservatism in the capillary forces of the liquid/vapor interface and are evaluated at depletion conditions in the tank when the hydrostatic head is at its largest.

For the case where 32 baffles are used in the tank, the maximum capability of the device is 2.3×10^{-6} g_0 for a flow rate of 500 L/h.

At this point the minimum radius of the liquid/vapor interface is 0.88 cm, which provides a capillary pressure of 9×10^{-4} g_0-cm. The hydrostatic

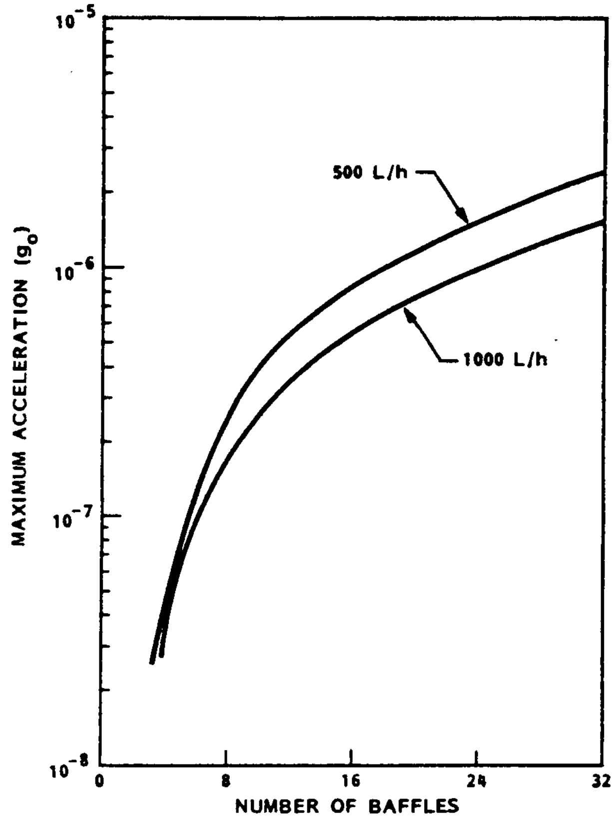

Fig. 3-2 Open-Baffle Device Capability

load is 6.7 x 10^{-4} g_0-cm and the dynamic load is 2.1 x 10^{-4} g_0-cm. This high dynamic load is due to the low-flow area caused by the required small-radius liquid/vapor interface. The capability of the device varies linearly with the hydrostatic head and therefore the size of the tank would have to be reduced by two orders of magnitude to achieve a small residual at 10^{-4} g_0.

In order to further increase the capability without having to install an impossible number of baffles, a ridged ribbon device was evaluated. This device is shown in Fig. 3-3 where the grooves in the ribbon provide a large number of small flow passages. The analysis is essentially the same as the baffle system except in evaluating the velocity, where n is now the number of grooves and δ is the angle of the groove.

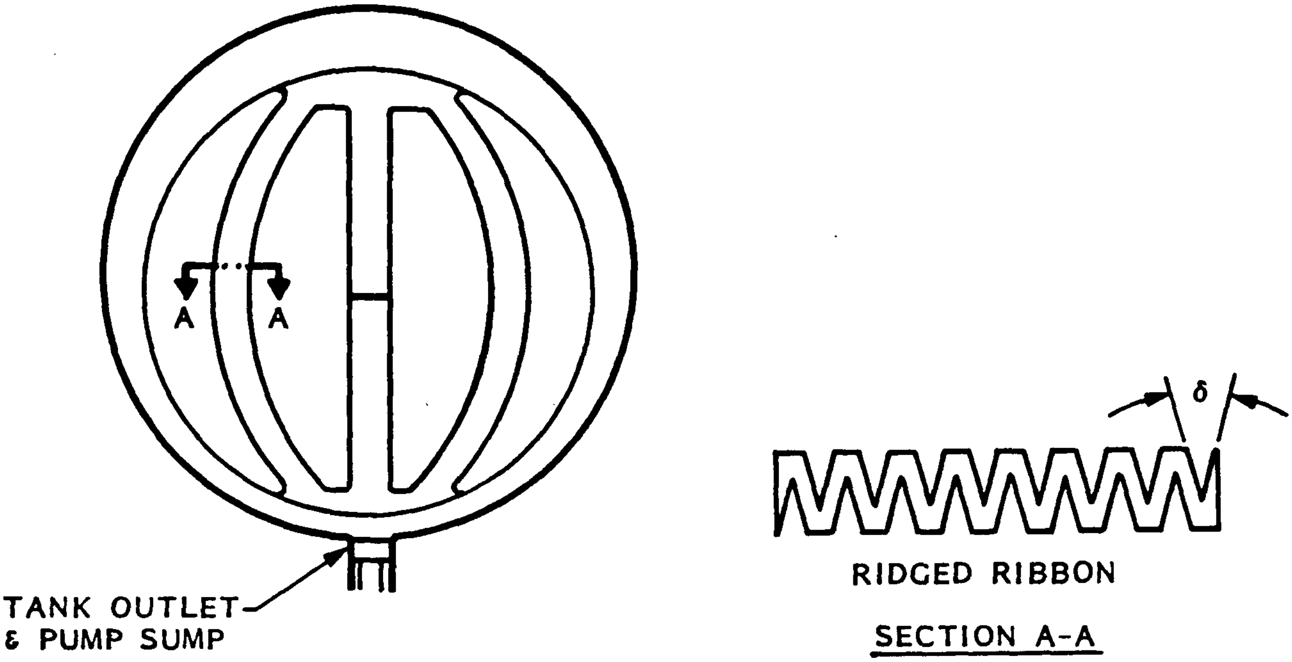

Fig. 3-3 Ribbon Capillary Device

The maximum number of grooves is determined by the minimum required liquid/vapor interface radius. As the radius gets smaller, the required depth of the groove goes down and therefore more grooves can be made per unit width of ribbon. The maximum number of grooves is thus

$$n = \frac{LB}{r \cos \delta/2}$$

where L is the width of the ribbon which has grooves made on both sides and B is the number of ribbons. Assuming that the flow is evenly distributed to each ribbon, the velocity of the liquid is:

$$V = \frac{Q_T}{LBr} \cos \frac{\delta}{2} \left(\frac{1}{\tan \delta/s} + \frac{\delta}{2} - \frac{\pi}{2} \right)^{-1} \qquad (3.4)$$

Substituting Eq. (3.4) into Eq. (3.2), a quadratic equation for the minimum meniscus radii of the liquid/vapor interface can be derived as

$$\frac{g}{g_o} r^2 - \frac{1}{h} \frac{\sigma}{\rho g_o} r + \left(\frac{Q_T K}{LB}\right)^2 \frac{1}{2hg_o} \tag{3.5}$$

where

$$K = \cos\frac{\delta}{2}\left(\frac{1}{\tan\delta/2} + \frac{\delta}{2} - \frac{\pi}{2}\right)^{-1}$$

This equation can be solved for the maximum acceleration that the capillary forces could overcome. This occurs when only one real root can be found. It can be shown that this occurs when

$$r = \frac{(\sigma/\rho h g_o)}{2g/g_o}$$

and solving for the acceleration gives

$$\frac{g}{g_o} = \frac{1}{2rh}\,\frac{\sigma}{\rho g_o}$$

This acceleration is half of the capability of a meniscus that is supporting a static column of liquid, thus the dynamic head is half of the load on the meniscus.

It can also be shown that the maximum acceleration from solving Eq. (3.5) is:

$$\left(\frac{g}{g_o}\right) = \left(\frac{\sigma}{\rho g_o}\right)^2 \frac{g_o}{h2K^2}\left(\frac{LB}{Q_T}\right)^2$$

The results are shown in Fig. 3-4 for ribbons 10 cm wide. It can be seen that this device would would only be capable of accelerations in the 10^{-6} g_0 to low 10^{-5} g_0 range. This is lower than the required 10^{-4} g_0. The capability varies linearly with the hydrostatic head. Therefore, the size of the tank would have to be decreased considerably in order to have low residual in the 10^{-4} g_0 range.

One can argue that a very large number of ribbons could be installed in the tank in order to reach the desired acceleration capability. The assembly and manufacturing of such a system would become prohibitive since a total width of ribbon of over 500 cm would be required. For the case where 24 ribbons are used, the maximum capability of the device is 1.98 x 10^{-5} g_0 with a flowrate of 500 L/h. At this point the minimum radius of the liquid/vapor interface is 0.069 cm and each ribbon has 150 grooves. The tolerances required for machining these ribbons to accommodate these small meniscus radii

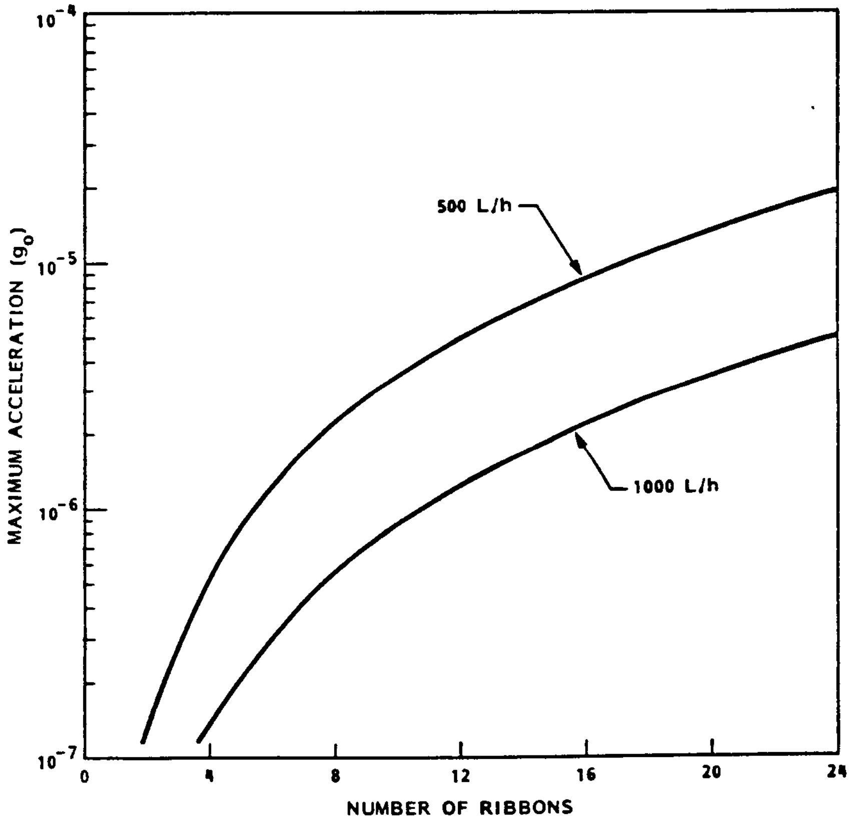

Fig. 3-4 Open-Ribbon Device Capability

make the device impractical. At the lower accelerations, in the low 10^{-6} g_0 range, the minimum meniscus radius increases to approximately 0.5 cm, which would be manageable.

In summary, neither open-capillary device examined here meets the requirement of managing the liquid against adverse accelerations of 10^{-4} g_0. This is unfortunate since these devices are the simplest capillary devices available and should be used whenever possible. Prior to entering the pump sump, the liquid is in direct contact with its vapor and it would seem that the chances of cavitation would be small. However, a gas-arrester screen or perforated plate is required at the entrance of the sump to prevent vapor ingestion. The flow of the liquid through this gas arrester would further drop the liquids' pressure and could induce cavitation. The question of cavitation is examined in detail in Section 4, which evaluates an enclosed-capillary device that can meet the requirements.

Section 4

ENCLOSED CAPILLARY DEVICE

An enclosed capillary device with gallery channels was selected as the primary device to provide liquid communication to the pump. A device for partial liquid retention was not selected, primarily because the acceleration may be continuously in an adverse direction, which would not allow the bulk liquid to replenish the device. Also not selected was perforated tank liner next to the tank wall, which provides constant communication and liquid feed from any bulk liquid location to the pump. Although the performance of this type of a device is approximately that of the gallery channel device, it would weigh a lot more.

4.1 DESIGN DESCRIPTION

The liquid-management device is a gallery device designed to allow most of the liquid to move about in the tank bulk space while maintaining fluid paths to the pump. Only the liquid in the screen-covered gallery channels and the lower and upper receivers will be contained. The device operates by providing surface-tension-dominated liquid paths from all locations within the tank to the lower receiver. The gallery assembly is shown in Fig. 4-1, where gallery channels connect an upper and lower receiver. The lower receiver encloses the He-II pump used to pump the liquid out of the tank.

The gallery assembly is composed of seven identical gallery channels, which are oval tubes shaped to conform to the tank walls. The spacing between the channels and the tank wall is 0.75 in. Openings in the tubes are covered with screen on their outer faces to allow a liquid flow path into the channels. The screens are attached by sandwiching the screen between two doublers which are electron-welded to the gallery channel. The screen is a 50 x 250 mesh plain dutch weave. A rib type of opening on the outboard side of the channel

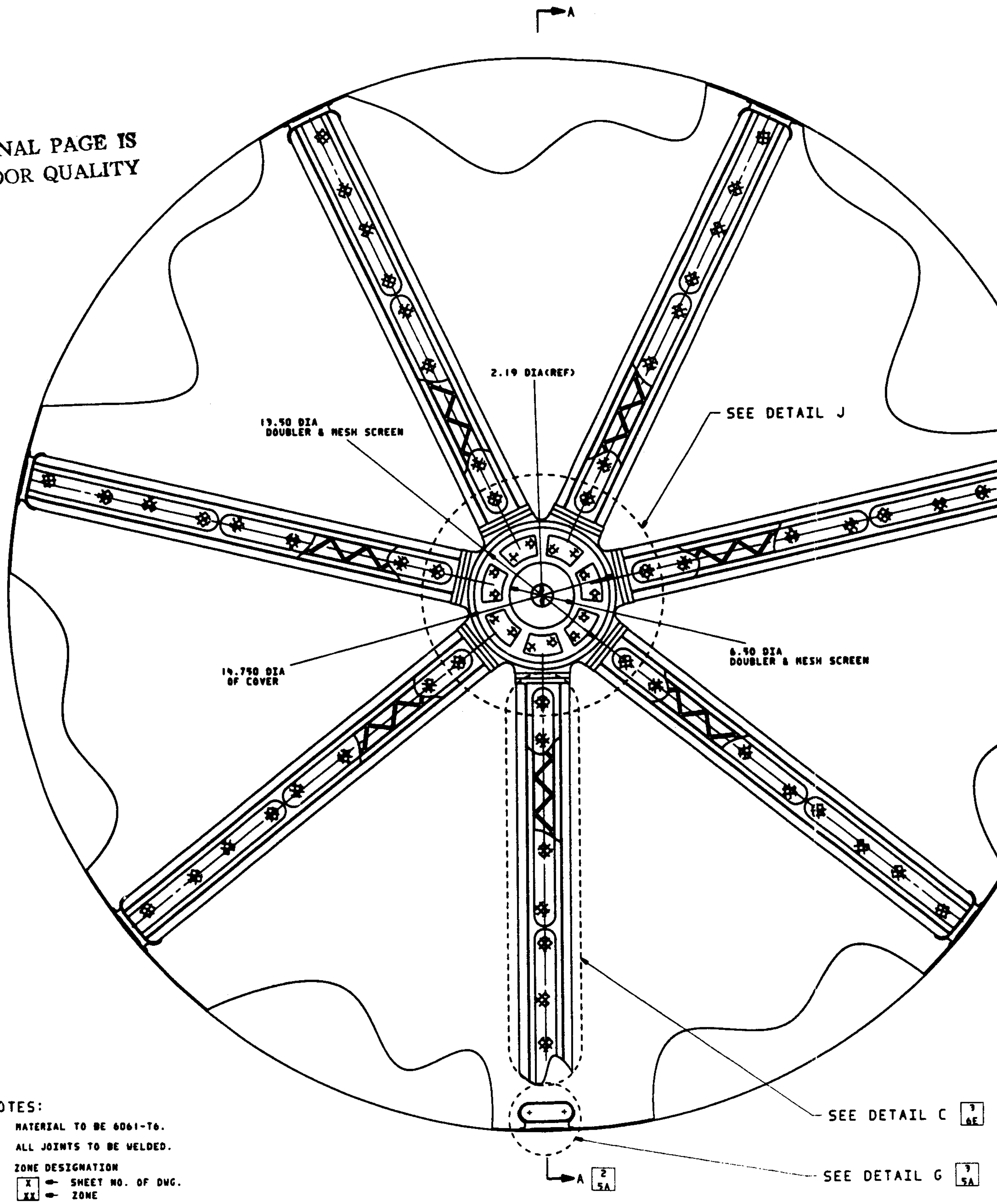

NOTES:
1. MATERIAL TO BE 6061-T6.
2. ALL JOINTS TO BE WELDED.
3. ZONE DESIGNATION
   X ← SHEET NO. OF DWG.
   XX ← ZONE
4 (BOTH END OF GALLERY ARM)

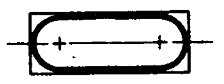

SECTION P-P
SCALE: 1/2

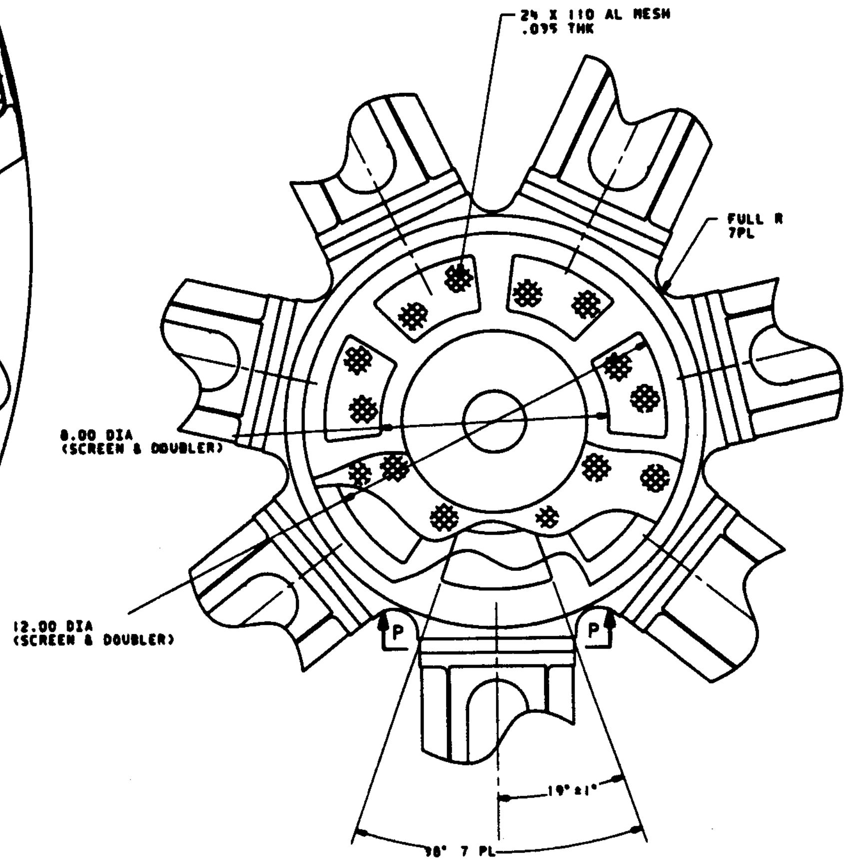

DETAIL J
SCALE: 1/2

Fig. 4-1 Gallery Device Tank Assembly
(1 of 4)

ORIGINAL PAGE IS
OF POOR QUALITY

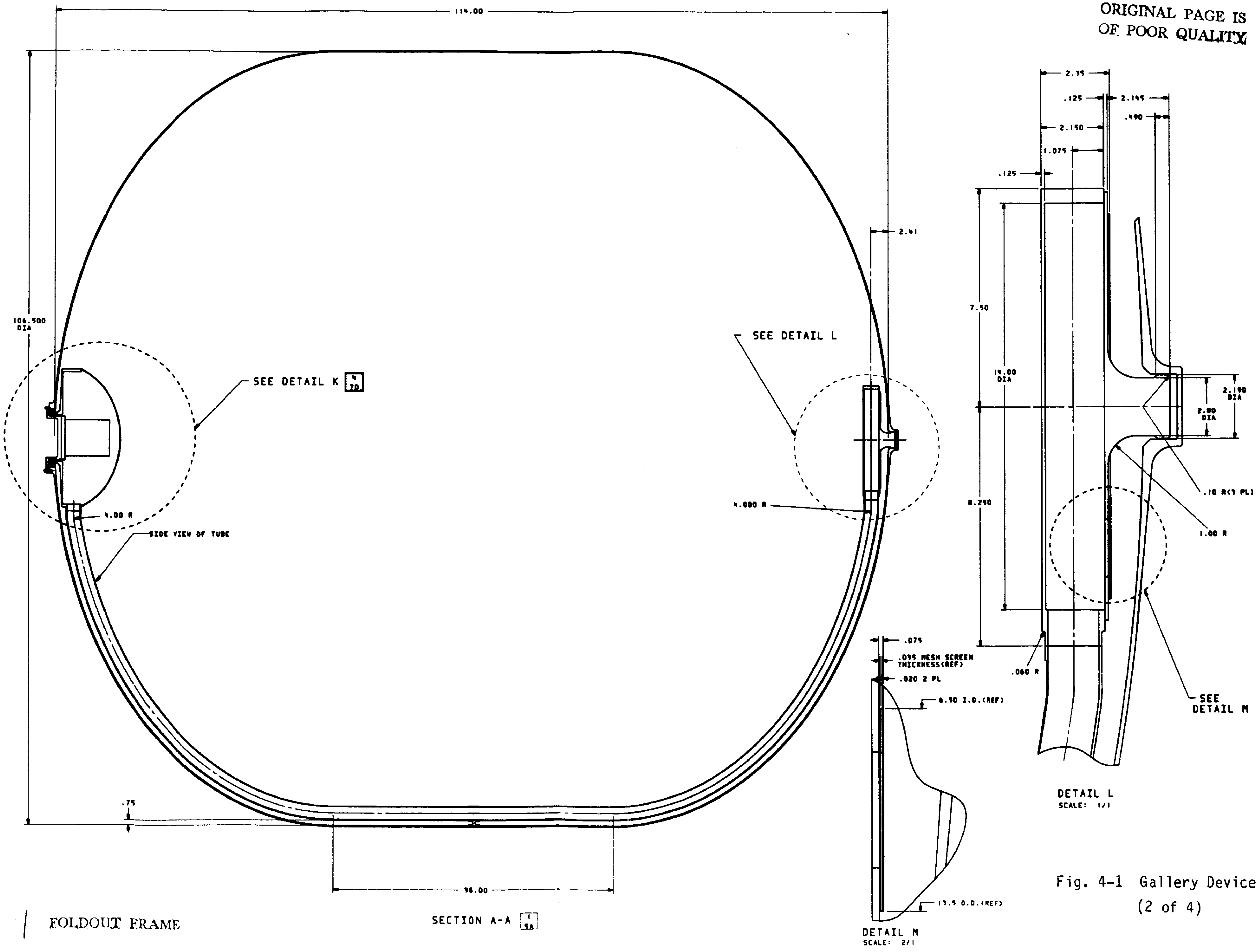

Fig. 4-1 Gallery Device Tank Assembly
(2 of 4)

1 FOLDOUT FRAME

2 FOLDOUT FRAME

ORIGINAL PAGE IS
OF POOR QUALITY

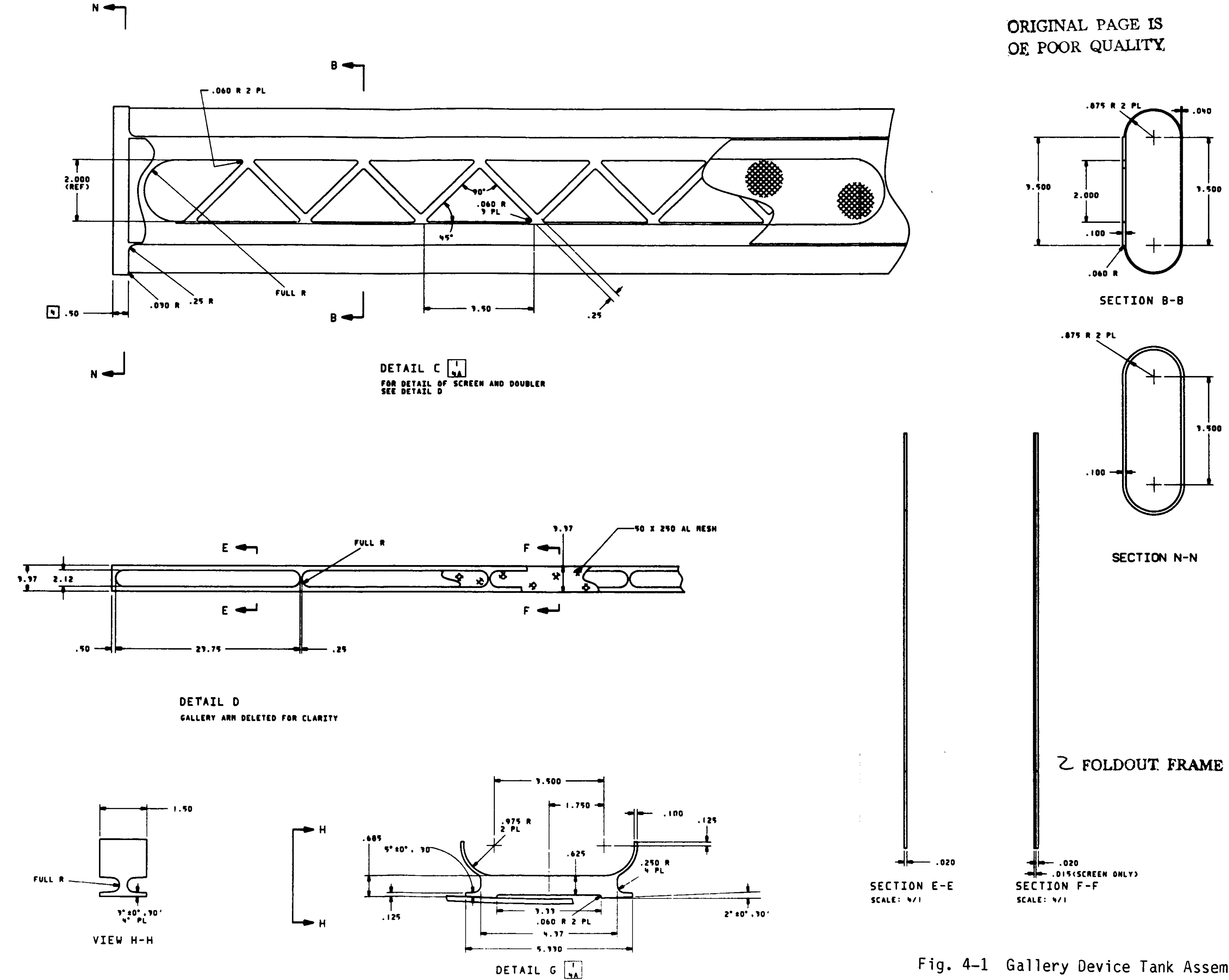

2 FOLDOUT FRAME

Fig. 4-1 Gallery Device Tank Assembly
(3 of 4)

1 FOLDOUT FRAME

ORIGINAL PAGE IS
OF POOR QUALITY

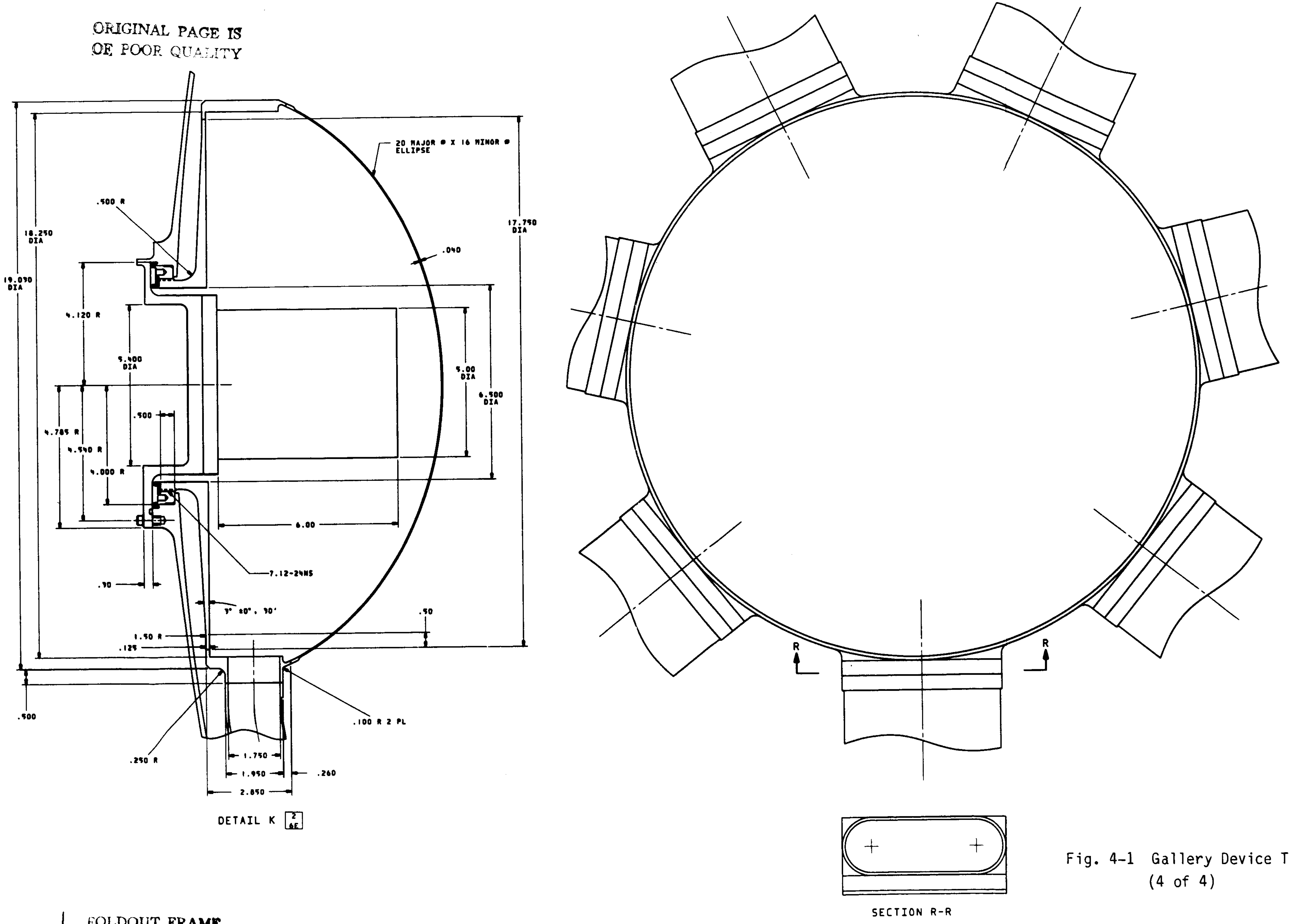

Fig. 4-1 Gallery Device Tank Assembly
(4 of 4)

is provided for resistance against torsion loads. The configuration shown provides over 80 percent open area to the screen. These arms are chemically milled to reduce weight while still providing the required weld thickening.

The tank gallery channels are supported at the lower and upper receivers. A structural support may be needed at the tank equator and is shown. This support may not be needed, but it could be retained to provide support of the liquid management system during integration into the tank.

The upper receiver is located at the upper intersection of the seven gallery channels. A coarser mesh, 24 x 110 plain dutch weave, is located at an annular opening in the receiver. The function of this coarser weave is discussed in the performance analysis. The support at the upper receiver is a sliding assembly that provides lateral support while allowing the tank to grow during pressure testing without stressing the management device.

The lower receiver consists of a bottom plate welded to a ring with fittings that connect to the gallery channels by butt welds. The top consists of a thin hydroformed shell welded to the ring. This lower receiver provides the region to store the pump. The volume was sized to accommodate a pump envelope of 5-in. diameter, 6 in. high.

The device is designed to be fully assembled prior to insertion into the tank. The device is lowered into the tank and secured by a large nut by use of a spanner wrench. Once secured, welds are made to prevent gas ingestion around the nut. Two concepts for sealing and insertion of the pump plate are shown. One design utilizes a bolted connection backed by a seal, the other welds the pump in.

4.2 DESCRIPTION OF OPERATION

Figure 4-2 shows the operation of the management device during all phases of the mission. In this sequence, the operations are separated into three categories: ground operations, boost operations, and orbital operations.

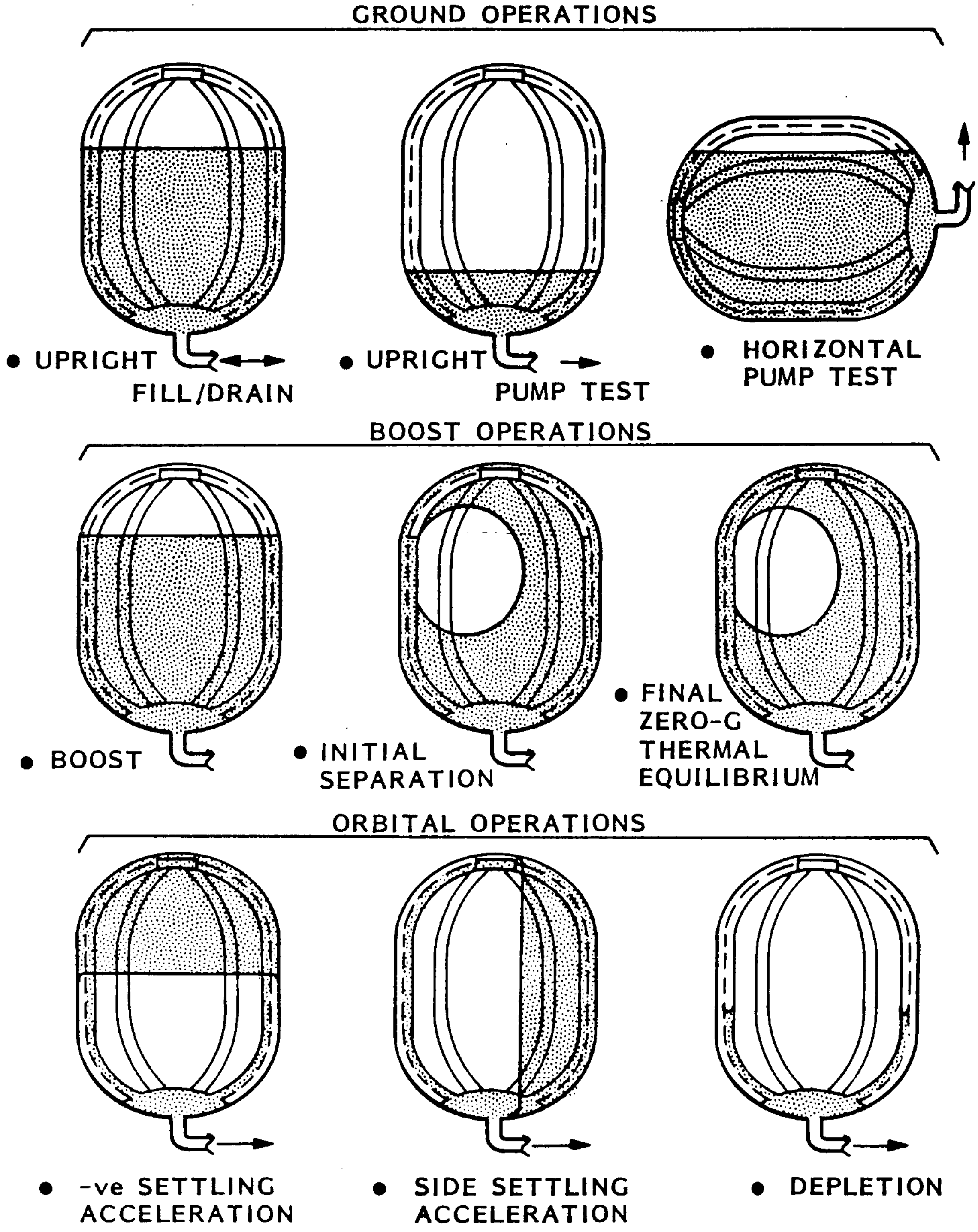

Fig. 4-2 Operational Sequence

The actual operations during the mission have not been established; therefore an estimate will be made in order to evaluate the management device.

The liquid-management device has been designed to function independently of any vehicle events before injection into orbit.

4.2.1 Ground Operations

The sequence of events on the ground is the least defined sequence at this point. These operations will be addressed by the NASA/JSC SFHT study. The primary sequences will be cool-down, fill, pump test, and drain. The orientation of the tank during these sequences has not been defined. In this study, the only plumbing identified is the outlet liquid drain during orbital transfer of He II. Any limitations on the orientation of the tank during cool-down and fill operations will be partially set by the plumbing required to vent the vapor ullage. The liquid fill may not be able to be done by backflowing through the pump; therefore some tanker orientation limitations may be imposed by this operation. If a liquid drain must be accomplished on the ground, the internal fill plumbing may or may not be used. The tank must be drained with the lower receiver down. The amount of liquid trapped in the tank when the liquid stops flowing out will vary depending on the orientation of the tank. Heat flow into the tank will cause residual liquid to vaporize, therefore the orientation of the management device will have no effect on liquid residual during ground draining.

Any requirements for demonstrating the performance of the pump with He II installed in the tank will put a limitation on the orientation. Since the management device cannot control the liquid against a 1-g_0 acceleration, some restrictions are imposed. With the tank upright (lower receiver down) or on its side the liquid fill level must be kept high enough to keep the lower receiver submerged. In any event, none of the limitations imposed by ground operations will have an effect on the orbital performance of the liquid-management device.

4.2.2 Boost Operations

During boost, the liquid body will be settled by the acceleration field and in the same position at the end of ground hold. During launch, when the acceleration increases to 3 g_0, the first fundamental frequency of the liquid will be between 0.90 and 1.2 Hz for a range of fill levels of 50 to 90 percent. The excitation frequency during launch will be much larger, and therefore no slosh forces are expected and no liquid damping during this operation would be required.

Once the tank achieves low gravity, the liquid will quickly assume a low-g configuration. The bulk-liquid configuration was described in section 1.2 and the vapor behavior at orbit injection is further discussed in section 4.3.

4.2.3 Orbital Operations

The liquid orientation on orbit is also shown in Fig. 4.2. The position of the liquid will depend on the direction of the acceleration. As shown in section 1.2, the liquid/vapor interface is essentially flat, since it is dominated by the acceleration.

Liquid flows from the bulk tank space through the tank gallery channel screens, down the channels, and into the lower receiver where the pump is located. The gallery channels ensure liquid access to the lower receiver for accelerations in any direction. When any one of the channels is in contact with liquid in the bulk tank space, all liquid withdrawl from the lower receiver is replaced by an equal volume of liquid from the bulk tank space. The screens on the gallery channels prevent vapor from passing through into the galleries when liquid contact exists.

4.3 ORBIT INJECTION

The bulk liquid in the tank will assume the flat surface configuration as shown in Fig. 4-2 on the pad and during boost. When the tanker enters a very low-g_0 environment, capillary forces will become dominant. The management device uses these forces to fill the gallery feed channels by capillary action and the space between the galleries and the tank wall.

The device was not sized so that the capillary fill velocity in the galleries would sufficiently exceed the velocity of the liquid rising outside or in the screens to enable vapor in the galleries to be displaced out through unwetted screen. With a noncondensable gas as the ullage, as with propellant tanks, gas can be trapped in the galleries. In these cases, gallery devices are designed with a trap in the lower receiver where the gas will be drawn into and remain there until depletion.

As discussed in section 2.3, it is expected that with He II and helium vapor this trapped vapor will condense and reappear in the larger radius vapor ullage space. Therefore no provisions have been made to design a vapor trap in the lower receiver.

4.4 ON-ORBIT PERFORMANCE ANALYSIS

The gallery assembly is designed to control the He II in the tank while the vehicle experiences any of the forces described in section 1.1. Most of the liquid in the tank is free to respond to the forces the vehicle experiences. The liquid behavior and device performance during the on-orbit phase of the mission are discussed below.

4.4.1 Capillary Retention

The liquid-management device must supply He II to the pump, regardless of bulk liquid location. To accomplish this, liquid communication must be maintained between the bulk liquid and the outlet receiver which houses the pump. This requires that the galleries remain full of liquid from injection until final depletion, which in turn requires that the capillary pressure difference at the gallery wall perforations exceed all adverse hydrostatic, dynamic, and frictional pressures by suitable margins of conservation:

$$\Delta P_{\substack{\text{min}\\ \text{capillary}}} > \Delta P_{\substack{\text{max}\\ \text{hydrostatic}}} + \Delta P_{\substack{\text{max}\\ \text{dynamic}}} + \Delta P_{\substack{\text{max}\\ \text{friction}}} + \Delta P_{\substack{\text{max}\\ \text{entrance}}}$$

The maximum hydrostatic head was determined by assuming that the tank is near depletion and that the adverse acceleration is such as to position the remaining liquid at the top of the tank producing the maximum hydrostatic head. Maximum dynamic and frictional pressure depressions were calculated by assuming that all the flow is in only one gallery channel, which would produce maximum flow velocities.

It must also be noted that the heat dissipation by the pump will set up a small temperature gradient across the walls of the gallery channels. This temperature difference may cause the screens to behave slightly as a fountain-effect pump and actually raise the pressure in the channels. This raise in pressure may more then offset the above pressure depressions depending on the thermal resistance of the gallery channel walls, the actual pump heat dissipation, and the type of screens used. This is further discussed in section 4.4.2.5. This effect is neglected in this performance analysis, however would have to be included once a final design of the management device is performed.

4.4.1.1 Gallery Material Capillary Retention Capability. The theoretical capillary pressure difference across a curved meniscus is given by

$$\Delta P_{\text{theoretical}} = \sigma \frac{1}{r_1} + \frac{1}{r_2}$$

or, for the case where the principal radii of curvature are equal

$$\Delta P_{\text{theoretical}} = \frac{2\sigma}{r}$$

This theoretical expression is generally sufficiently accurate for preliminary design calculations, but actual capillary capability must be determined before the prototype hardware can be developed. Tests should be conducted to establish the capillary retention capability of the gallery material with He II, and also with any test fluids and materials that would be used in modeling aspects of the system, to assure correct scaling when substitute fluids are used during testing.

The containment capability of a capillary tube can be examined by simply dipping one end of the tube into a dish of liquid. A balance of gravitational and surface-tension forces on the liquid rising into the tube yields the expression

$$\rho g h = \frac{2\sigma}{r} \cos\theta$$

where

ρ = liquid density
g = acceleration
h = contained height
σ = liquid surface tension
r = tube radius
θ = contact angle

The above expression is in good agreement with empirically determined liquid-support heights in glass capillary tubes, but when applied to retention devices that use screens or perforated grid materials, it does not account for some of their geometric factors. Therefore, a dimensionless parameter ϕ equal to $\rho g h r/\sigma$ is used to evaluate the capillary support limits of these materials.

This empirical constant ϕ is an expression of the stability limit for capillary-supported systems, much the same as the bond number serves as the stability limit for pressure-supported systems. In the case of screen mesh, ϕ is a function of the geometry of the mesh and the wetting character of the liquid to the screen and wire contraction effects on cool-down. It incorporates any uncertainties in the actual value of r, the pore radius, for complicated geometries such as the dutch twill mesh. The definition of ϕ provides a convenient organization of the parameters which influence a capillary-supported system. By accepting the value of pore size provided by the manufacturer or obtaining it by a geometric measurement, one can measure the height of a column of liquid that can be supported below a capillary surface and derive a value of ϕ. This derived value then incorporates all the uncertainties in the relationship between the capillary bubble radius and pore size in the screen. In effect, values of ϕ less than the theoretical upper limit of 2 for wetting liquids amount to a derating of the screen mesh pore size.

A typical test rig is shown in Fig. 4-3. The test sample is clamped at the top of a glass tube and the assembly is slowly immersed in the test fluid. After assuring the ejection of all trapped gas, the test fluid is slowly drained (or the assembly slowly raised), leaving liquid contained in the glass tube. Withdrawal is continued until gas is pulled through the test sample and at this point the height is recorded. This procedure should be repeated several times to assure consistency of the results.

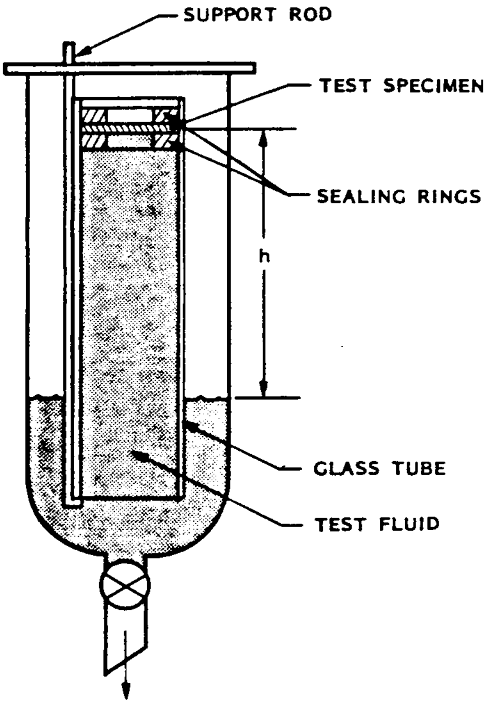

Fig. 4-3 Bubble-Point Measurement Device

This test is similar to the bubble-point test commonly used to test screens. In this test the glass tube is submerged in the test fluid and gas is injected into it, displacing the fluid. This test would be difficult with He II as a test fluid since all gasses (except He^3) would condense at He-II temperature.

Table 4-1 shows the results of tests previously performed for woven mesh screen. Since there are no data on the retention capability of He II with perforated grids or screens, a value of $\phi = 1.0$ was used in this study. The screens that are to be selected for the He II management device must meet the capillary requirements for the tank size and acceleration levels specified in section 1.1. Figure 4-4 is a capillary-supported stability map for He II. The line marked LHe II represents a value of $\phi = 1.0$. The ordinate represents the static head in g_0-cm that can be supported by a capillary pressure in screen pores of diameter d. Also shown on the abscissa at the location of their respective nominal room-temperature pore sizes are various screen mesh weaves. The relationship between the requirements for static support in the screen and its pore size is readily apparent.

It can be seen that, for a steady acceleration of 10^{-4} g_0 at the maximum height of 290 cm, any of the screens shown would be sufficient. If the acceleration requirement is increased to 10^{-2} g_0, a 200 x 1400 mesh screen would be required.

Table 4-1 WOVEN SCREEN CAPILLARY STABILITY LIMIT

Liquid	Gas	ϕ
Isopropyl Alcohol	Air	1.1
Benzene	Air	1.1
UDMH	Helium	1.4
IRFNA	Helium	1.3
Water	Air	1.5
Methyl Alcohol	Air	1.8
LH_2	Helium	1.6
LO_2	Helium	1.2

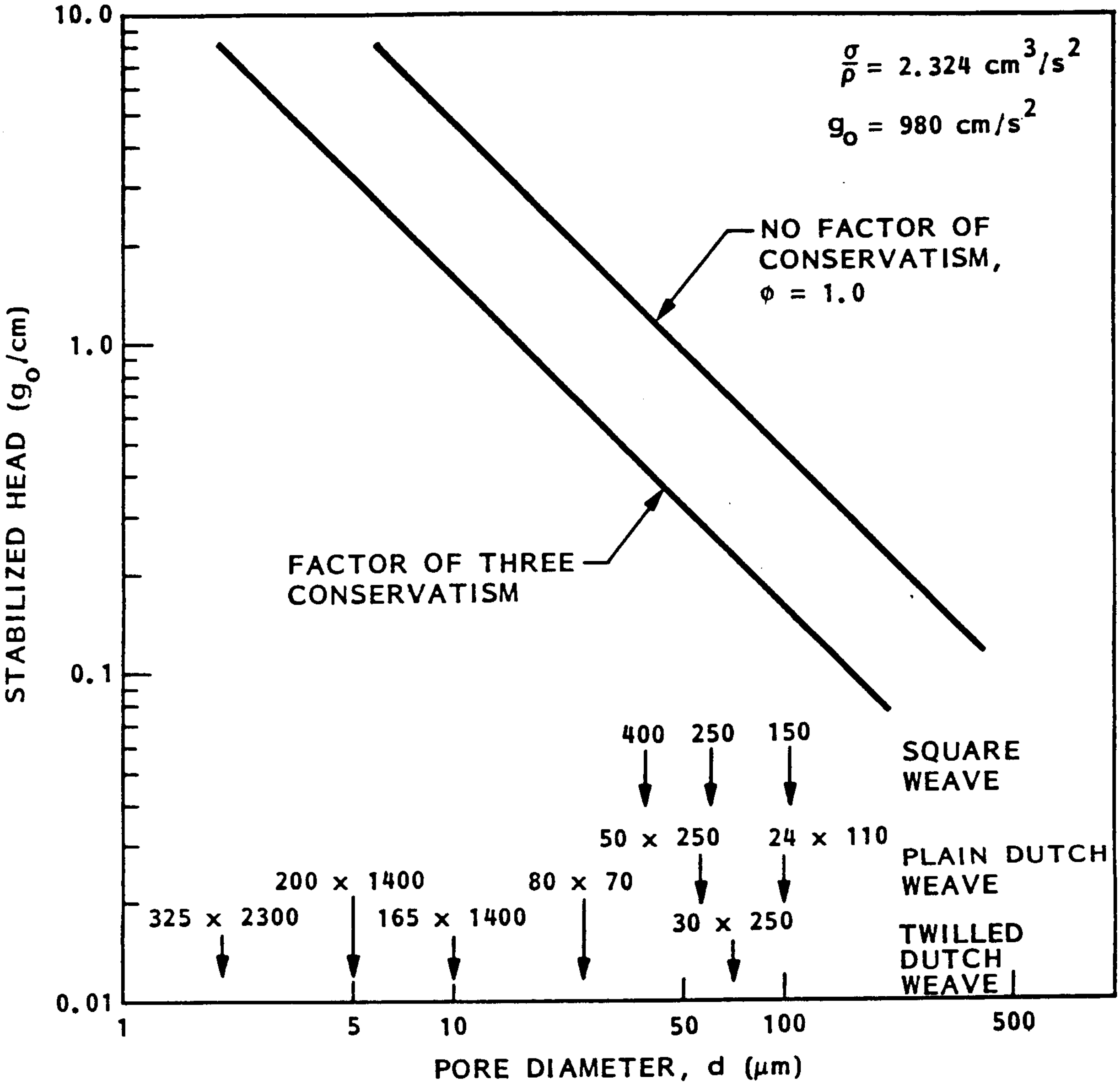

Fig. 4-4 Capillary Stability Map for He II

4.4.1.2 Effect of Vaporization at Retention Meniscus. One effect which would cause failure to retain liquid in the gallery channels is the vaporization of liquid from part of the capillary retention material. In this event, the gallery must resupply any liquid lost or a large radius bubble could grow at the vaporization site and eventually result in a loss of gallery retention. Under very low accelerations, capillary action will cause liquid to be retained, in the form of a fillet, in the area between the outboard side of the gallery and the tank wall. Since the gallery capillary retention material is on the outboard side of gallery, it will be covered by liquid during very low accelerations and vaporization is impossible. Due to the high hydrostatic head near depletion and during most of the mission under normal expected acceleration, the liquid will not be retained in the fillets and the outboard side of the gallery will be exposed to vapor.

When the capillary retention material is exposed a local meniscus will become either a liquid-vapor interface or, if there is a vapor bubble trapped inside the gallery in contact with the material, a vapor-liquid-vapor interface. Illustration a shows a liquid-vapor interface and illustration b shows a vapor-liquid-vapor interface.

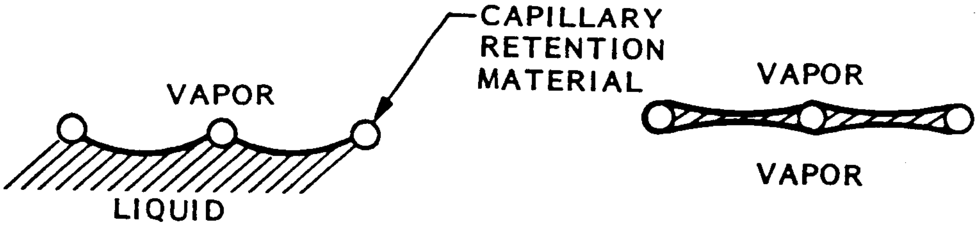

If vaporization occurs on the meniscus, it is possible for the meniscus to break if the rate is greater than the bulk liquid's capability to replenish the vaporized liquid.

Evaporation tests were performed on several capillary retention materials with isopropyl alcohol, which has a near-zero contact angle like He II (Ref. 4-1). The material specimens used were perforated plates and woven screens. The plate specimens where tested with various surface finishes to evaluate capillary liquid feed effects along the materials. Woven screen was found to be the most desirable material for use as the capillary retention material in the galleries and was selected for this study.

For the case of He II, it is expected that once vapor is ingested into the gallery channel, it will condense and liquid will be drawn into the channel to replenish the difference in volume. In this case, a vapor-liquid-vapor interface is not expected. If this is not the case, then it would be more desirable to utilize a screen that provides wicking, which would be able to replenish the interface as it vaporizes. Experiments have shown that square-mesh screens do not wick, therefore a dutch-weave screen would be a more desirable retention material (Ref. 4-2).

The bulk liquid's capability to replenish vaporized liquid at the liquid-vapor interface of the woven screen under the maximum predicted steady acceleration needs to be demonstrated. This test can be performed with a 1-g_0 scaled model. The only scaling parameter of importance for static testing is the dimensionless Bond number ($\rho g R^2/\sigma$). To test with a factor of two conservation, the predicted acceleration should be doubled before scaling. Because He II has some unique properties, it sould be used as the test fluid.

Simulating a prototype acceleration of 10^{-4} g_0 leads to a scale ratio of 0.014. Both the gallery dimensions and screen pore diameters should be scaled down by this ratio for the test model. The maximum hydrostatic head that the test model should be subjected to is 4.06 cm. For a prototype screen of 24 x 110 mesh, the corresponding model screen would be approximately a 325 x 2300 mesh. This scaling leads to an extremely small model of the gallery channel, with hydraulic diameter of 971 μm. It would be very hard to make such a model, therefore a gallery channel model with a larger cross section would have to be utilized. This should not effect the results of the test.

In this test, it would be desirable to allow the gallery to be left undisturbed for a period of time. The gallery must be in contact at some location with a He-II supply in order to replenish any vaporization taking place at the screen vapor-liquid meniscus. This test would demonstrate the bulk liquid's capability to replenish the screen.

4.4.2 Liquid Withdrawal

During liquid withdrawal, the capillary capability of the gallery channel screens must also overcome the liquid dynamic head and frictional losses. The total frictional loss is the sum of the pressure loss due to flow through the screen and down the gallery channel to the outlet receiver. These pressure drops are shown in Fig. 4-5. The flow losses must be kept small relative to the capillary strength of the retention material to assure that maximum expulsion efficiency can be achieved.

The frictional loss along the gallery channel is a function of the length the liquid must travel. The farther the bulk liquid is from the lower receiver, the higher the frictional loss; therefore, the maximum frictional pressure loss was calculated by assuming that the He II must travel the full length of a gallery channel and that all the flow was in a single channel producing a maximum velocity.

The pressure loss through the screen depends on the area that the liquid is passing through. It is obvious that as the bulk liquid is depleting, less of it is in contact with a gallery channel; therefore, the area of flow through the screen diminishes and the pressure drop increases. The pressure drop increases until it overcomes the capillary retention capability of the screen. At this point, vapor is ingested into the gallery arms and communication between the lower receiver and bulk liquid vanishes.

The cross-sectional area and shape of the gallery channels are governed by the following parameters:

1. Bond number (Bo)
2. Dynamic and frictional pressure losses down the channel

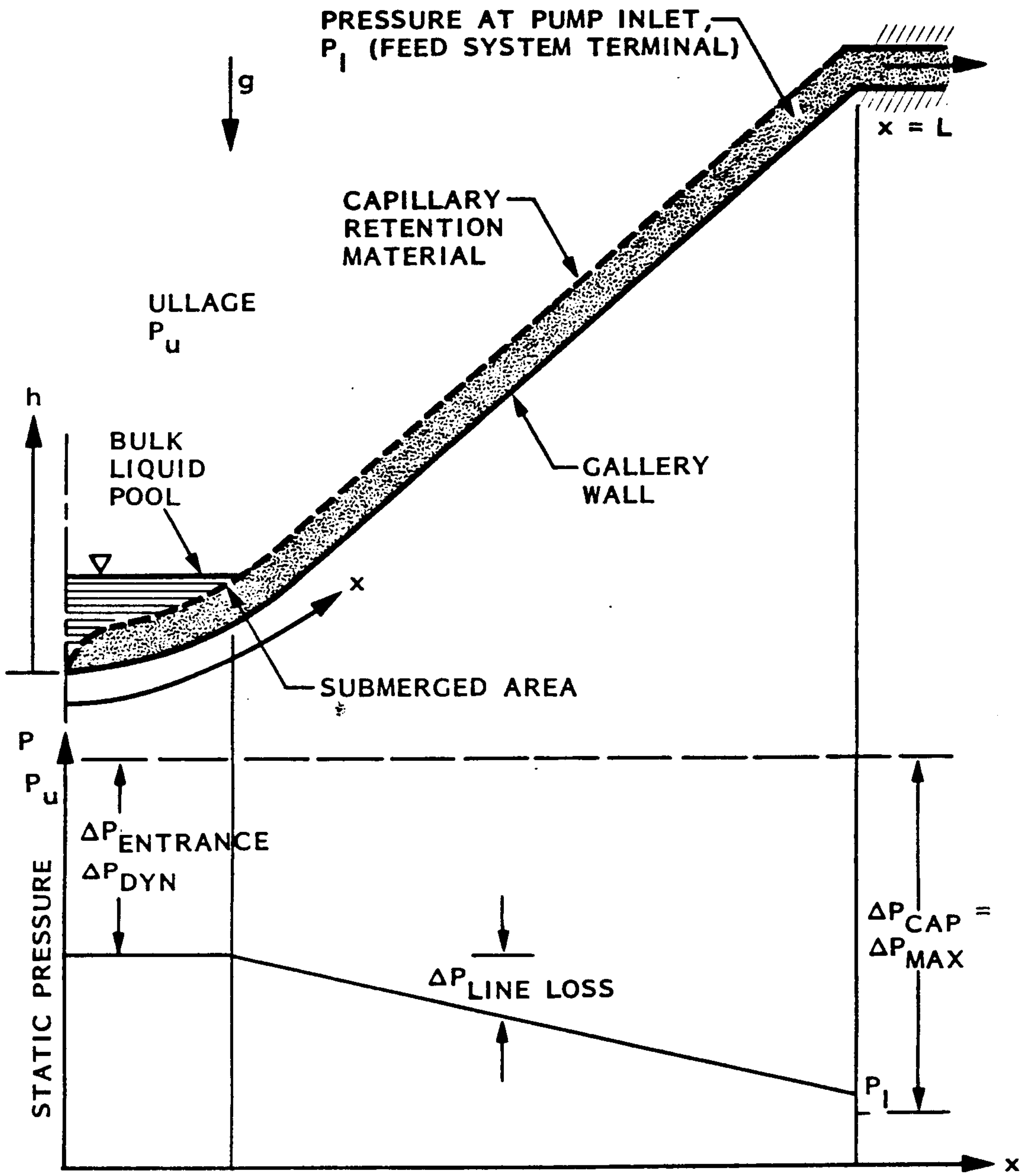

Fig. 4-5 Liquid-Feed System and Pressure-Drop Representation

3. Screen area per unit length
4. Gallery channel internal volume
5. Gallery channel mass

The Bond number is of importance to achieve capillary stability in the channel to allow at least partial consumption of the liquid in the channel at depletion in order to minimize residuals. To achieve capillary stability of the liquid-vapor interface during draining of the channels, the Bond number must be less than 0.842 during the peak acceleration. This critical Bo is applicable to wetting liquids, such as He II, and channels of circular cross section. For channels of other shapes, the hydraulic diameter appears to be a valid means of estimating the Bo.

For the maximum acceleration of 1×10^{-4} g_0, the maximum channel hydraulic diameter is calculated to be 8.94 cm (3.52 in.). For an acceleration of 1×10^{-2} g_0, it is reduced to 0.89 cm. A minimum gallery cross section is desired to minimize the mass of the management device and its internal volume; however, as the flow area decreases, the frictional and dynamic pressure drops of the liquid down the channel both increase. In addition, as the channel gets smaller, the quantity of exposed screen to the bulk liquid decreases, which would cause the losses through the screen to be higher.

The cross section illustrated in Fig. 4-1 was chosen to minimize mass and maintain adequate margin on the various parameters listed above. The channel hydraulic diameter (4A/P) is 6.93 cm (2.73 in.) leading to a Bo of 0.51 at 1×10^{-4} g_0.

4.4.2.1 Channel Pressure Losses. Once the liquid is in the gallery channel, the pressure will be reduced further by the dynamic pressure ($V^2/2$), the hydrostatic pressure (ρgh), and the frictional flow loss due to the fluid viscosity. These flow losses occur once the fluid has experienced a pressure loss due to flowing through the gallery screen.

The dynamic pressure depression in a single channel is 0.0069 g_0-cm based on 500 L/h and 0.0277 g_0-cm based on 1000 L/h.

The frictional pressure drop of the He II as it flows down the gallery channel was calculated by assuming that all the flow is in only one channel and must travel the whole length. The pressure drop of He II in wide ducts was reported by Stass et al. (Ref 4-3) to obey a modified Blasius equation

$$\frac{\rho D^3}{32\ \eta_n^2} \Delta P = 4.94 \times 10^{-3} \left(\frac{D\rho V}{\eta_n}\right)^{7/4}$$

where

ΔP = pressure gradient
D = diameter of the channel
η_n = bulk liquid viscosity

For a flow rate of 500 L/h, the pressure drop is computed to be 0.0063 g_0-cm and for the maximum, 1,000 L/h it is 0.021 g_0-cm

The sum of these pressure losses and that of the flow through the screens must remain small compared to the capillary strength. No data on the pressure loss of He II across screens has been measured or reported, therefore an effort was undertaken to estimate it.

4.4.2.2 Flow Resistance Across Woven Screens. The pressure drop across various candidate screens that can be used is being estimated. Due to its quantum effect, the transport of He II is quite different from any Newtonian fluid. An analysis based on the two-fluid model is used to predict the pressure drop of liquid helium across the screens. Similar attempts by Staas et al. (Ref 4.3) for the flow of He II in wide capillaries have been proven successful. According to this model, the velocity of liquid helium can be divided into two terms, namely the normal fluid velocity and the mutual friction term

$$\begin{aligned} V &= V_n + \frac{\rho_s}{\rho}(V_s - V_n) \\ &= V_n + \frac{\rho_s}{\rho}\left(\frac{\nabla P}{A_{GM}\rho\rho_n}\right)^{1/3} \end{aligned} \tag{4.1}$$

where ρ is the density, ∇P is the pressure gradient across the screen, and A_{GM} is the Gorter-Mellink coefficient. Subscripts n and s stand for normal and superfluid component respectively. The second term of Eq. (4.1) arises due to the interaction between the normal fluid and the vortex tangles.

The normal fluid velocity V_n of Eq. (4.1) assumes that the normal fluid behaves like a Newtonian fluid and thus should follow the empirical equation proposed by Armour and Cannon (Ref 4-4). These authors adopted a packed-bed model to correlate the transport of Newtonian fluids through all types of woven-metal screens. By substituting the normal fluid velocity and viscosity for that of the Newtonian fluid, the Armour and Cannon equation can be written as

$$V_n = \frac{-\alpha}{2\beta} \frac{a^2 \varepsilon D_o \eta_n}{\rho} + \left(\frac{\alpha^2 a^4 \eta_n^2 D_o^2}{4\beta^2 \rho^2} + \frac{\varepsilon^2 D_o}{\beta Q \rho} \nabla P\right)^{1/2} \tag{4.2}$$

where α and β are constants (with values of 8.61 and 0.52 respectively), η_n is the viscosity of the normal fluid, D_o is the screen pore size, a is the surface-area-to-unit-volume ratio of screen wire, ε is the screen-volume void fraction, and Q is the tortuosity factor.

By substituting Eq. (4.2) into (4.1), the pressure drop across various screens can be obtained as a function of He approach velocity. Figure 4-5 shows plots of ΔP versus fluid velocity for different types of screens. The Armour and

Cannon correlations for Newtonian fluids (Eq. 4.2) are presented in the same graph with He-II results. The maximum velocity of each curve corresponds to the capillary stability limit (maximum ΔP) of each screen where:

$$\Delta P_{max} = \Delta P_{cap} = \phi \frac{\sigma}{r}$$

If the pressure drop of He II across the screen is larger, the capillary retention forces will be ruptured, resulting in the collapse of the liquid/vapor interface. The maximum velocities are also shown in Table 4-2 where U_N is the Newtonian velocity, U_{GM} is the Gorter-Mellink velocity due to mutual friction, and U_T is the sum of the two.

It should be noted from Fig. 4-6 that the coarsest screen has the largest pressure drop across it, as contrast to the Newtonian transport where the three curves almost coincide with each other. This is due to the fact that the fine screens are much thinner than the coarse ones, which results in a much larger pressure gradient (of the mutual friction term) or velocity according to Eq. (4.1).

4.4.2.3 Depletion Residuals. The depletion residual of the tank is defined as the quantity of He II remaining in the tank once vapor has been ingested into the lower receiver. When the bulk liquid volume decreases, the area of screen in contact with the bulk liquid decreases and thus, the flow loss through the screen increases. As previously stated, once the sum of all the losses and the hydrostatic load increases to the bubble point of the screen, vapor will be ingested into the gallery channels.

The maximum allowable flow loss through the screen prior to vapor ingestion is:

$$h_{screen} = h_{\substack{max\\cap}} - h_{hyd.} - h_{dyn} - h_{friction}$$

ORIGINAL PAGE IS
OF POOR QUALITY

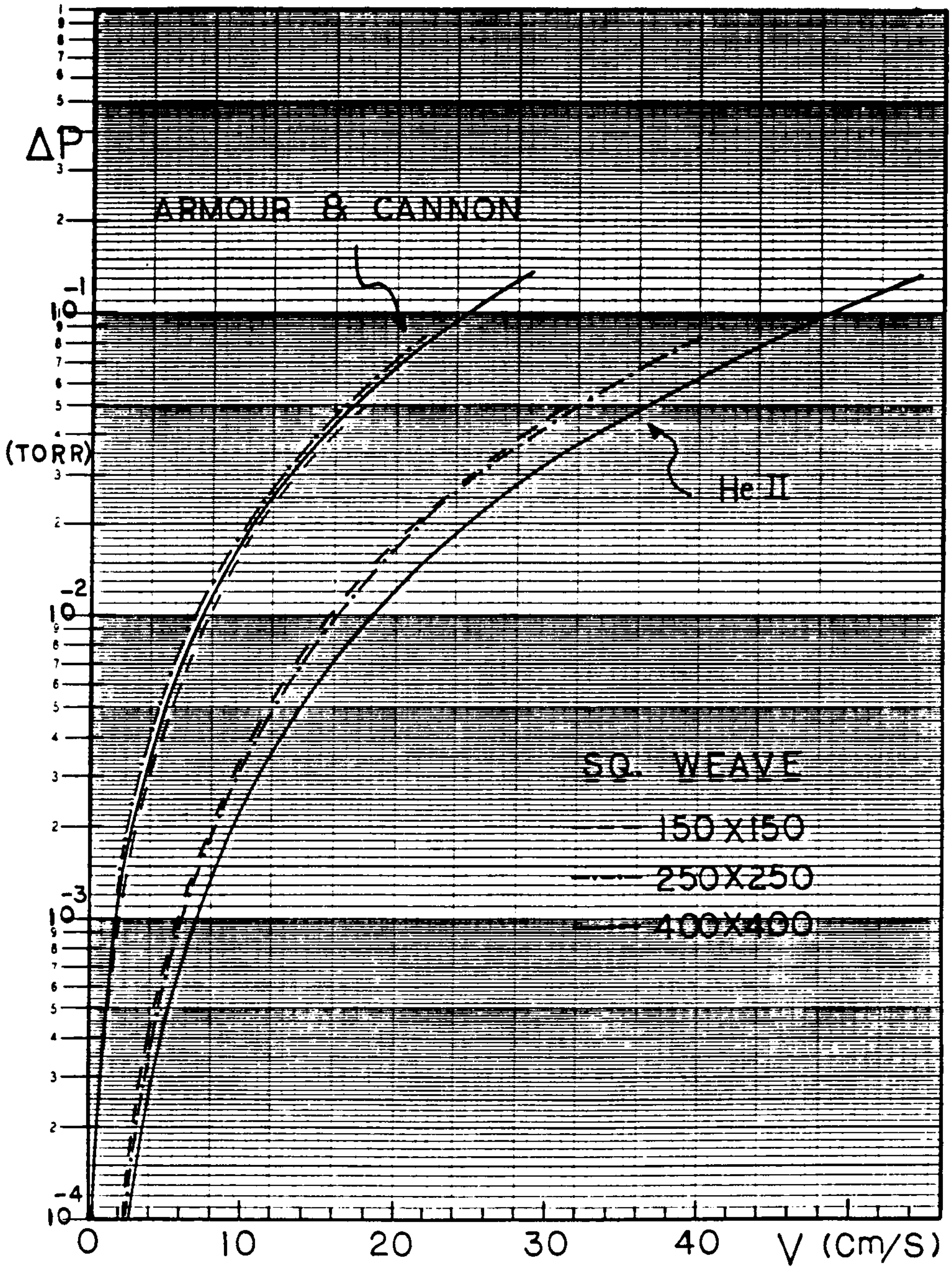

Fig. 4-6 Screen Pressure Drop versus Velocity (1 of 2)

ORIGINAL PAGE IS
OF POOR QUALITY

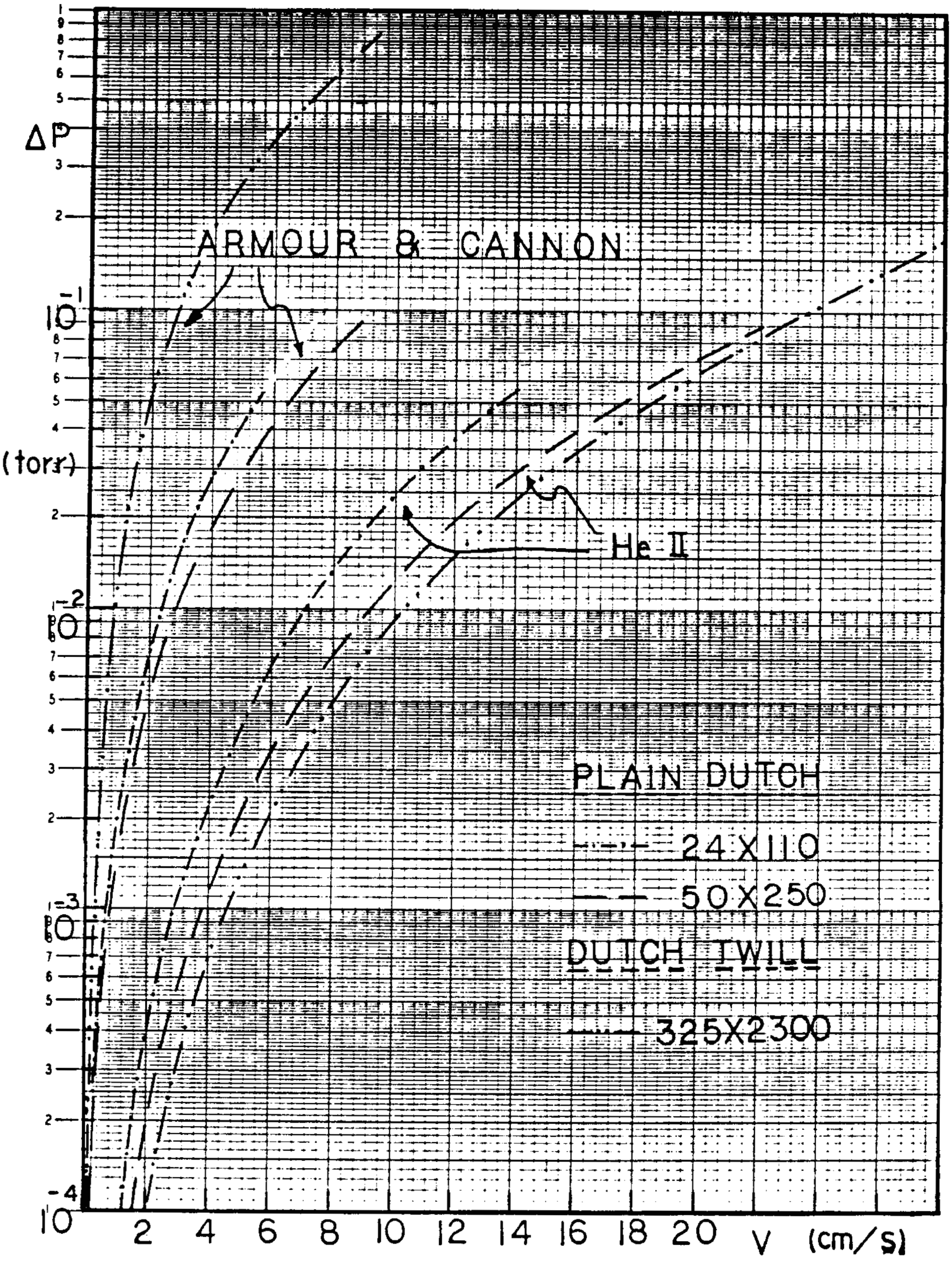

Fig. 4-6 Screen Pressure Drop versus Velocity (2 of 2)

Table 4-2 MAXIMUM SCREEN APPROACH VELOCITIES

Mesh Type	U_N (cm/s)	U_{GM} (cm/s)	U_T (cm/s)
Square Weave			
150 x 150	18.05	13.28	31.33
250 x 250	21.93	18.19	40.12
400 x 400	28.83	26.37	55.20
Plain Dutch			
24 x 110	5.39	7.00	12.39
50 x 250	8.80	11.71	20.51
Dutch Twill			
325 x 2300	9.40	39.34	48.74

The hydrostatic, dynamic, and channel pressure drops are summarized in Table 4-3. The difference between the screen maximum capillary strength and these losses is the maximum allowable pressure loss of the flow through the screen. Exceeding this loss could cause vapor to be ingested into the gallery channels. For the 50 x 250 mesh gallery channel screen with a capillary retention capability of 0.2818 g_0-cm, the screen maximum allowable loss is 0.2396 g_0-cm (2.57×10^{-2} torr) for a flowrate of 500 L/h and 0.2039 g_0-cm (2.19×10^{-2} torr) for 1000 L/h. Based on the predicted screen flow losses, the maximum approach velocity is 13.4 cm/s and 12.3 cm/s respectively for the two flowrates. The minimum area of screen required to ensure losses less than the maximum allowable is 10.4 cm^2 and 22.6 cm^2 for the flow rates of 500 and 1000 L/h respectively.

Given the gallery channel with 4.18 cm^2 of screen per centimeter of gallery length, the length of one gallery which must be covered with liquid to prevent vapor ingestion is 2.49 cm at a flowrate of 500 L/h and 5.41 cm at 1000 L/h.

Table 4-3 CHANNEL PRESSURE LOSSES

Pressure Losses (g_0-cm)	Flowrate (L/h)	
	500	1,000
Hydrostatic	0.0290	0.0290
Dynamic	0.0069	0.0277
Channel friction	0.0063	0.0212
Total	0.0422	0.0779

For the 1.91-cm (0.75-in.) gap between the tank wall and the gallery channel, the liquid will rise approximately 8.3 cm at an acceleration of 1×10^{-4} g_0 with a factor of three conservatism. At an acceleration of 1×10^{-2} g_0, the rise will only be 0.083 cm. Therefore, as long as liquid touches a gallery channel with an acceleration of 1×10^{-4} g_0, it will fill the gap between the tank wall and the gallery arm, and will provide more than the required 5.41 cm of gallery arm in liquid. Thus, vapor will not penetrate the gallery channel screens until liquid in the bulk space no longer contacts a gallery.

The maximum residual quantity in the bulk space occurs when the acceleration settles the liquid between two gallery channels. The highest residuals occur during a lateral acceleration where the gap between gallery channels is the largest. Determining this residual quantity requires the definition of the fluid surface in the tank. Due to surface-tension forces, the surface will not be totally flat but will be curved and will attempt to climb the tank walls. The exact solution to determine the shape of the liquid-vapor interface was not solved. A more conservative approach was taken by assuming that the interface was completely flat as shown in Fig. 4-7. The trade between the number of gallery channels and residual is shown in Fig. 4-8. The residual decreases as more channels are introduced because the gap separating them decreases and thus the volume of the pool of liquid between two channels decreases at depletion. Included in the figure is the residual of the management device if the gallery channels do not deplete before vapor is

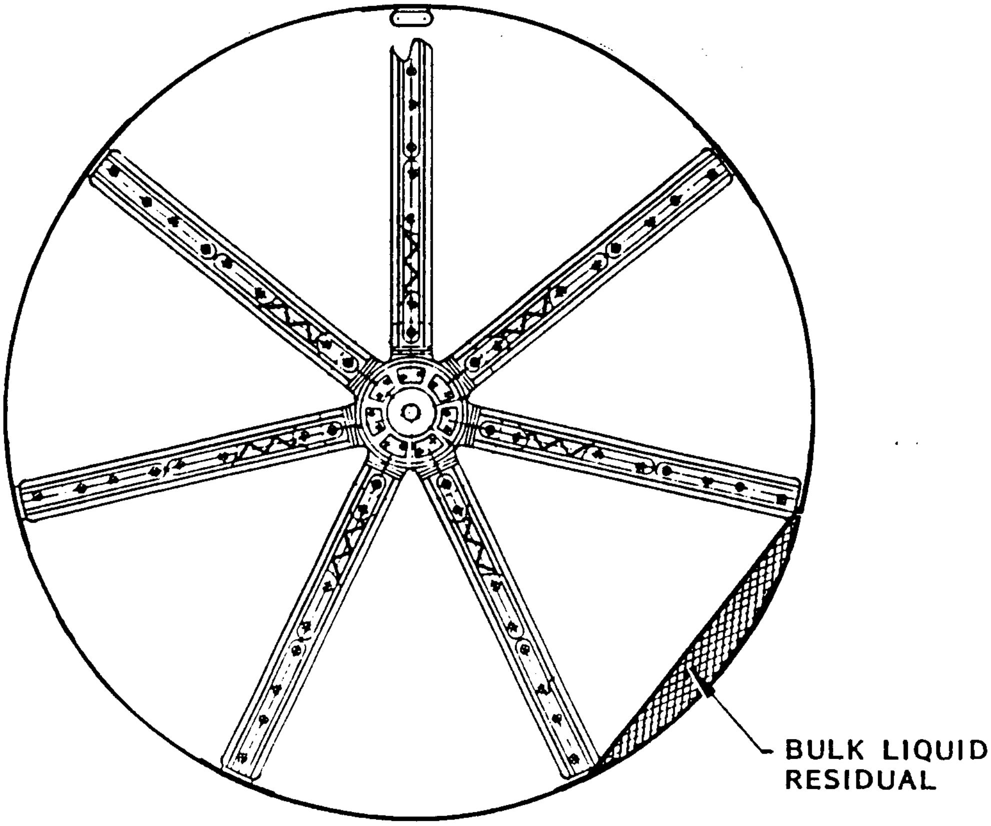

Fig. 4-7 Bulk Liquid at Depletion

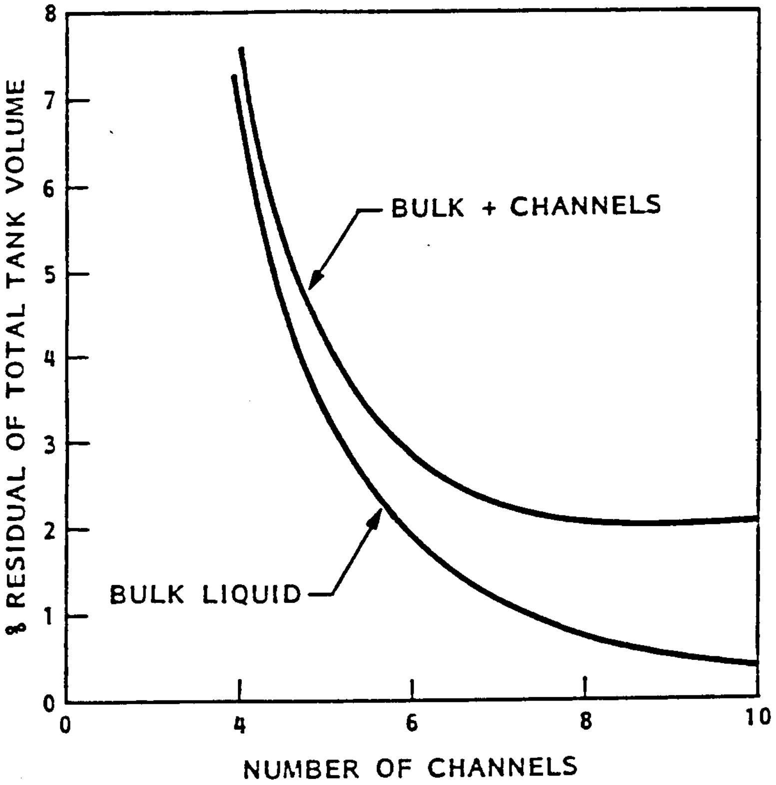

Fig. 4-8 Gallery Device Residuals

ingested into the lower receiver. The volume of the lower receiver is not included in these calculations since no provisions to drain it have been considered. The main reason is that the inlet of the pump is not defined at this point. The volume of the lower receiver is ~27 L including the volume of the pump envelope.

The gallery channels in the management device have been designed to empty completely during normal depletion at an acceleration of 1×10^{-4} g_0. This is accomplished with two features. First, as stated previously, the channel cross section was designed to be capillary stable. This means that if a bubble enters the gallery channel, it can only move with the fluid. Second, coarser screen windows are located in the upper receiver. These coarser screens will admit vapor into the channels sooner than the finer screens used over the length of each channel. The combination of these two features assures that when the bulk fluid has been depleted, vapor will enter each gallery channel from the end and will force nearly complete depletion of the channels. Under these circumstances, the nominal residual volume is approximately 150 L or 1.15 percent of the total tank volume. This volume is not the only volume of liquid left in the tank at depletion. Isolated liquid fillets forming at various structural junctions may not be accessible. This would include liquid under the lower receiver and in the screens, corners of the management device, and the gallery/tank wall flange. This volume was not estimated since most of it would be under the lower receiver and only concepts of that section have been designed. Once the final requirements of the pump/tank interface have been established, that section can be fully designed and the actual trapped liquid fillets can be determined. No provisions have been made to deplete the lower receiver, whose volume is 0.21 percent of the total tank volume.

A more conservative residual budget must use worst-case residual volume. Under worst-case conditions, the gallery channels may not deplete. First, the gallery channels may not have capillary stability as designed due to either vibrations during depletion, the capillary fillet created by the screen reinforcement ribs, or higher than 1×10^{-4} g_0 acceleration during depletion. Second, due to manufacturing tolerances on the screens, the bubble point of the upper receiver screens may be at the same level or higher than the gallery screens. If this is the case, then vapor would be ingested in the gallery channels and not necessarily restricted to the upper receiver. This would cause the channels to not fully deplete. For this case, if none of the arms empty, the bulk liquid residual would be as high as 2.32 percent, excluding the lower receiver and trapped fillets. The 24 x 110 screen in the upper receiver has pore openings twice as large as those of the 50 x 250 screen on the gallery channels. Therefore, with proper bubble-point testing of the screens, it could be assured that the upper receiver would ingest vapor before the galleries do.

4.4.2.4 Cavitation Potential. Cavitation or bubble formation within He II is discussed in this section. As liquid helium is drawn into the gallery channels, pressure drops result. Although the typical pressure drops are extremely small, cavitation is still a concern because He II is a saturated fluid. Any decrease in pressure will drop below the vapor-pressure curve and might result in boiling of the liquid. However, liquid He II is known to exist in metastable-state liquid phase below its vapor pressure. Therefore, the possibility of cavitation within the gallery channels really depends on whether the He II is in a vapor-liquid equilibrium (VLE) with the ullage or in a metastable state. The behavior of bubbles within the gallery channel under VLE was discussed in section 2.3. It was concluded that any bubble that might form in the channel will collapse and reappear in the bulk vapor phase of the ullage tank. Therefore, this section is mainly devoted to the study of cavitation within the metastable state.

The experimental measured tensile strengths of most liquids are considerably lower than those predicted by the classical nucleation theory. Fisher has applied classical nucleation theory (CNT) to liquid and has derived the following expression for the fracture pressure (Ref 4-5).

$$P_t = - \frac{16\pi}{3}\left(\frac{\sigma^3}{(KT\ln NKTt/h) - \Delta f_0}\right)^{1/2} \tag{4.3}$$

where σ is the surface tension, Δf_0 is the free energy of activation for the motion of a molecule of the liquid into or away from the bubble surface, and t is the waiting time for bubble formation, K is the Boltzmann constant, and h is the Planck's constant.

To explain the wide discrepancies between the predicted and the experimental tensile stress, it can be concluded that nucleation sites must be present. Possible sites for cavitation in liquid include:

- Suspended foreign particles
- Trapped gas or vapor filled bubbles
- Solid particles unwetted by the liquid
- Cosmic rays and radioactivity

For obvious reasons, He II has received a lot of attention in the cavitation research. First of all, because of its low viscosity and density, He II cannot carry any solid particles in suspension. The presence of trapped vapor or unwetted surfaces are also extremely unlikely because of its zero contact angle with any solid. He II is among the purest liquids in the nature; therefore, one will expect the tensile strength of liquid helium to match the classical nucleation prediction. Using Eq. (4.3), the tensile strength of He II was estimated to be ~ 5 bar at 2.09 K (Ref. 4-6). Unfortunately, the experimental threshold pressure (negative pressure) required for the formation of macroscopic (or visible) cavities in He II is still an order of magnitude lower than that of the classical nucleation theory. Beams (Ref. 4-7) measured the tensile strength of liquid helium by a spinning capillary method at about 1.9 K (according to Beams, the actual temperature might be higher). He found that the negative pressure necessary for the rupture of He II by centrifugal forces was 0.14 ±0.2 atm. Using a bubble chamber, Fairbank et al. (Ref. 4-8) detected nucleation of bubbles at a negative pressure of about 100 mm Hg (~ 0.13 atm). These values agree roughly with the incipient threshold pressure for visible ultrasonic cavitation determined by Chu (Ref. 4-9).

Therefore, it can be concluded that the negative pressure necessary to nucleate macroscopic cavities in He II is about a tenth of an atmosphere. Usually, the incipient pressures measured for the formation of microscopic bubbles using acoustic techniques are much lower than that (please refer to the review article by Apfel, Ref. 4-10). As it will be pointed out later, the cause of the lower values may be that such acoustic methods detect bubbles before they reach the critical radius. These bubbles will collapse unless more energy is supplied.

Since foreign particles and trapped vapor are not likely to be present in He II, the discrepancy between the experimental result and the CNT must be due to some other nucleation sites, e.g., He-3, cosmic rays, and vortices. Jarman and Taylor (Ref. 4-11) removed impurities and He-3 in He II by filtering and heat flushing. No appreciable change in the nature of the cavitation or in its threshold could be detected after this treatment. Thus, the only remaining possible nucleation sites are cosmic rays and vortices. It is quite obvious that bubbles could be induced by cosmic rays and radioactivity. A number of phenomena are reported in the literature for these types of cavitation (Refs. 4-12 through 4-16). However, Shadley and Finch (Ref. 4-17) concluded from their experiment that nucleation occurs on the vortices created by α particles. Therefore, it is conceivable that vortices are responsible for the cavitation in He II. The vortex-nucleation hypothesis was first suggested by Edwards, Cleary, and Fairbank (Ref. 4-18) who used a bubble chamber to produce visible cavities in He II and found nucleation to occur readily after vortices had evidently been formed within the chamber. Further support of this hypothesis was reported by Finch and Chu (Ref. 4-19). They used acoustic methods to nucleate bubbles in a chamber where a rotating paddle was used to generate vortices. The threshold voltage for cavitation was found to be constant until a critical angular rotation rate was reached, beyond which the threshold reduces sharply. The experimental angular velocity of the paddle is found to be

$$\omega_c = \frac{n\hbar}{m} \frac{1}{r_p^2} \tag{4.4}$$

where m is the mass of one helium atom and n is an integer. The radius of the shaft is designated by r_p. These results are consistent with the theory of quantized vortex formation and appear to indicate that vortices play a definite role in the cavitation nucleation process.

The exact mechanism for the formation of bubbles from vortex structures is not known. McCloud (Ref. 4-20) suggested that the nucleation of rupture was due to the convolution of vortex lines or rings into a spherical volume, the size of a bubble nucleus. The concentration of energy in this case was thought to be sufficient to nucleate a bubble. McDonnell, Chu, and Finch speculated that the breaking up of vortex filaments is responsible for the nucleation process.

The question arises whether vortex lines or vortex rings are accountable for the nucleation process. Edwards et al. (Ref. 4-18) indicate that rectilinear vortex lines do not act as nuclei for visible bubbles; they found that vortex rings have this property. Moreover, as pointed out by Jarman and Taylor (Ref. 4-11) it is possible that Finch and Chu's (Ref. 4-19) paddle-wheel observations can be attributed to vortex rings peeling off the tips of the wheel rather than to their "solitary macroscopic quantized vortices." All these observations point towards the fact that the low threshold pressure for cavitation in He II is due to the nucleation of bubbles from vortex rings.

Mechanism for the Cavitation of He II from Quantized Vortex Rings

A mechanism is proposed for the nucleation of bubbles from vortex rings. This model assumes that the bubbles are initiated from the cores of the vortex rings. The vortex core, which is thought to be constituted of normal fluids, provides thermal insulation for the nucleation of a cavity. Once the bubble is formed, two opposite forces act on it. The growth of the bubble requires PdV work

$$W = P\frac{4}{3}\pi r^3 \qquad (4.5)$$

where r is the radius of the bubble and P is the pressure of the liquid. When the liquid is under negative pressure, P is negative and the bubble will tend to grow. On the other hand, the growth of the bubble will be constrained by the energy associated with the vortex ring, because it takes energy for the ring to expand.

$$W = \frac{1}{2} \rho_s (\Gamma)^2 R \left(\ln \frac{8R}{a} - \frac{7}{a}\right) \tag{4.6}$$

where Γ is the quantum of circulation and R and a are the radius of the ring and the radius of the core respectively. By further assuming that the size of the bubble is directly proportional to that of the vortex ring, $R = \psi r$, one can combine Eqs. (4.5) and (4.6) to get

$$W = \frac{1}{2} \rho_s(\Gamma)^2 R \left(\ln \frac{8R}{a} - \frac{7}{a}\right) + \frac{4}{3} \pi \left(\frac{R}{\psi}\right)^3 P \tag{4.7}$$

In Fig. 4-9, the work needed for the growth of the bubble is plotted as a function of the vortex radius. For $R < R_c$, the PV work created by the negative pressure is not large enough to overcome the vortex energy which tries to prevent the ring (or the bubble) from expanding, and the bubble will collapse. For $R > R_c$, further increase in the bubble radius requires decreasing free energy, and the cavity will grow. As the cavity grows, a stage will be reached where the vortex ring ruptures releasing the free bubble.

In Fig. 4-10 the work required for the formation of bubble is plotted as a function of the radius of the vortex ring. The critical ring radius ranges from about 25 Å at $P_t = -0.7$ bar to 80 Å at $P_t = -0.1$ bar. Analytical solution to Eq. (4.7) is not possible. One can employ graphical methods. Figures 4-11 and 4-12 represent the maximum work and critical vortex radius versus the pressure of the liquid. The maximum work is plotted as a function of the critical radius in Fig. 4-13. From graphical methods, the solution to Eq. (4.7) can be represented by an equation of the following form

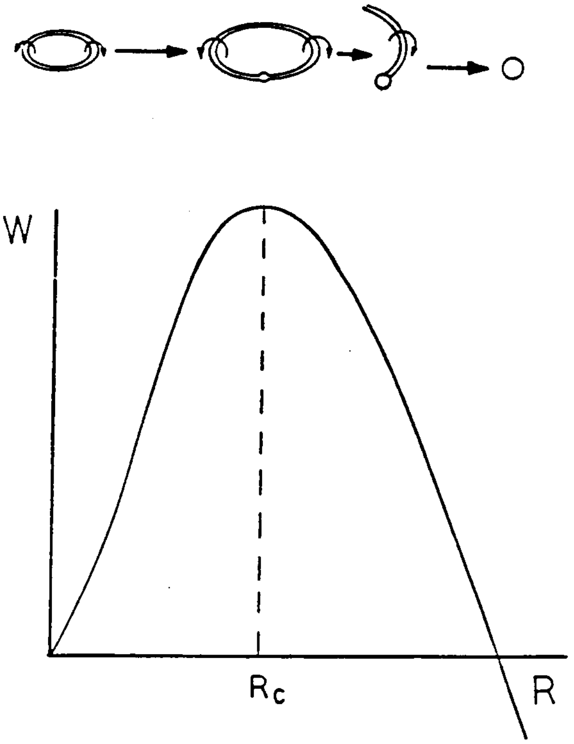

Fig. 4-9 Mechanism for Nucleation of Bubbles from Vortex Rings

$$W_{max} = \frac{A}{P} + BP + C \tag{4.8}$$

where A, B, and C are constants.

The theory of nucleation states that the rate of bubble formation is proportional to $\exp(-W_{max}/KT)$. The proportionality factor can be estimated from the theory of absolute reaction rates to be $(NKT/h)\exp(-\Delta f_0/KT)$, where N is the number of molecules in the liquid, and Δf_0 is the free energy of activation for the motion of an individual molecule of liquid past its neighbors into or away from the bubble surface. Due to the low viscosity of He II, one can set $\Delta f_0 = 0$. The rate of formation of bubbles of vapor in a mole of liquid subject to negative pressure P is therefore equal to

$$\frac{dn}{dt} = \frac{NKT}{h} \exp[-W_{max}/KT] \tag{4.9}$$

ORIGINAL PAGE IS
OF POOR QUALITY

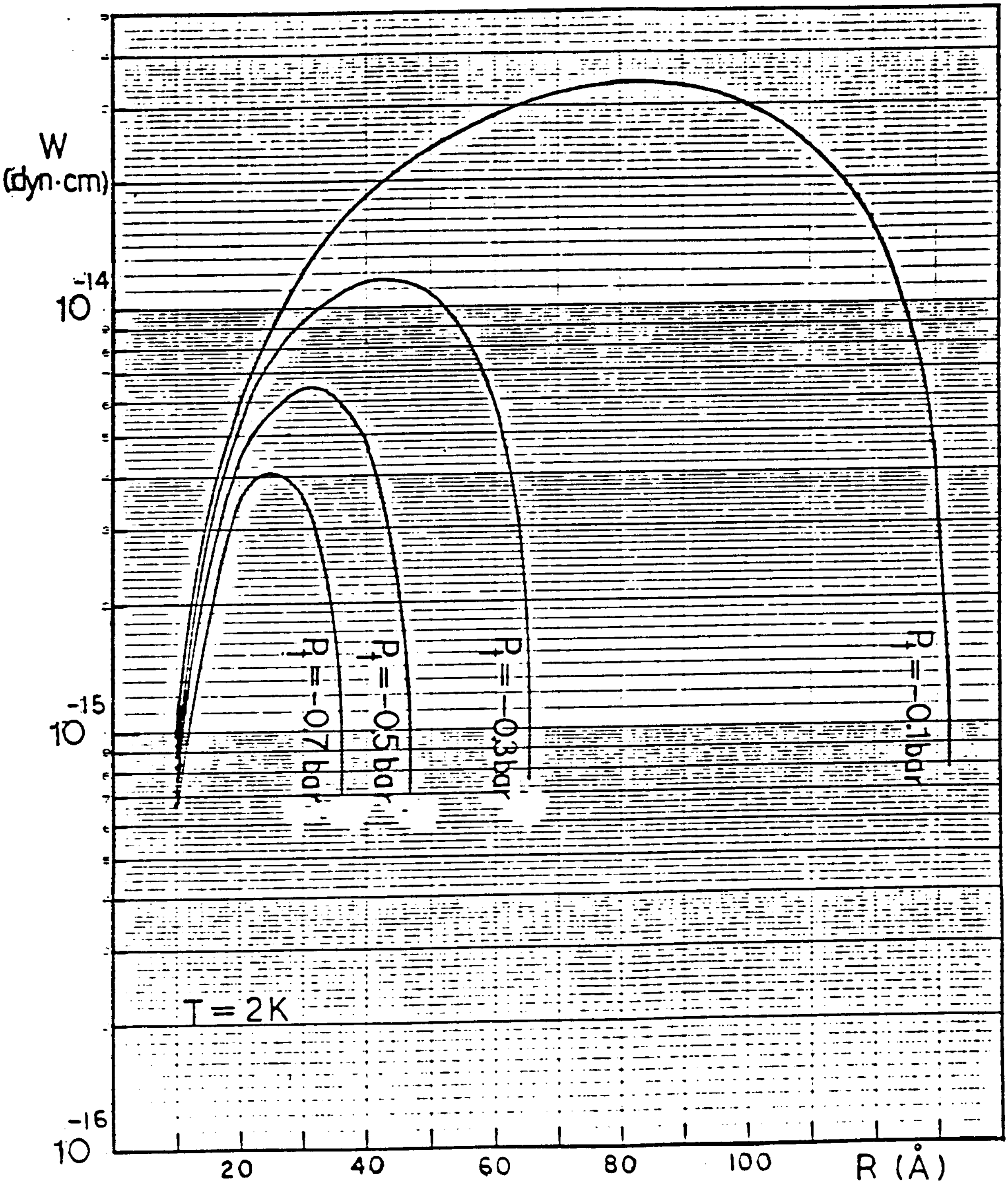

Fig. 4-10 Work Required for the Formation of Bubble versus R

ORIGINAL PAGE IS
OF POOR QUALITY

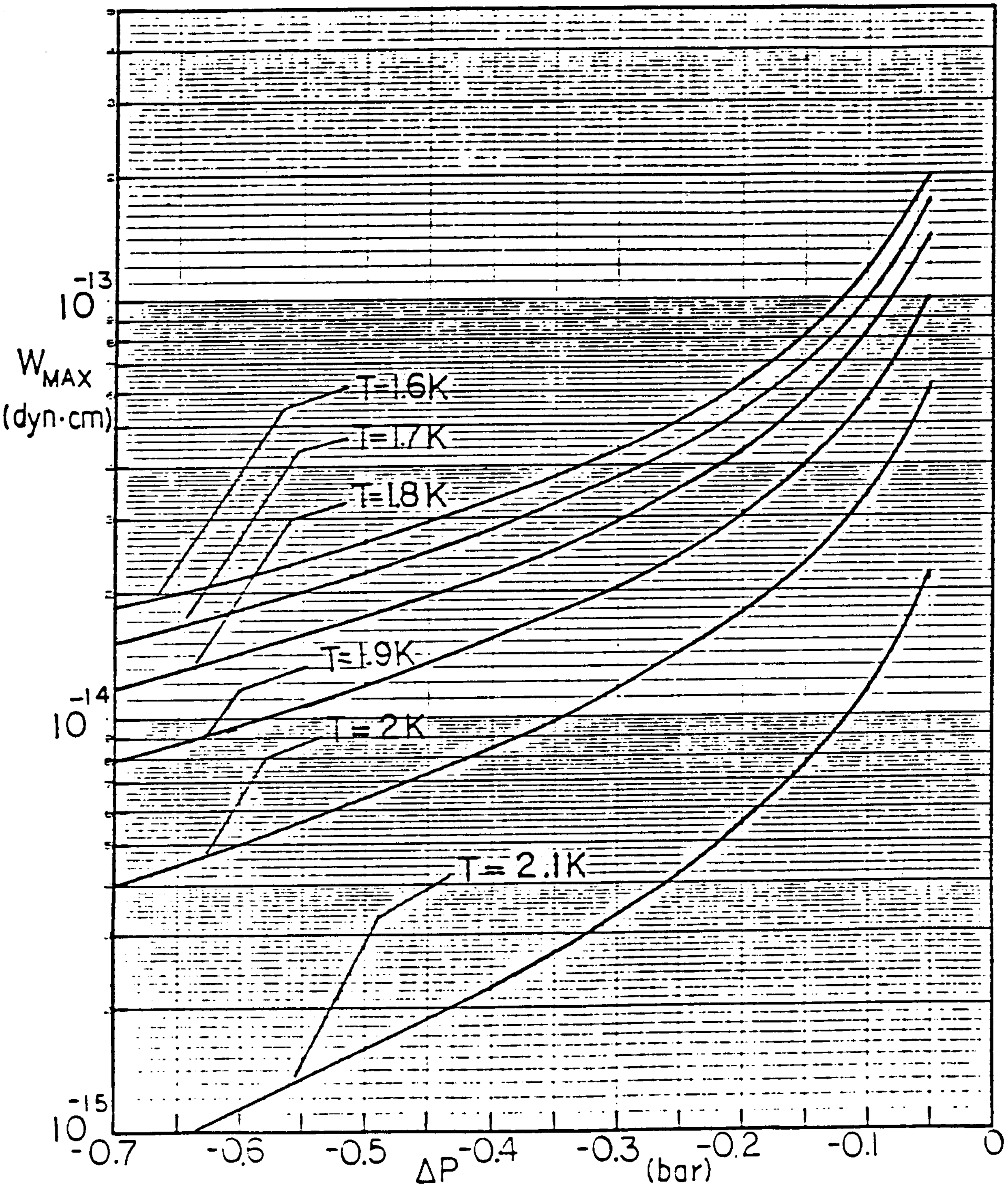

Fig. 4-11 Maximum Work Required for Cavitation as a Function of Fracture Pressure

ORIGINAL PAGE IS
OF POOR QUALITY

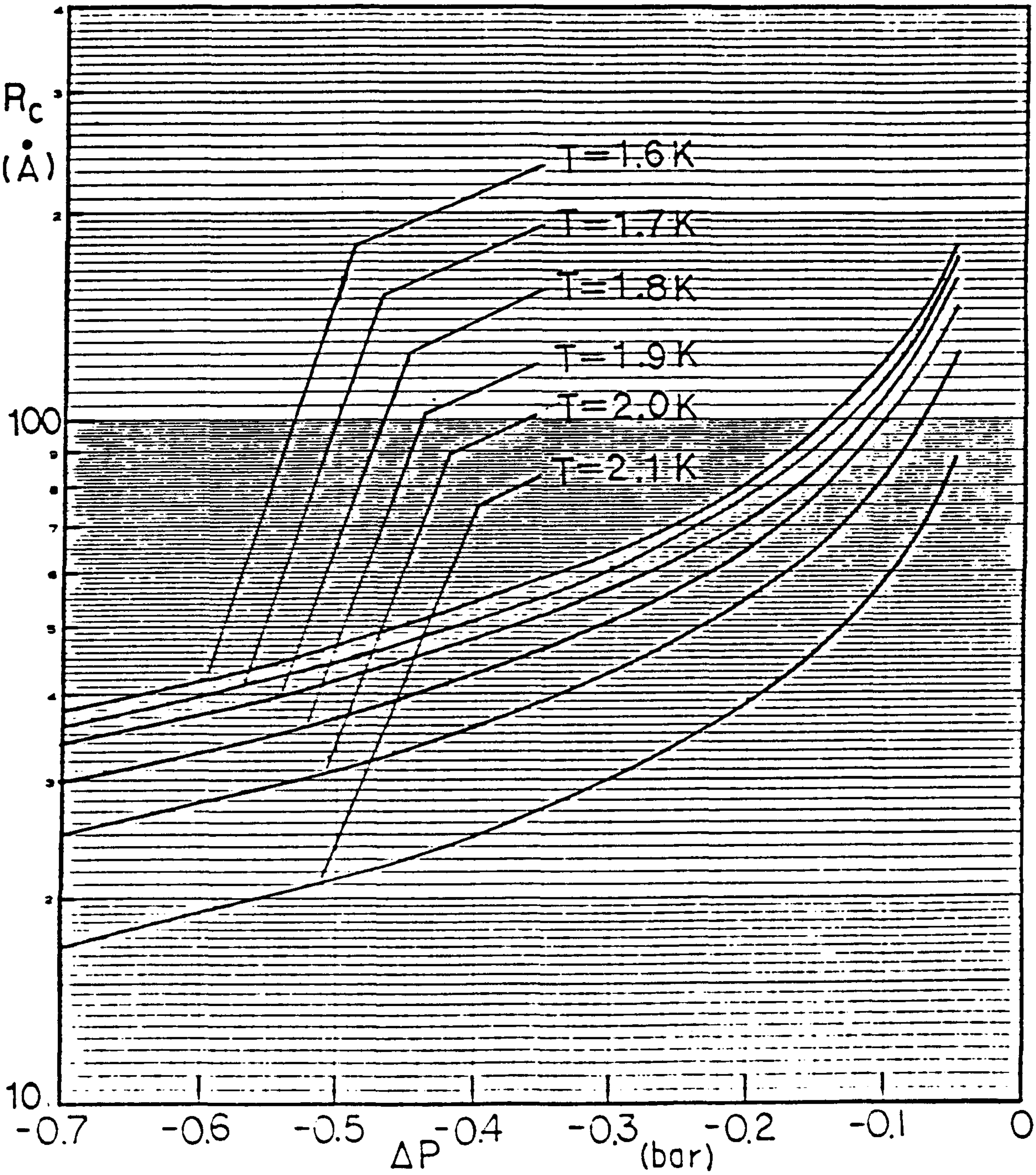

Fig. 4-12 Critical Vortex Radius as a Function of Fracture Pressure

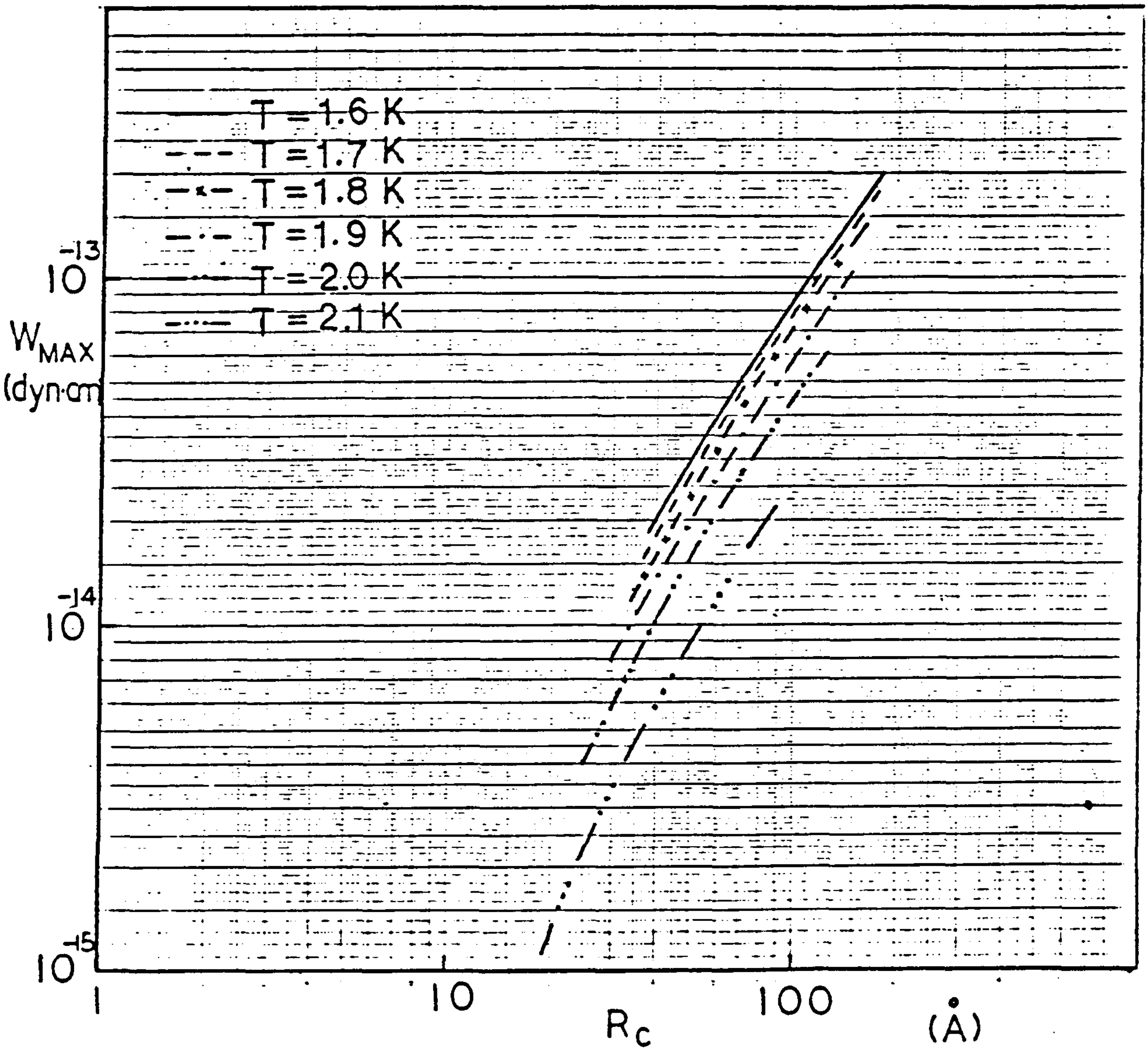

Fig. 4-13 Maximum Work Required for Cavitation Versus Critical Vortex Radius

where n is the number of bubbles. If we look at the formation of one bubble in t seconds we can set dn/dt = 1/t. Equation (4.8) can be substituted into (4.9) and the fracture pressure required for the nucleation of a cavity can thus be solved. The calculated pressure is presented in Fig. 4-14 for various bath temperatures. At 2 K, the fracture pressure is $P = -0.16$ bar. This result is consistent with the experimental findings of Fairbank, Beams (Ref. 4-7) and Chu (Ref. 4-9). Note that the threshold pressure increases with decreasing temperature. This temperature dependency of the tensile stress agrees with the results reported by Akulichev (Ref. 4-22).

Experimental work to measure the cavitation threshold of He II is being conducted at the National Bureau of Standards (NBS) in Boulder, Colorado. This work is being conducted in support of testing a centrifugal He-II pump. In the apparatus being used, cavitation thresholds of 1.0 to 5.0 torr at 1.8 K have been measured (Ref. 4-23). It must be noted that these values are being measured in very turbulent He II at Reynolds numbers in the range of 10^6 to 10^7.

The NBS data is very interesting in that it is showing a much lower threshold than our analysis predicts. Our analysis is more applicable to stagnant He II. It is conceivable that in highly turbulent flow, the vortex ring would rupture prematurely due to tangle of the vortices and therefore release the bubble. In the fluid-management device, the He-II Reynolds number is much lower; therefore, the cavitation threshold may be closer to the prediction presented here. In any case, the maximum negative pressure of the He II in the management device is only a tenth of a torr and therefore no cavitation is expected.

Critical Velocity of He II Across Screens

According to the present findings, bubbles are nucleated from vortex rings which act as thermal barriers. However, vortex rings could only be generated if the critical velocity of superfluid is exceeded.

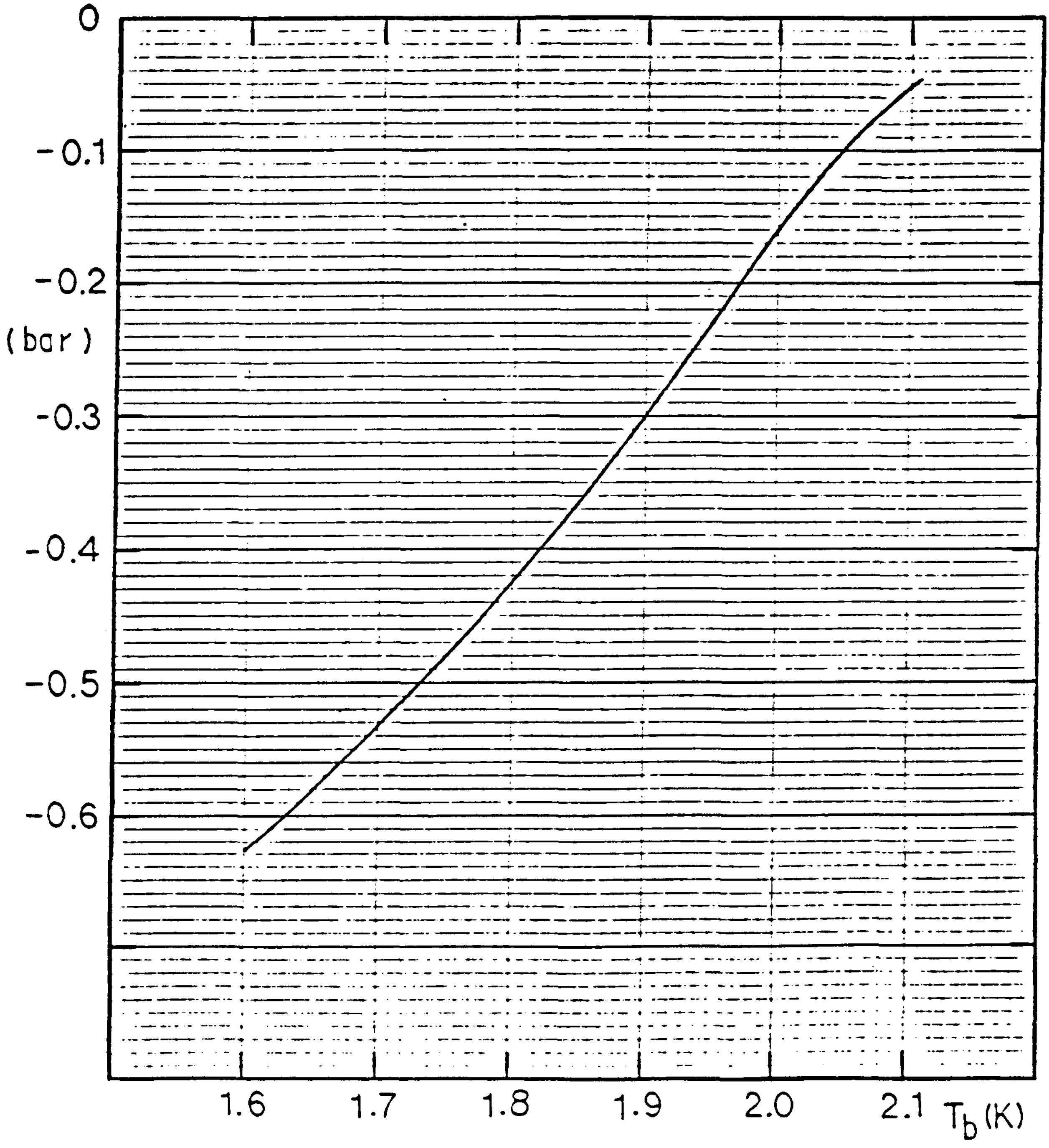

Fig. 4-14 Negative Pressure Required for Cavitation Versus Bath Temperature

The critical velocity (V_{sc}) of the He II is the velocity at which the superfluid turns turbulent. Transportation below this limit is known as the Landau regime where the flow is not associated with any dissipation losses. Above this critical value, quantized vortices are generated and vortex shedding occurs, resulting in energy dissipation. This kind of transition is better understood for the transport of He II in capillaries through the works of Van Alphen et al. (Ref. 4-24). Figure 4-15 is a plot of the product of V_{sc} and capillary diameter (D) versus D (for the description of symbols, please refer to the original work of Van Alphen et al.). One can see that most of the data lie on a straight line represented by

$$V_{sc} = D^{-1/4} \tag{4.10}$$

However, for $D > 10^{-3}$ cm, some of the data follow the equation

$$V_{sc} = C\ D^{-1} \tag{4.11}$$

where C is a constant. This discrepancy might be due to the observation limits or different experimental setups. There is very little data on the critical transport of He II in screens or porous media. Hendricks and Karr (Ref. 4-25) measured the V_{sc} of liquid helium across porous media of various pore sizes. From the analogy between the Poiseuille equation and the Darcy Law, one can obtain a correlation between the capillary diameter and the permeability (K_p) of the porous plugs

$$D_{EP} = \sqrt{32\ K_p} \tag{4.12}$$

Equations (4.11) and (4.12) can thus be combined to estimate the critical velocity of He II in porous media.

$$V_{sc} = (32\ K_p)^{-1/8} \tag{4.13}$$

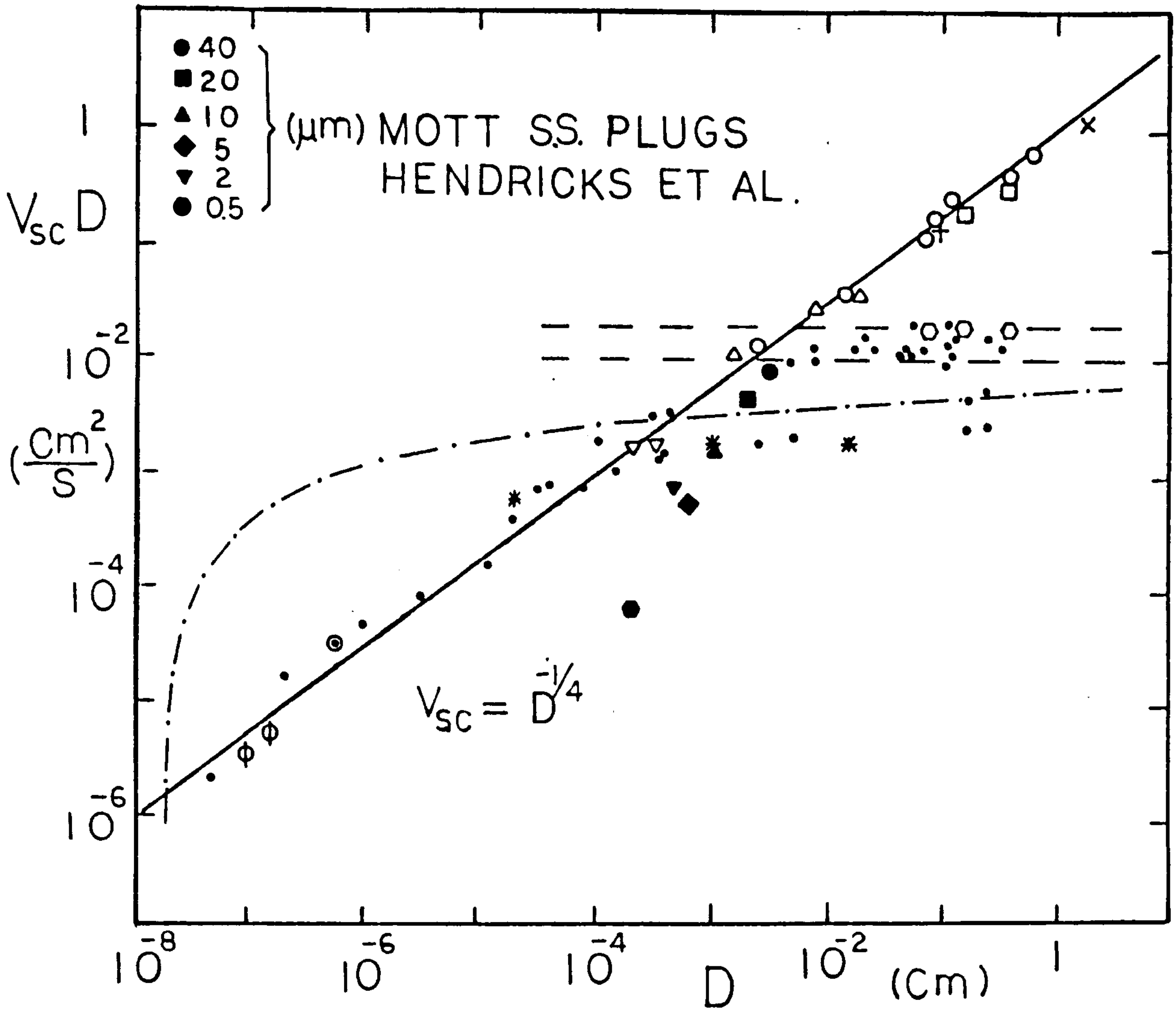

Fig. 4-15 $V_{sc}D$ Versus Diameter

The results of Hendricks and Karr are also included in Fig. 4-15. For materials with large pore sizes, these data tend to agree with Eq. (4.13). As the pore size or permeability decreases, deviation from the preceding equation is observed. Since, generally speaking, screens have higher premeability than porous plugs, Eq. (4.13) should be valid for predicting the critical velocity of He II across screens. One can either measure the K_p of the screens experimentally or one can derive an equivalent capillary diameter and substitute that into Eq. (4.10). From the Armour and Cannon correlation, an equivalent capillary diameter can be obtained readily through the analogy of the Poiseuille law

$$D_{ES} = \left(\frac{32\varepsilon}{\alpha a^2 Q}\right)^{1/2} \tag{4.14}$$

The critical velocity of He II across woven screens can be expressed as

$$V_{sc} = \left(\frac{32\varepsilon}{\alpha a^2 Q}\right)^{-1/8} \tag{4.15}$$

These critical values are listed in Table 4-4. Therefore, the flow is not expected to reach critical velocities until all the flow is through a small portion of a gallery channel. This will not occur until near depletion of the bulk liquid.

Conclusions

From the experimental works of Fairbank, Beam, and Chu, it was found that the tensile stress of He II is about $P_t = -0.14$ atm. A mechanism is proposed in the present work that can predict this value. It can be concluded that a negative pressure of a tenth of an atmosphere is required to cavitate He II. The tensile stress measured for the formation of microscopic bubbles by acoustic techniques are much lower than that. This can be explained through the present model that microscopic bubbles were detected by acoustic methods

Table 4-4 SCREEN CRITICAL VELOCITIES

MESH TYPE	D_E	V_{sc}	V_c
150 x 150 Sq. Weave	1.03×10^{-2}	3.14	2.14
250 x 250 Sq. Weave	5.6×10^{-3}	3.66	2.50
400 x 400 Sq. Weave	3.15×10^{-3}	4.22	2.88
24 x 110 Plain Dutch	1.94×10^{-2}	2.68	1.83
30 x 150 Plain Dutch	1.58×10^{-2}	2.82	1.93
50 x 250 Plain Dutch	8.58×10^{-3}	3.29	2.24
x 70 Dutch Twill	3.77×10^{-3}	4.04	2.76
x 1500 Dutch Twill	1.54×10^{-3}	5.05	3.45
325 x 2300 Dutch Twill	1.05×10^{-3}	5.55	3.79

before they reach the critical radius. In order for these bubbles to grow to visible sizes, free energy is required. Without externally supplied energy, these bubbles will collapse.

Let us look at the potential of cavitation within the gallery channels. The largest negative pressure in the gallery occurs at depletion when it reaches the maximum capillary retention capability of the screen. For a 50 x 250 mesh, this is 0.2818 g_0-cm (3×10^{-2} torr), and for a 325 x 2300 mesh, this is 3.0993 g_0-cm (3.3×10^{-1} torr). The present study shows that these pressures are not sufficient to cavitate He II. The above analysis assumes that the helium within the gallery channel is in metastable state. If the liquid in the gallery is in VLE, the issue was addressed in Section 2.3. Any bubble that would tend to form should collapse and reappear in the bulk vapor phase at the ullage tank. Therefore, it can be concluded that cavitation of the He II in the gallery is extremely unlikely under metastable or vapor-liquid equilibrium state. The only conceivable way for cavitation to occur within the gallery is by pushed-over vapor. During short-duration high g-acceleration pulses, vapor might be pushed into the gallery through the screens. The introduction of vapor into metastable liquid will result in spontaneous boiling. The only way to prevent this is by using a thicker screen with finer pore size.

4.4.2.5 Effect of Pump Heat Dissipation. The potential of cavitation of He II due to isothermal pressure drop was addressed in the previous section. The possibility of boiling from isobaric heating of liquid helium is studied in this section. The heater power from the FEP or dissipation heat from the mechanical pump may result in nucleation of boiling. In terrestrial tests with different types of heaters one should be able to deduce peak values in principle for film flow. The Van Der Waals forces of the film enhance the pressure locally. Therefore, the boiling onset at low-g is not the same as the value predicted from usual peak flux equations when the acceleration "g" goes to zero. As mentioned earlier, He II can exist in metastable (liquid) state when its pressure has dropped isothermally below the vapor-pressure (V-P) curve. Similarly, metastable state of liquid helium is also noted when the fluid temperature is raised above the saturation temperature isobarically (Refs. 4.26 and 4.27). The temperature above the saturation temperature at which nucleation of bubbles is observed is known as the superheat. From the classical nucleation theory, the amount of superheat required for nucleation depends on the surface tension of the liquid. Cole (Ref. 4-28) has derived an approximate expression for the superheat value

$$T - T_{sat} = \frac{T_{sat}}{\rho_v \lambda} \left(\frac{16 \pi \sigma^3}{3KT \ln(NKTt/h)} \right)^{1/2} \qquad (4.16)$$

where ρ_v is the vapor density and λ is the latent heat of vaporization. The above correlation predicts that He II can tolerate superheating without boiling until a temperature of about 4 K is reached. This limit was verified experimentally by Saji et al. (Ref. 4-29). They showed that He II could be superheated isobarically beyond the vapor-pressure curve, as shown in Fig. 4-16. The superheated He II then transformed into superheated He I at T_λ and did not cavitate until the classical nucleation theory limit (~ 4 K) was reached. The superheated He II regime is divided from the superheated He I regime by T_λ (2.17 K). The He I phase is distinguished by a sharp rise

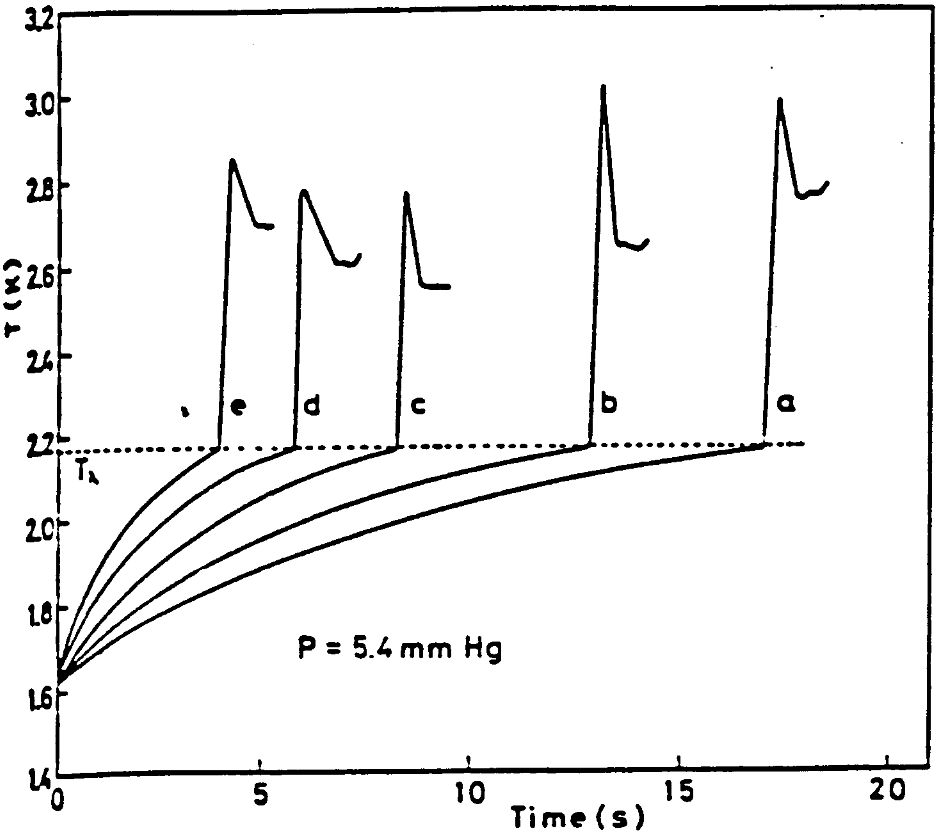

Fig. 4-16 Thermograms for Various Values of Applied Power q. The letters on the curves represent the applied power in milliwatts: a. 70.6; b. 94.2; c. 132.3; d. 196.2; e. 272.6 mW. (Ref. 4-29)

in temperature due to poor heat conduction. The boiling of the liquid is characterized by a sudden drop in temperature, caused by the energy consumed during bubble formation. The experimental transition temperature from superheated He II to He I is plotted in Fig. 4-17. The dashed lines on the data points represent uncertainty in measuring the peak boiling temperature. This temperature is found to be 2.17 K ±0.005 K. The experimental boiling temperature is compared with the classical nucleation theory (solid line) in Fig. 4-18. Good agreement is found within data scatter. It should be noted that since the authors did not measure the actual pressure within their experimental chamber, they might be pressurizing the He II along the constant chemical potential line instead of superheating the liquid (Ref. 4-30).

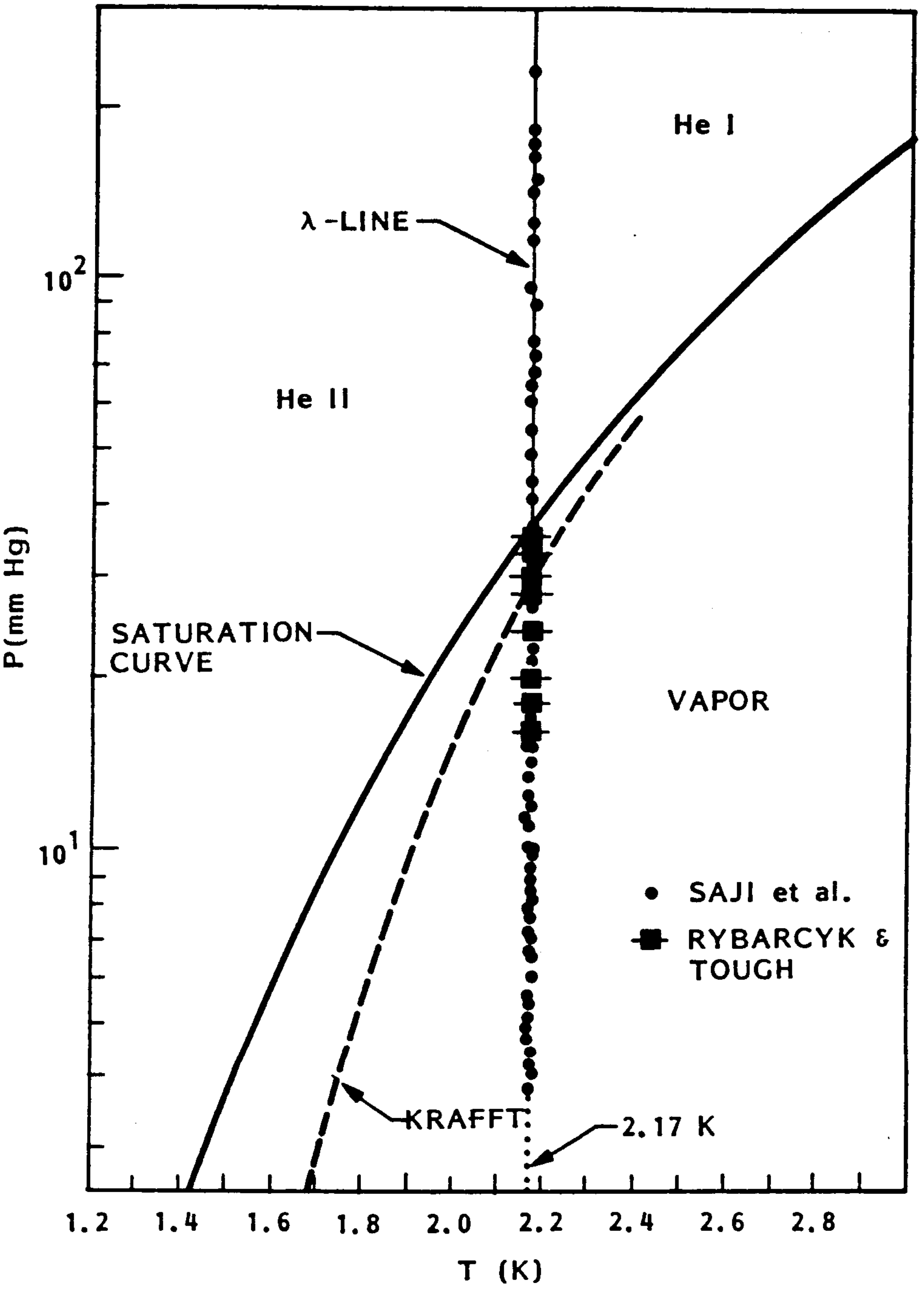

Fig. 4-17 Phase Diagram of Helium with Equilibrium Lines (Solid Lines) and Maximum Superheating Temperatures (Solid Circles). The experimental upper limits of superheating found by Krafft (dashed curve) and Rybarcyk and Tough (solid squares) are also indicated (Ref. 4-29)

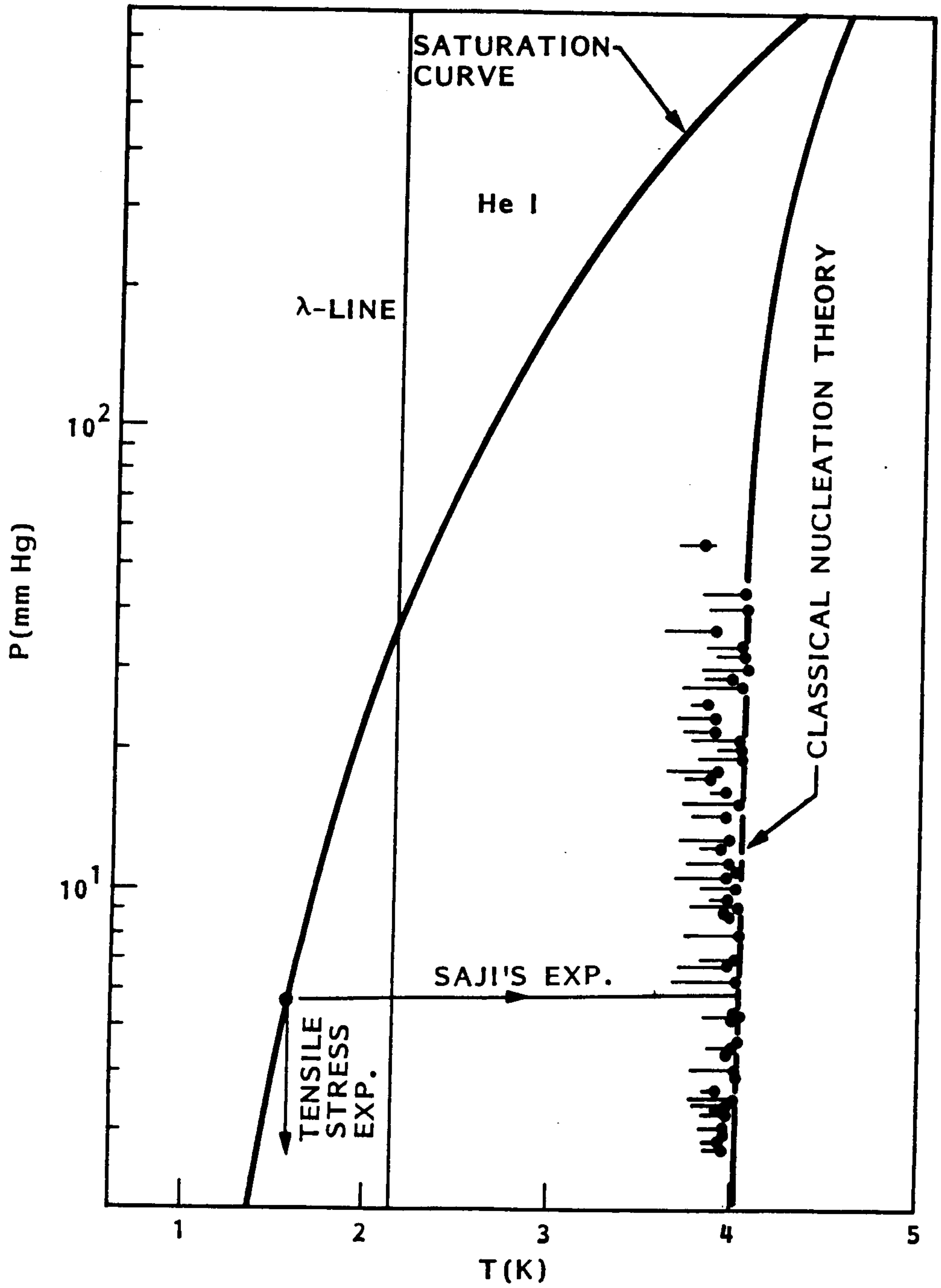

Fig. 4-18 Phase Diagram of Helium with Equilibrium Lines (Solid Lines) and Maximum Superheating Temperature (Solid Circles). (Ref. 4-29)

At first glance, Saji's findings seem to contradict the vortex theory or the isothermal tensile stress experiments, which show that the threshold value for cavitation is much lower than that predicted by the classical nucleation theory. However, there is really no abiguity if one realizes the difference in the nature of the two experiments. For the isothermal reduction of pressure (e.g., the tensile stress experiment), the metastable state of liquid helium is always within the He-II regime (Fig. 4-18). The cavitation of helium from the vortex rings that act as nucleation sites reduces the threshold pressure required for the bubble formation. As for the isobaric heating of He II (Saji's experiment), the vortex theory predicts that one needs to superheat He II to temperature above T_λ for cavitation. However, as the superheated He II transforms into superheated He I (at T_λ), all the vortex rings vanished (Fig. 4-18). No nucleation sites are present, resulting in the agreement between the classical nucleation theory and the experimental results.

The FEP or mechanical pump will dissipate up to 50 W. Based on the thermal resistance of the gallery arms, the maximum temperature gradient across the gallery channels will be approximately 1 mK. The fluid within the gallery channels will remain below T_λ and, based on the findings of Saji et al., the heat dissipated by the pump is not going to cavitate the fluid.

It is noteworthy that the estimated 1-mK rise in temperature within the gallery channels (due to dissipation of the pump) might be enough to set up a thermomechancal effect across the screen. According to the London's equation, a fountain pressure of about 1 torr could be generated by the above temperature gradient. This overpressure within the gallery channels is much higher than the summation of pressure drops mentioned in 4.4.1. Therefore the gallery might be slightly pressurized instead and cavitation might never occur in the channels. This 1-torr pressurization would be sufficient to overcome the capillary retention capability of the screens in contact with vapor and cause liquid breakthrough. However if the screens are fine enough, breakthrough can be avoided and liquid can be retained as in the case of a conventional vapor-liquid phase separator.

The actual temperature gradient across the screens will not be uniform, especially when some sections of the channels are submerged and others are exposed to vapor because of the highly different heat-transfer coefficients. These gradients will therefore be a function of the amount of liquid remaining in the tank.

Once the final pump heat dissipation and gallery wall thickness are established, this effect would need to be carefully modeled and analyzed. A coarse screen (50 to 100 μm) is baselined for the gallery device and it is possible that the pore openings may be too large to set up a sizable thermomechanical effect to pressurize the gallery channels.

Section 5

INTEGRATED FEP/ENCLOSED CAPILLARY DEVICE

An alternative to the gallery device using screens is the integrated FEP device (IFD) which uses the capillary action of porous plugs instead of screens along the gallery channels to collect liquid He II. Figure 5-1 is a schematic diagram of the IFD. The downstream pump is removed and the porous plugs along the gallery channels are also responsible for the transport of the liquid as FEPs. For this reason heaters have to be installed within the gallery channels. The channels also have to be constructed of insulating materials to allow the required temperature difference to be sustained across them. The porous plugs in this system can be divided into two groups: (1) the FEP plugs (where both sides of the porous media are in contact with the liquid - they are responsible for conveying He II) and (2) the vapor-liquid phase separation plugs (where only one side of the plugs is

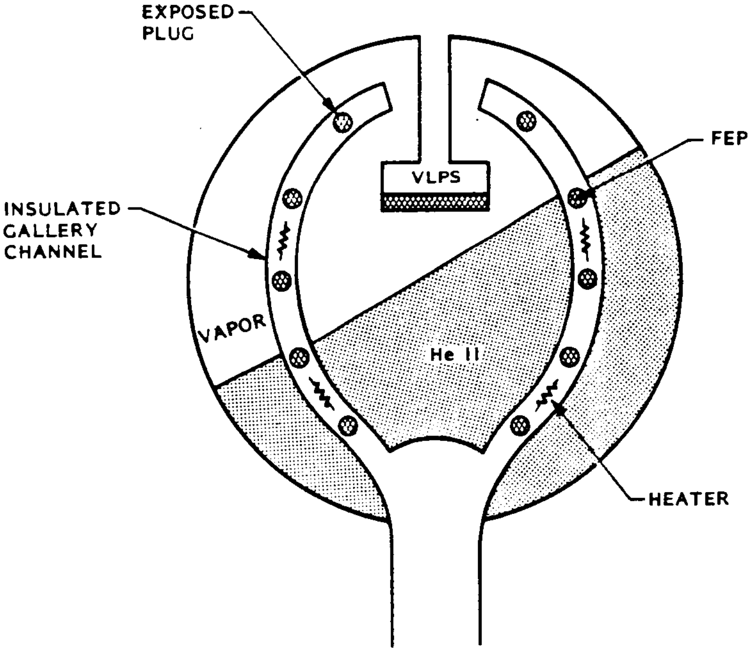

Fig. 5-1 Schematic Diagram of the Integrated FEP Device

submerged in liquid with the other side open to vapor - these porous media prevent the vapor from entering or the liquid from escaping the gallery channels). The performance of these plugs will be discussed in detail in the following sections.

5.1 DESCRIPTION OF OPERATION

As the heaters of the IFD are activated, liquid helium is pumped across the FEP plugs into the gallery channels. Vapor is introduced into the ullage tank through the VLPS plugs to replace the volume vacated by the liquid being transferred and to reject part of the heat input from the FEP. The net transfer rate into the receiver tank is the difference between the mass flow through the FEP plugs and that of the VLPS plugs.

The advantage of this device over the screen system is that the gallery channels are always pressurized. In the screen device, liquid helium is drawn through the screen, resulting in pressure drops that might cause cavitation problems. Although it was concluded in Section 4.4.2.4 that the boiling of He II under metastable conditions is highly unlikely, there is still a slim chance that cavitation might occur under the vapor-liquid equilibrium state (VLES). Under equilibrium conditions, it is conceivable that any bubble that formed in the gallery channel would condense and reform in the ullage. However, this scenario is complicated by the heater input from the fountain-effect pump. Moreover, during the short-duration high-g-acceleration pulses (SDHGP) and startup transients, vapor might be pushed across the screens into the gallery channels. This would convert metastable He II into VLES with vigorous boiling. However, these problems are not likely to occur in the IFD, because the gallery channels are always pressurized and vapor is much less likely to transfer through a porous plug during SDHGP than through a screen.

5.2 LIQUID WITHDRAWAL

5.2.1 Performance of the Submerged Porous Plugs

These plugs are in contact with the liquid helium on both sides and behave as typical fountain-effect pumps when subjected to a temperature difference. Recently the performance of FEPs was found to obey the following empirical equation (Ref. 5-1)

$$\dot{m}_{FEP} = \rho_s A_F \frac{K_4}{K_p}\left[\frac{\eta_n^2 S \Delta T K_p{}^{3/2}}{L\,\rho^2}\;\frac{\rho_s}{\rho_n}\right]^{1/4} \qquad (5.1)$$

where $\dot{m}_{FEP}$ is the mass flow rate and K_4 is the throughput factor. It was found that K_4 is inversely proportional to the square root of the permeability (K_P),

$$K_4 \sim \frac{6.32 \times 10^{-6}}{K_p} \qquad (5.2)$$

Combining Eq. (5.2) with (5.1) one gets:

$$\dot{m}_{FEP} \cong C\frac{A\rho_s}{K_p{}^{5/8}}\left[\frac{\rho_s}{\rho_n}\;\frac{\eta_n^2 S\Delta T}{\rho^2 L}\right]^{1/4} \qquad (5.3)$$

where C is 6.32×10^5 cm.

The preceding equation is used as the criterion for the design of the submerged porous plugs of the integrated FEP device. As the supply tank is continously being drained, the area of the submerged porous plugs decreases and the area of the exposed plugs increases. The mass flow rate of the FEP is governed by its heater power ($\dot{Q}$), i.e.,

$$\dot{Q} = \dot{m}T_H S_H \tag{5.4}$$

This means that the temperature difference across the plugs has to rise according to Eq. (5.3). Figure 5-2 is a plot of the temperature across the porous media as a function of the submerged plug area over the total plug area (A_F/A). The material used is the 0.5-μm stainless steel Mott plug with a permeability of $K_p = 8 \times 10^{-10}$ cm^2. The study is based on a flow rate of 500 liter of He II per hour and a total plug area of 2000 cm^2 (which is approximately the surface area of the screen for one arm of the gallery device). The ΔT increases as the pump area decreases until the limit is reached, when the downstream temperature or T_H exceeds T_λ. When this happens, the superfluid downstream of the pump transforms into He I, and the pumping power would be reduced sharply. The area ratio at which $T_H = T_\lambda$ is the minimum value allowable in the design is designated by $(A_F/A)_{min}$.

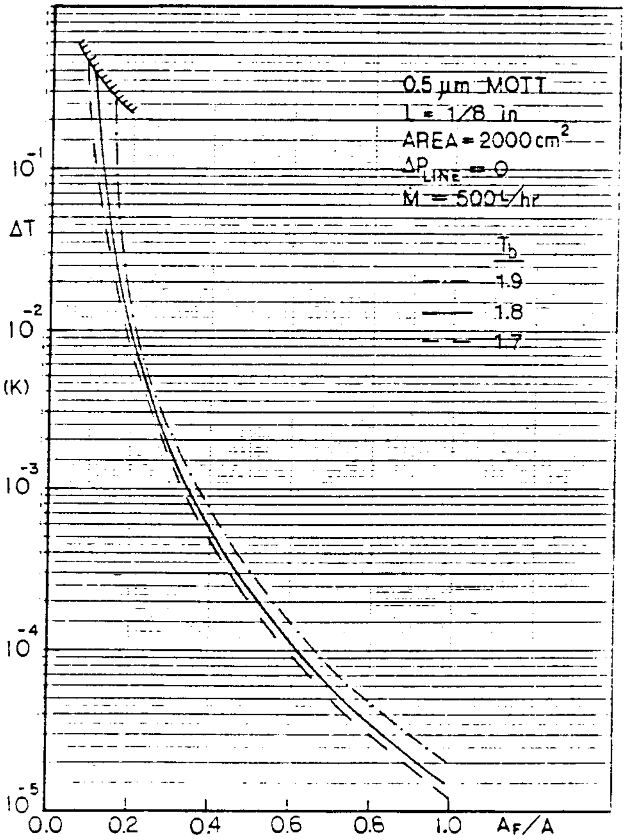

Fig. 5-2 ΔT Versus FEP to Total Area of Porous Media

Note that in Fig. 5-2, it was assumed that there was no pressure drop in the plumbing downstream of the FEPs. However, in actual situations there is quite a bit of flow resistance due to friction losses and back pressure (especially during the initial phase of transfer). The maximum amount of pressure head that can be generated by a single-stage FEP is

$$\Delta P_{max} = \int_{T_b}^{T_\lambda} \rho S dT$$

$$= \rho \int_{T_b}^{T_\lambda} S_\lambda \left(\frac{T}{T_\lambda}\right)^{5.6} dT$$

$$= \rho \left[\frac{S_\lambda T_\lambda - S_b T_b}{6.6}\right] \tag{5.5}$$

where S_λ is 1.5378 J/gK. Equation (5.5) is plotted in Fig. 5-3 together with the ΔP_{max} obtained from evaluating TS at the mean temperature. For small ΔT, the two curves almost coincide as expected. At low bath temperature the integration method tends to predict a higher fountain pressure. For example, it is clear that a single-stage FEP is not operational at 2 K if the flow resistance in the plumbing exceeds 230 torr.

With a pressure drop along the pipe line (ΔP_{LINE}), the fountain-effect pump Eq. (5.3) can be modified to

$$\dot{m} = \rho_s A_F \frac{C}{K_p^{5/8}} \left[\frac{\rho_s}{\rho_n} \frac{\eta_n^2}{\rho^3} \frac{1}{L} (\rho S \Delta T - \Delta P_{LINE})\right]^{1/4} \tag{5.6}$$

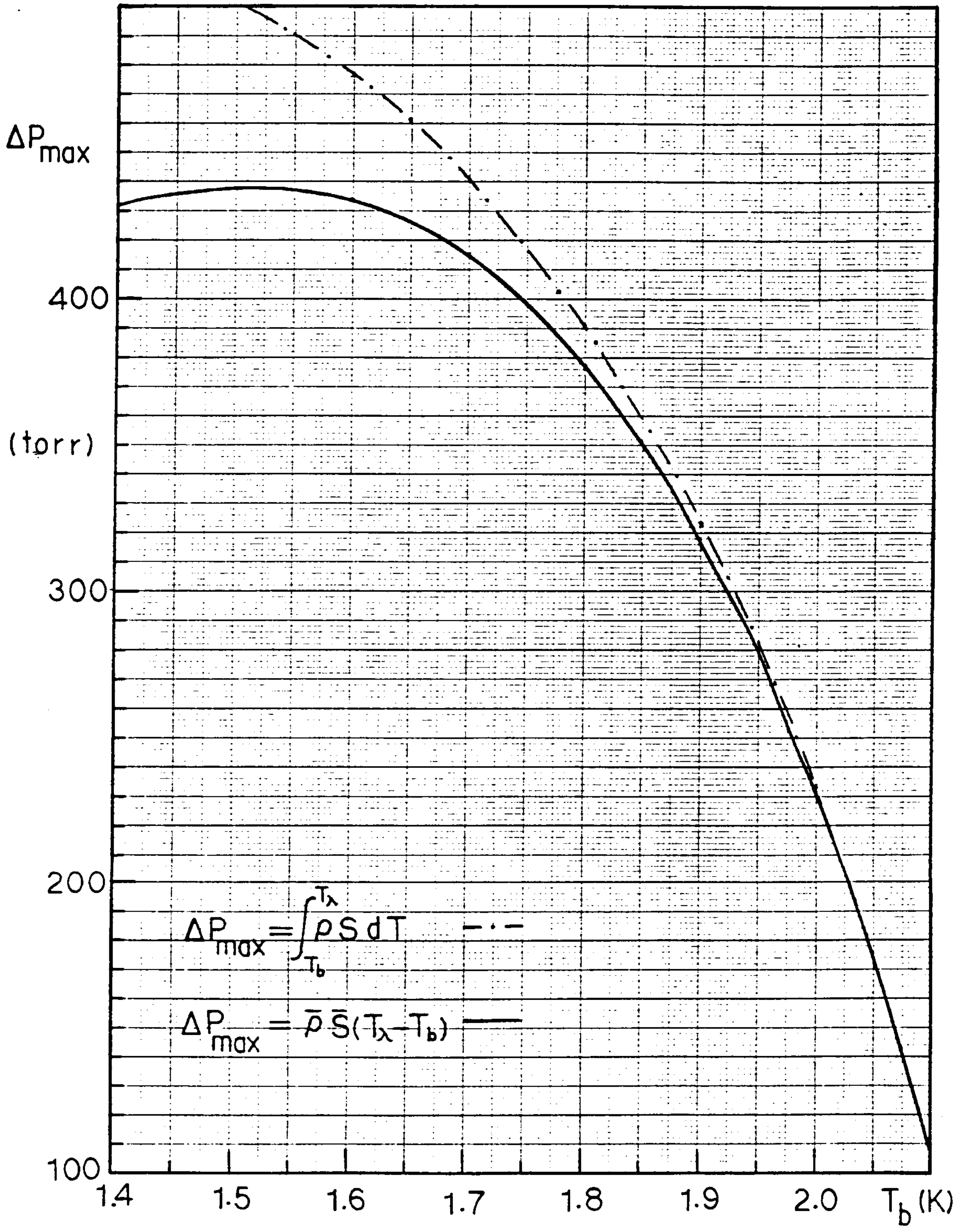

Fig. 5-3 Maximum Pressure Head that can be Generated by a Single-Stage FEP

From this equation, $(A_F/A)_{min}$ can be calculated as in Fig. 5-2 and is presented in Fig. 5-4 versus the total plug area (A) for various ΔP_{LINE}'s. For a certain $\Delta T_{max} = T_\lambda - T_b$, one can calculate the required fountain-effect-pump area (A_F) or the minimum surface-area ratio $(A_F/A)_{min}$ to pump 500 L of He II per hour. From $(A_F/A)_{min}$ one can estimate the amount of residual fluid left in the receiving tank. Based on Fig. 5-3, the minimum area of FEP that must be in contact with the bulk fluid is 180 cm^2 to 320 cm^2 for a range of ΔP_{line} of 0 to 300 torr. Using the same area of FEP per length of gallery channel as the screen device, the length of the gallery channel that must be submerged is 43 to 76 cm. This small value essentially assures that the residuals will be the same as for the screen capillary device.

One important factor in the design of the integrated FEP device is the selection of the porous material. As it is seen from Eqs. (5.1) and (5.6) that the mass flow rate of an FEP is roughly proportional to the inverse square root of the Darcy permeability (actually $\dot{m} \propto K_p^{-5/8}$), the total pump area A_F can be greatly reduced if one uses material with a fine pore size instead of a coarse one. Accordingly, the amount of residual fluid left in the tank is much smaller. Figure 5-5 is a plot of $(A_F/A)_{min}$ versus the Darcy permeability of the plug for three different bath temperatures at 1.8 K $(A_F/A)_{min}$ ranges from about 0.007 with $K_p = 1 \times 10^{-11}$ cm^2 to 0.5 with $K_p = 1 \times 10^{-8}$ cm^2. It is obvious that any porous material with $K_p \geq 10^{-9}$ cm^2 is not feasible for use in the integrated FEP device. For comparison, the classical permeability of the 325 x 2300 Dutch Twill screen is included in Fig. 5-5. The K_p was determined from manufacturer-supplied data, which was obtained by passing air through a single screen, by correcting for helium gas (using the ratio of the molecular weights) and for the thickness of the stack of screens (0.318 cm). Among the finest screens available, the Dutch Twill 325 x 2300 has a pretty small permeability, comparable to some of the coarse-pore sintered metal plugs. Usually, the permeability obtained by different flow media are related by the following correlation (Ref. 5-2)

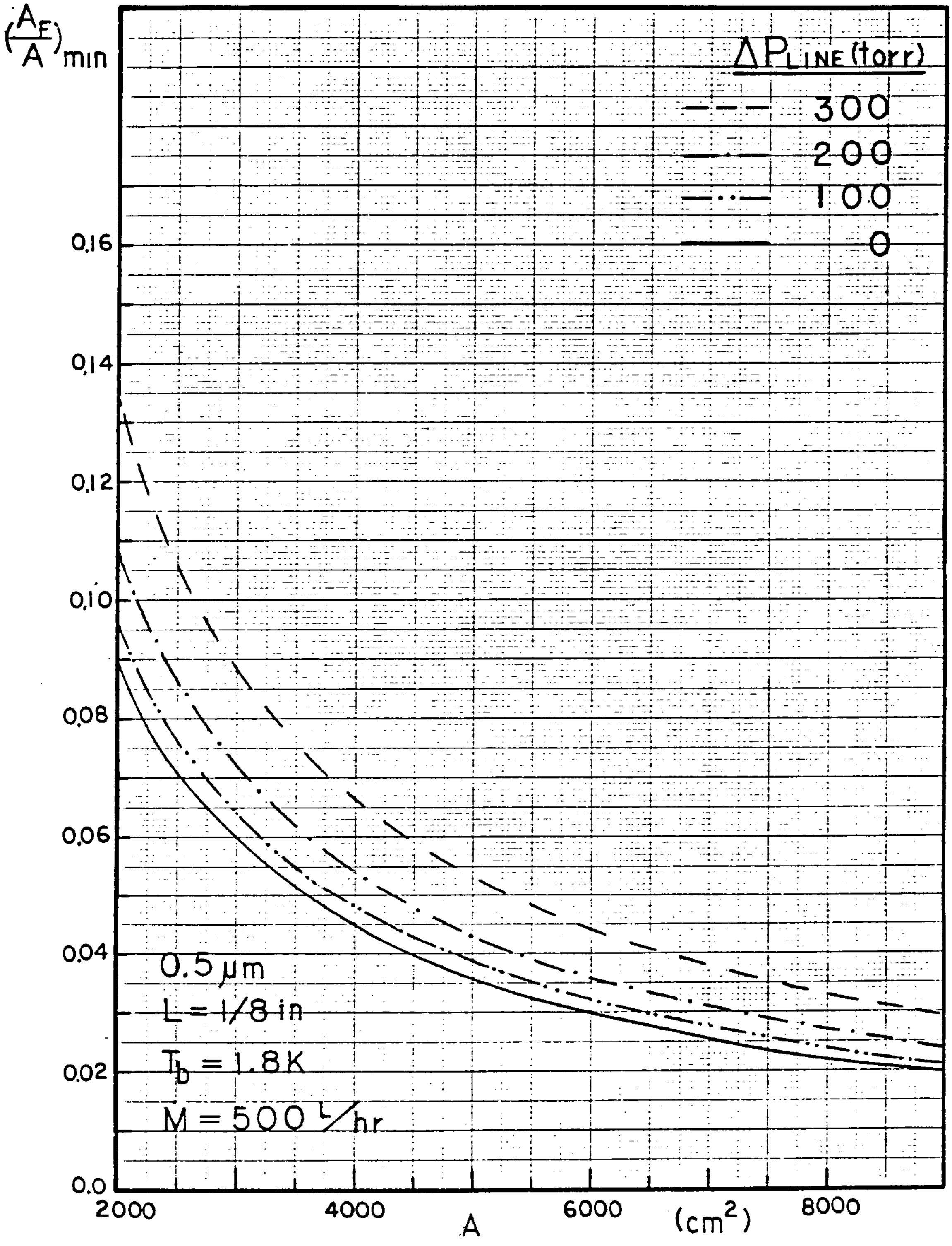

Fig. 5-4 $(A_F/A)_{min}$ as a Function of Total Plug Area for Various ΔP_{line}'s

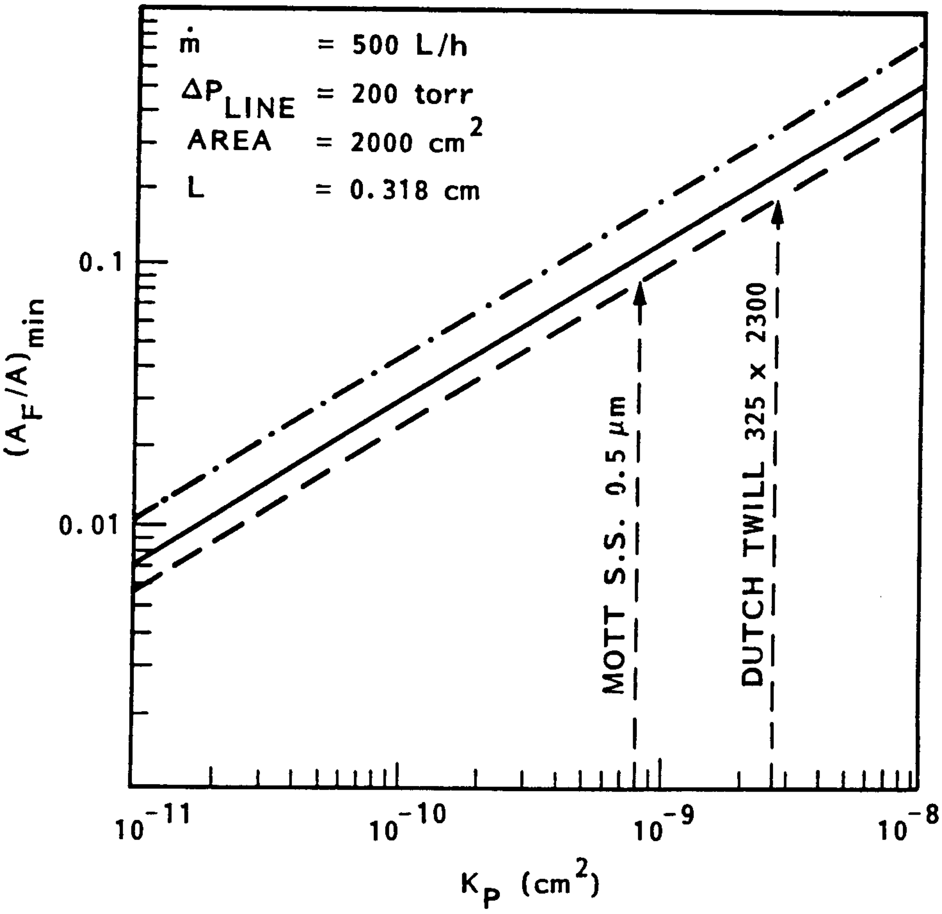

Fig. 5-5 $(A_F/A)_{min}$ as a Function of Permeability for Various Bath Temperatures

$$\frac{(K_p)_A}{(K_p)_B} = \sqrt{\frac{M_A}{M_B}} \tag{5.7}$$

where M_A and M_B are the molecular weights of the flow media.

Therefore, the actual permeability for helium should be $\sqrt{4/29}$ times the measured value using air, or about $2.86 \times 10^{-9} cm^2$. It should be noted that the curves in Fig. 5-5 are generated for a porous plug thickness of 1/8 in. In order to compare with the performance of the Dutch Twill screen, one needs to stack the screens to the appropriate thickness. Even with a K_p of 2.86×10^{-9} cm^2, the screen is marginal for use in the integrated FEP device, because more than 20 percent of the screen has to be submerged when ΔT_{max} is reached. This translates into a large residual fluid volume. An ideal material for used as the integrated FEP is a fine-pore ceramic plug with a K_p of the order of 1×10^{-11} cm^2 (Ref. 5-6).

5.2.2 Performance of the Exposed Porous Plugs

The performance of the exposed porous plugs is not easily predictable. For a conventional vapor-liquid phase-separation system, the upstream of the porous plug is at P_u (saturation pressure of T_u) when the downstream is at a very low pressure. The liquid that penetrates the plug is immediately evaporated. Latent heat of vaporization is removed and the temperature difference across the porous media is sustained. This kind of transport was found to be dominated by the thermal convection of the two-fluid system (Ref. 5-3). The mass flow rate across the phase separator can be expressed as

$$\dot{m}_{VLPS} = K^{*}_{GM} A_{VL} \frac{\rho_s}{\rho} \frac{\eta_n ST}{(\lambda + ST)} \left(\frac{\rho^2 \rho_s S \Delta T}{L \rho_n \eta_n^2} \right)^{1/3} \tag{5-8}$$

where A_{VL} and L are the area of the phase separation plugs and their thickness. The latent heat of vaporization is represented by λ. K^{*}_{GM} is the Gorter-Mellink constant for porous media. From the experimental results of varoius VLPS data, the following relationship was obtained

$$K^{*}_{GM} \propto \sqrt{K_p} \cong \delta \sqrt{K_p} \tag{5.9}$$

where δ is 10^7.

Assuming that the exposed plugs perform ideally as conventional phase separators, one can estimate the area ratio A_F/A_{VL} for which the FEP flow rate is equal to the mass loss rate through VLPS. When this happens, liquid helium is circulated between the bulk liquid and the gallery channel with no transfer of fluid into the receiving tank. In combining Eqs. (5.6) and (5.8), the area ratio of FEP to VLPS can be calculated by equating $\dot{m}_{FEP}$ to $\dot{m}_{VLPS}$. A_F/A_{VL} is plotted versus bath temperature in Fig. 5-6 for a 0.5-µm Mott stainless steel plug with a thickness of 1/8 in. The area ratio is less than 10 percent for $T_b < 2$ K. This limit is smaller than the $(A_F/A)_{min}$ value estimated in the previous section for ΔT (across the FEP) to exceed $T_\lambda - T_b$. Which implies that total circulation of fluid (with no transfer) will not occur before the downstream temperature (of the FEP) reaches T_λ. It can be shown (by combining Eqs. (5.8), (5.6) and (5.9) that the area ratio of FEP to VLPS for total recycle of fluid within the ullage tank is roughly equal to

$$\left(\frac{A_F}{A_{VL}}\right)_1 \sim \frac{(K_P)_1}{(K_P)_2}\left(\frac{A_F}{A_{VL}}\right)_2 \tag{5.10}$$

where subscripts 1 and 2 stand for two different porous materials with different Darcy permeabilities. Therefore, by choosing a fine-pore plug, one can reduce the (A_F/A_{VL}) limit substantially.

The net transfer rate from the supply tank to the receiver tank can be written as

$$\dot{m}_{NET} = \dot{m}_{FEP} - \dot{m}_{VLPS} \tag{5.11}$$

ORIGINAL PAGE IS
OF POOR QUALITY

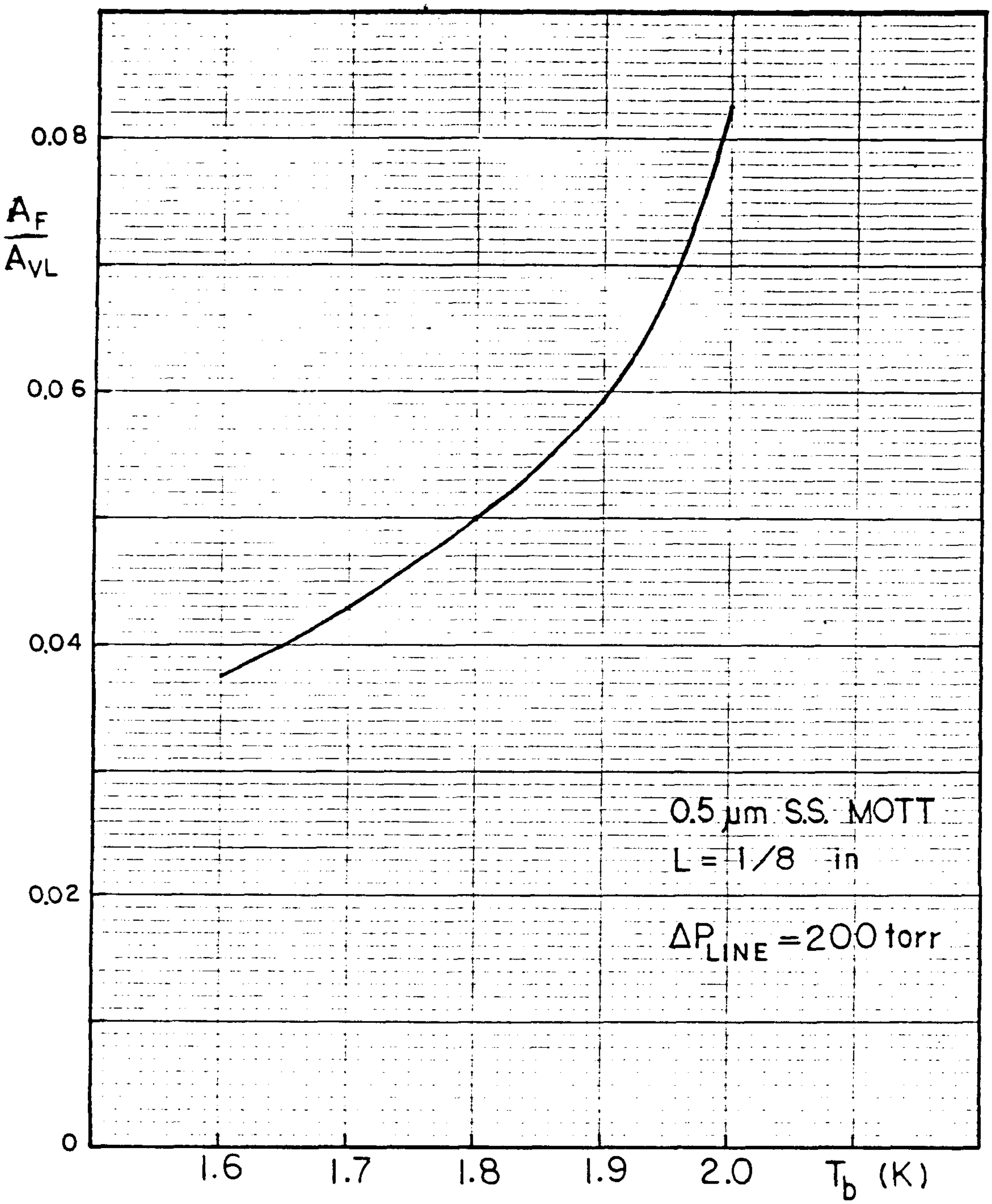

Fig. 5-6 Area Ratio of FEP and VLPS for Total Circulation of He II Within Supply Tank.

Unfortunately, as A_F/A_{VL} decreases, $\dot{m}_{NET}$ also decreases. This might result in extremely low flowrate when the tank is close to empty. One way to ensure adequate transport rate is again by careful selection of porous material for the integrated FEP device. The calculated net volumetric flowrate ($\dot{V}_{NET} = \dot{V}_{FEP} - \dot{V}_{VLPS}$) of the IFD by using a 0.5-µm Mott plug and a 1-µm ceramic plug is compared in Fig. 5-7 for a total plug area of 2000 cm^2. As expected, the losses due to VLPS in the low-throughput material is almost negligible as compared to the FEP transfer rate. (Although the ceramic plug has a larger pore size than the 0.5-µm Mott plug, it has a lower throughput as indicated by its permeability.) In using a 0.5-µm Mott plug, $\dot{V}_{VLPS}/\dot{V}_{FEP}$ can be as high as 40 percent at $(A_F/A)_{min}$. The ceramic plugs also tend to have a lower $(A_F/A)_{min}$ value than the 0.5-µm Mott plug.

The above analysis is based on the assumption that the exposed plugs perform ideally as conventional VLPSs. However, one might argue that there are some differences between these exposed plugs and the conventional VLPS plugs. The main difference between the two systems is depicted in Fig. 5-8. The pressure within the gallery channel of the IFD is quite high (due to the pressure drop in the transfer line), while the upstream pressure of the conventional VLPS is close to the saturated vapor pressure of T_b or T_u. With this large pressure difference across the exposed plugs, the main concern is breakthrough (BT). Breakthrough will occur if the thermomechanical pressure ($\rho S \Delta T$) is not large enough to overcome the external pressure forces (ΔP_{LINE}). Liquid begins to penetrate the plug faster than it can be evaporated, resulting in massive liquid loss. The onset to breakthrough in VLPS systems is not fully understood. However, conceivably breakthrough in a fine-pore plug requires a much larger external pressure difference. Figure 5-9 illustrates the breakthrough in an active phase separator (APS) device (Ref. 5-4). The APS data are usually characterized by two distinctive transport regimes. The flat portion of the curve with low mass flowrate represents Gorter-Mellink (GM) transport (Ref. 5-5) close to zero net mass flow of He II in wide ducts. The steep rise in mass flowrate indicates the onset of breakthrough. Due to the large throughput value of the APS ($K_p \sim D^2/12 = 6.75 \times 10^{-8}$ cm^2), the

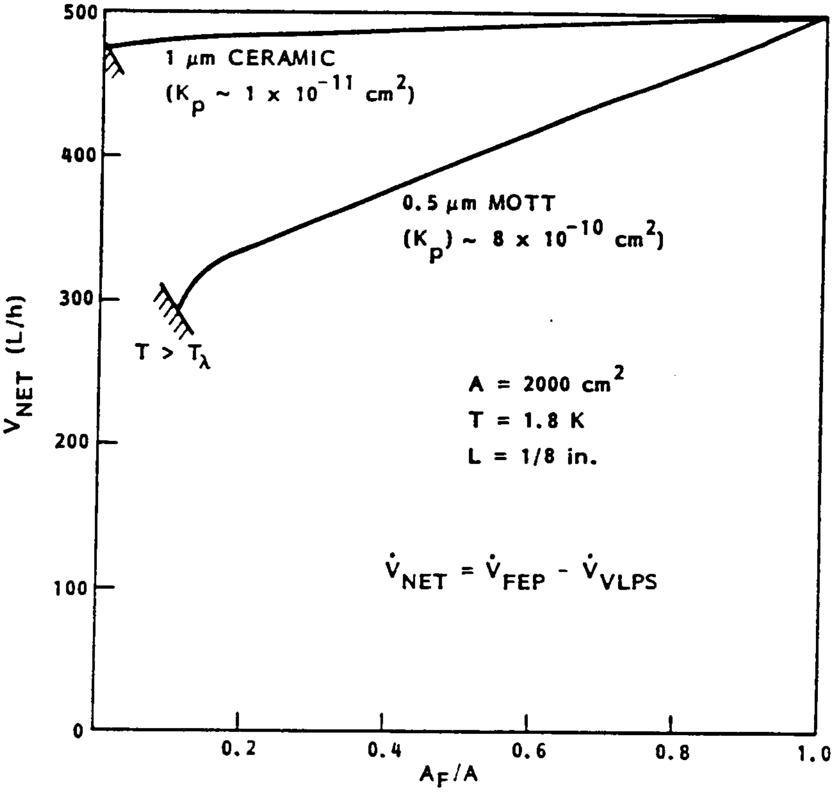

Fig. 5-7 IFD Net Volumetric Flow Rate

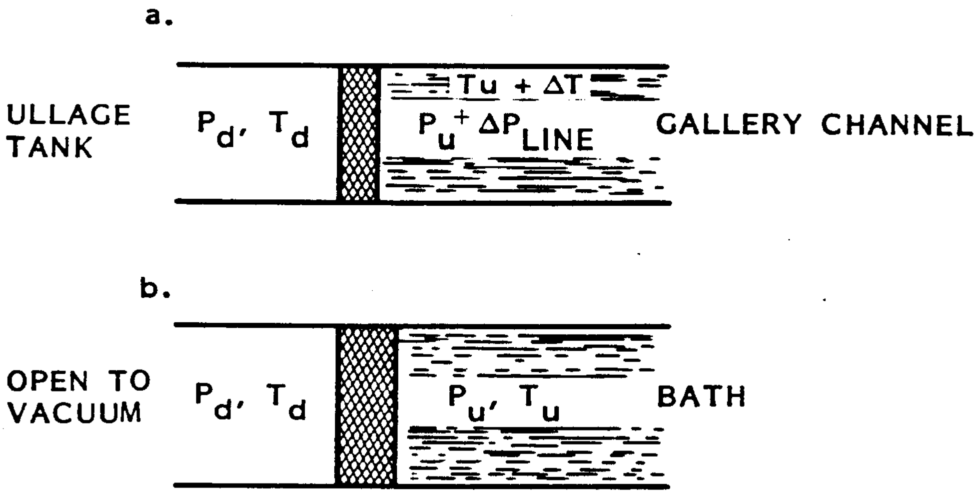

Fig. 5-8 Comparison Between the a) IFD and b) Conventional VLPS

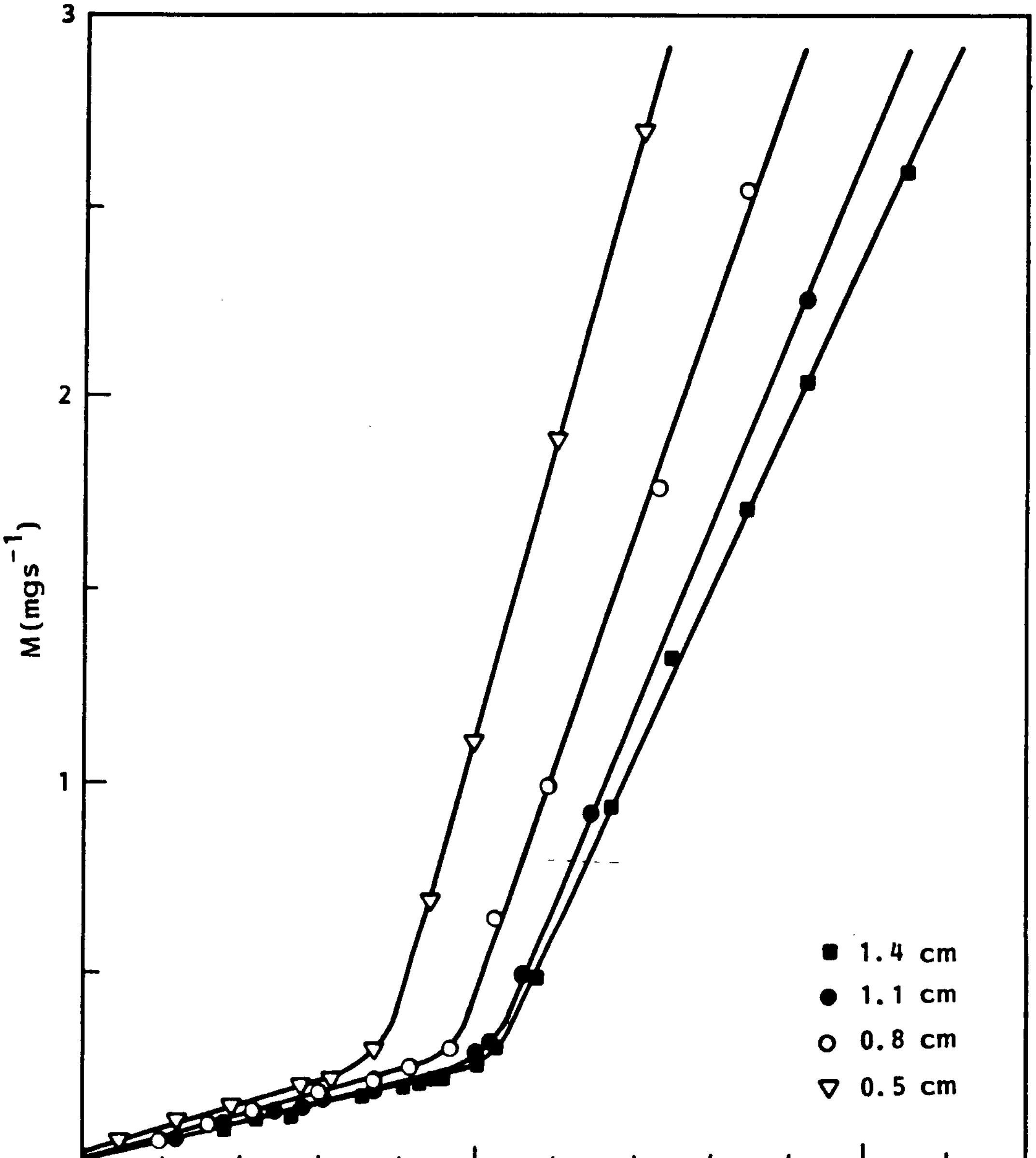

Fig. 5-9 Example of Experimental Mass Flow Results for the APS at Fixed T_B = 1.9 K for a 9-μm-Wide Slit and Radius of 0.25 cm

C-2

liquid tends to break through at very low external pressure difference, $\Delta P_C < 10$ mbar. Figure 5-10 shows the various transport regimes of VLPS using a 1 μm ceramic porous plug (Ref. 5-6). The porous-media phase-separation data that resemble the APS result are also characterized by a low-flowrate GM transport and a steep BT regime. Laminar flow within the phase separator is hard to achieve. Unlike the APS data, the critical pressure difference for the onset of BT in the ceramic plug is very high (about 500 mbar at a bath temperature of 1.8 K). This is because of the fine pore size of the ceramic plug, with $K_p \sim 10^{-11}$ cm^2. It can be concluded that breakthrough will occur if the external pressure difference is too high. However, the critical pressure difference ΔP_C for the onset of BT is a strong function of the pore size or the Darcy permeabilty of the porous material. The heat conduction of He II across low-K_p plugs is low. This enables a large ΔT to be sustained across the plug and the thermomechanical forces prevent the BT of the fluid until a large ΔP_C is reached. As for the slit device or high K_p plugs, it is hard to maintain the required ΔT across it and BT occurs at a much lower ΔP_C. It is obvious from the above analysis that a fine-pore medium should be selected as the material for the IFD to prevent breakthrough. It should be pointed out that the operation of a phase separator parallel to the FEP has been demonstrated by Klipping et al. (Ref. 5-7). Since the phase separator in their experiment was a large throughput slit device, massive circulation of He II was observed. However, for the case of the IFD, we propose to use a low throughput material for the phase separator which should avoid this problem.

5.3 REMARKS AND RECOMMENDATIONS REGARDING THE IFD

The main disadvantage of the IFD can be summarized as follows:

1. When the VLPS plug area is large (close to the end of the mission) the total transfer rate is low, due to the fact that $\dot{m}_{VLPS}$ is comparable to $\dot{m}_{FEP}$.
2. Breakthrough might occur, resulting in the recycle of fluid between the gallery channels and the bulk liquid with little or no net transfer of liquid helium out of the tank.

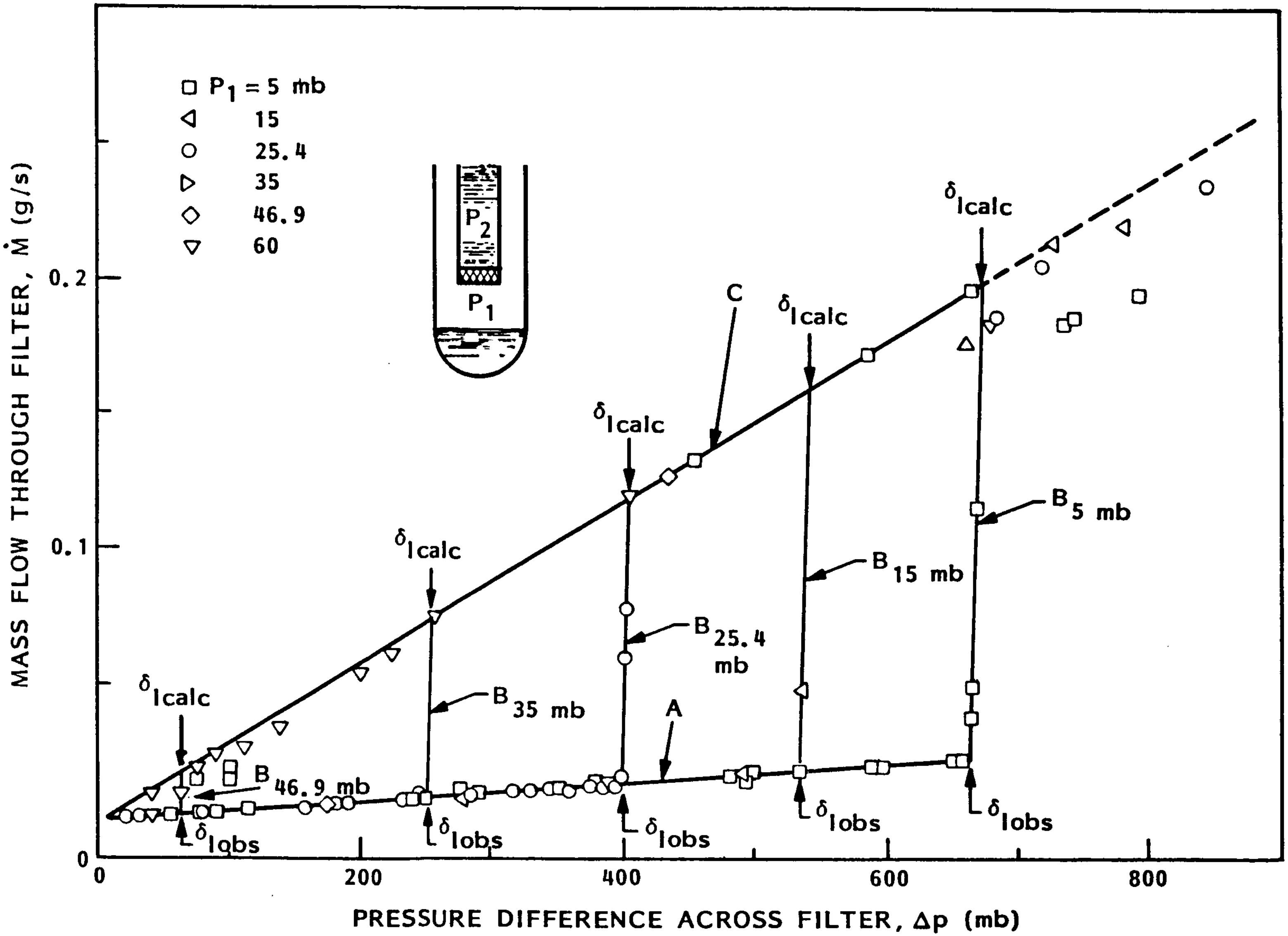

Fig. 5-10 Mass Flow of Helium as a Function of Pressure Difference For Fixed P_1

These shortcomings can be avoided by the selection of a very-fine-pore material as mentioned previously.

The differences between the screen gallery device and the IFD are quite obvious:

- The fluid within the gallery channels is always pressurized due to the TM forces (as a result of the large ΔT) across the porous plugs between the liquid in the ullage tank and the gallery channel. This further reduces the risk of cavitation within the channels.
- It is more difficult for the vapor to be pushed across the porous plugs as compared to screens during SDHGP or start-up transients. This also reduces the possibilities of boiling due to the conversion of metastable He II into VLES by the introduction of vapor phase.
- The capillary retention capability of the IFD against adverse accelerations is much greater due to the much smaller openings in the porous media.

5.4 DEMONSTRATION OF DEVICE PERFORMANCE

The performance of the IFD can be demonstrated easily by a simple experiment. The schematic diagram of the experimental setup is illustrated in Fig. 5-11. The heart of the system is an FEP made of a cylindrical porous pipe. The bottom part of the pump is sealed and the top of the porous pipe is connected to the transfer line. He II penetrates the porous wall of the pump and is forced into the receiver tank via the transfer line. A mass flowmeter and an absolute pressure transducer are mounted along the transfer tube to record the flow rate and the pressure. A flow restricter is also installed to simulate various pressure drops along the transfer line of the IFD. The entire FEP resides within a cryostat which is equipped with a fill line and an evacuation line. The liquid level within the cryostat can be measured by a superconducting liquid-level sensor.

The operation of this experiment is relatively simple. The cryostat is filled with normal liquid helium at 4.2 K. The entire system is pumped down to the

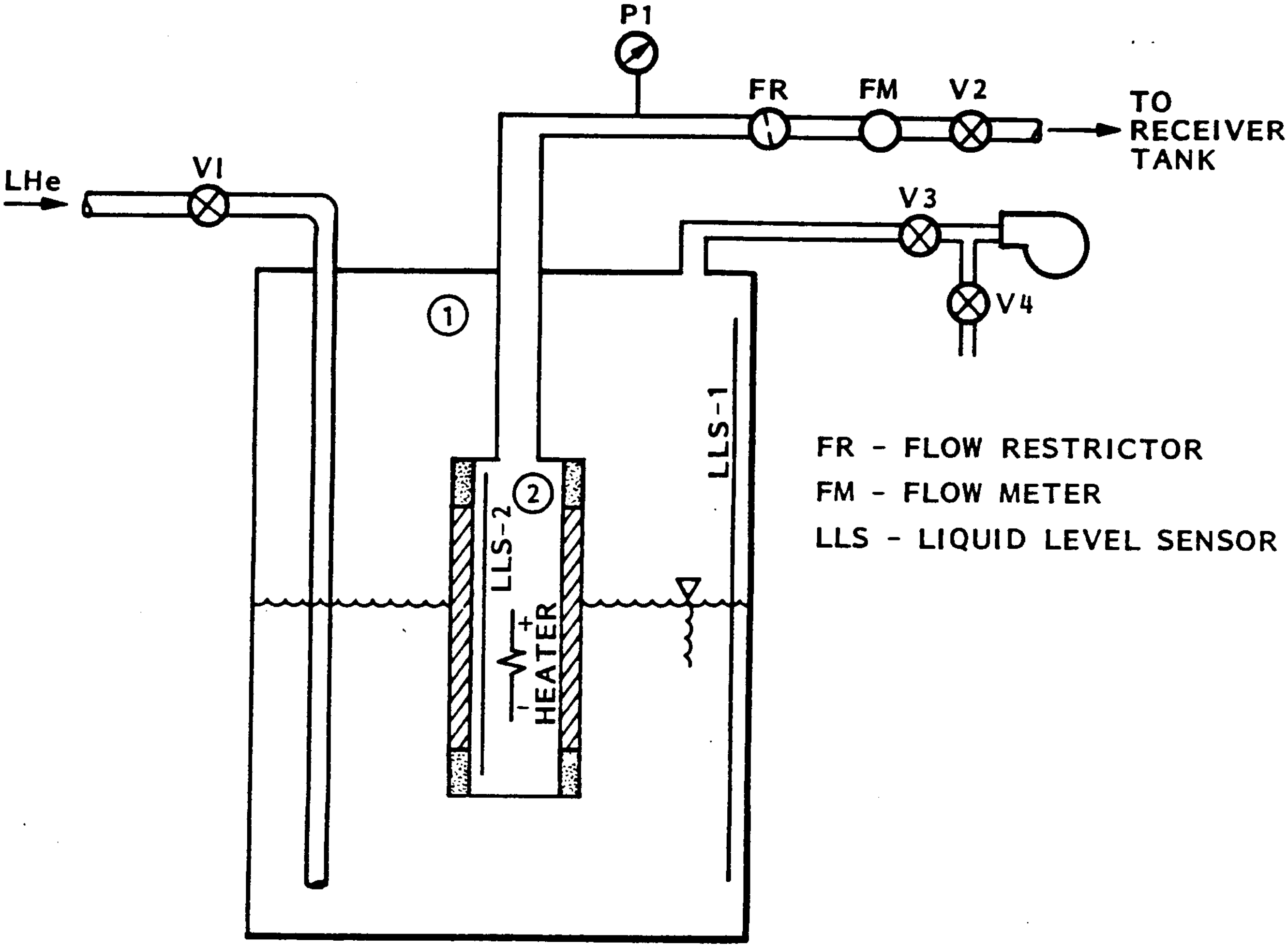

Fig. 5-11 Demonstration Experiment for the IFD

appropriate temperature below the λ point. Topping off may or may not be needed. Valve V2 is then opened with valve V1 closed and the apparatus is ready for the experiment. Valve V3 may be partly open to maintain a constant bath temperature. During the initial period of the experiment, the entire FEP is submerged, simulating a full supply tank. As the liquid level recedes, part of the porous material is epxosed to vapor, to demonstrate the performance of a partly filled IFD. This experiment can be repeated with different flow-restriction positions. The mass flow rate, temperature, and pressure differences across the FEP are recorded for different area ratio of FEP to VLPS.

This experiment is not only useful for the demonstration of the IFD, but will also provide invaluable information about the performance of a conventional FEP when in contact with vapor.

Section 6
SUMMARY AND RECOMMENDATIONS

The analysis reported in this study shows that the management of He II under low gravity is feasible. Four devices were analyzed, two of which were enclosed-capillary devices and two open capillary devices. The open devices could not manage the liquid against an acceleration of 10^{-4} g_0. The enclosed devices appear to be able to meet all of the requirements. One of the enclosed devices incorporates a fountain-effect pump (FEP) which can be used to provide the transfer flow rate at the required pressure.

Both of the enclosed devices have characteristics which have not been tested and need to be resolved before a final design can be performed. Any of these tests that need to be performed in low gravity could be incorporated in the NASA/Goddard SHOOT experiment. The SHOOT experiment will be addressing many aspects of on-orbit He-II transfer and will require a liquid-management device.

6.1 ENCLOSED CAPILLARY DEVICE

The enclosed-capillary device described in Section 4 will provide the means of supplying liquid helium to the pump inlet under an adverse acceleration of 10^{-4}g.

The acquisition device shown in Fig. 4-1 for the large 13,000-L tank weighs approximately 81 kg. Once detailed structural and thermal analysis is performed, it is estimated that this weight could be reduced. The wall thicknesses used in this design are much larger than those typically used in smaller tanks.

The following summarizes the items that need further analysis or testing. The effect of utilizing He I as a fluid is described.

6.1.1 He II

For the screened-gallery device, four different aspects require further attention with He II.

- Screen capillary retention capability
- Screen flow resistance
- Effect of pump heat dissipation
- Cavitation

The screen capillary retention capability can be characterized with one-g_0 testing with only the finest-mesh screens with the apparatus shown in Fig. 4-3. From this test, the empirical constant ϕ can be determined. Previous tests with LO_2, LH_2, and storable propellants have shown that capillary retention is fairly constant for screens of different pore sizes, therefore results of tests with fine-mesh screens can be extrapolated to coarser screens that can't be tested in a 1-g_0 environment because of their low capillary retention of He II. This test program should also include the effect of liquid vaporization at the liquid-vapor interface as described in section 4.4.1.2.

The flow-resistance characteristics of the screen are needed for the final design of liquid-management devices. This information is required to accurately determine residuals in the tank at depletion. The pressure drop across various screens was estimated in this study, using of a two-fluid model of He II. The results are presented in Fig. 4-5, and the effect of pressure drop on residuals is described in section 4.4.2.3. The depletion residual was found to be as high as 2.32 percent excluding the lower receiver and trapped liquid fillets. This is lower than the 5 percent requirement by a factor of two. Therefore if the actual flow resistance of screens was not measured, and predicted values were used, it is felt that the 5 percent requirement could be met.

The effect of the pump heat dissipation on the performance of the screens has not been characterized and needs further analysis and testing. Depending on the final size of the management device, the thickness of the gallery arms, the amount of liquid remaining in the tank, and the actual heat dissipation of the pump, the screens will be subjected to various temperature gradients across them. Screens of different thickness and pore size will also affect the temperature gradient. This gradient may set up a thermomechanical effect and possibly pressurize the gallery channels. This pressurization may offset pressure depressions described in section 4.4 and eliminate any potential for cavitation within the channels. The analysis of this effect is very lengthy and depends on a clear understanding of the heat-transfer process in the tank for all levels of fill. This analysis was judged to be beyond the scope of this study.

The size selected for the screen was therefore not based on any of these possible effects but was based solely on capillary retention capability. It is recommended that development be initiated to fully characterize these effects. Some tests are being performed at NASA/Goddard for the SHOOT experiment, however tests and analysis related to the full-size tank are needed.

Cavitation is another issue that needs further attention. This study showed by analysis that cavitation would not occur within the gallery channels. The question of whether the He II in the channels is metastable or in thermal equilibrium with the vapor ullage needs further attention to be resolved. It is felt that the pore size of the screens plays an important role. This issue can be resolved with ground tests and is directly coupled with the thermomechanical potential of the screens; therefore, it is recommended that these cavitation tests and analysis be carried out in parallel with the screen thermomechanical tests and analysis.

6.1.2 He I

Helium transfer may occur slightly above the lambda point. There are two possible causes for this. First, a mechanical pump may be required if the performance of a FEP is not sufficient to overcome the high back pressure that will be encountered during cool-down of the receiver system or if the FEP cannot achieve the desired flowrate. At present, the mechanical pumps do not perform with He II without a net positive suction head (NPSH), due to cavitation of the fluid. If a mechanical pump is selected, the liquid-management device may therefore be required to perform with He I. It is possible that utilizing a new inlet inducer or other modifications to the pump will allow it to be used with He II without a NPSH. The second reason is that the ground-hold conditions may force the choice of a mechanical pump in case the helium is allowed to warm up above the lambda point. A FEP will not operate with He I.

The primary concern regarding the management device is that, with He I, the device may have vapor trapped in the system. Due to possible thermal stratification in the fluid and the lack of the tremendous thermal conductivity of He II, the vapor may not achieve a minimum capillary area. In this case, the trapped vapor in the device will not condense. Without a trap in the lower receiver, vapor can be ingested into the pump inlet. Tests with the NBS mechanical pump have shown that the pump will be able to pump the vapor through and subsequently pump liquid without any degradation in performance. Therefore there is no need to design the management device with a vapor trap in the lower receiver in the case He I is used as the fluid.

The kinematic surface tension of He decreases with increasing temperature, and therefore the capillary retention capability of the screen is degraded. The mesh size of the screen selected in this study is small enough to accommodate this lower retention capability. With He I, the viscosity of the fluid is higher and therefore the pressure drop across the screens and down the channels will be larger than with He II. This can lead to slightly higher residuals in the tank at depletion. The temperature of the fluid in the channels will still remain below 4 K because of the heat dissipated by the pump, and therefore no cavitation due to superheating is expected. The negative pressure that the fluid will be subjected to is still too small to cause cavitation. There are no nucleation sites due to vortex rings in He I, and therefore the threshold pressure for cavitation may be closer to the classical nucleation theory. However, unlike He II, vapor can be trapped in the channels and act as nucleation sites. The tests performed at NBS with the mechanical pump have shown that He I can be subjected to a negative pressure of 10 g_0-cm in its acquisition device without affecting the performance of the transfer. This negative pressure is over 30 times the maximum what the liquid acquisition device will be subjected to at depletion.

6.2 INTEGRATED FOUNTAIN EFFECT DEVICE (IFD)

In the analysis of the IFD, two aspects were identified that would require further attention.

- o Selection of gallery channel material
- o Selection and characteristic of the porous material

In order for the IFD to perform, a temperature gradient across the gallery channel material is required in order to set up the thermomechanical effect of the porous material. Material selection must be based on thermal and structural properties. The selection of the porous material is the primary concern. As the tank fill level decreases, more and more of the porous material is exposed to vapor. The exposed material would recycle helium back into the bulk space, which would cause the net transfer rate to decrease. Since the porous material that is acting as a FEP may be required to provide large pressures to overcome transfer losses, the exposed material might be subjected to helium breakthrough. The analysis in Section 5 showed that a very-fine-pore material would overcome these shortcomings. It is these aspects that need to be characterized and demonstrated. The required test apparatus and test sequence are described in section 5.4.

6.3 SMALL-SCALE ORBITAL TEST

As previously mentioned, the SHOOT experiment will be addressing on-orbit He II transfer. This experiment will use a mechanical or fountain-effect pump. The tank is fairly cylindrical, with a diameter of 22.25 in., a length of 36.625 in., and a capacity of approximately 200 L. Under a $10^{-4} g_0$

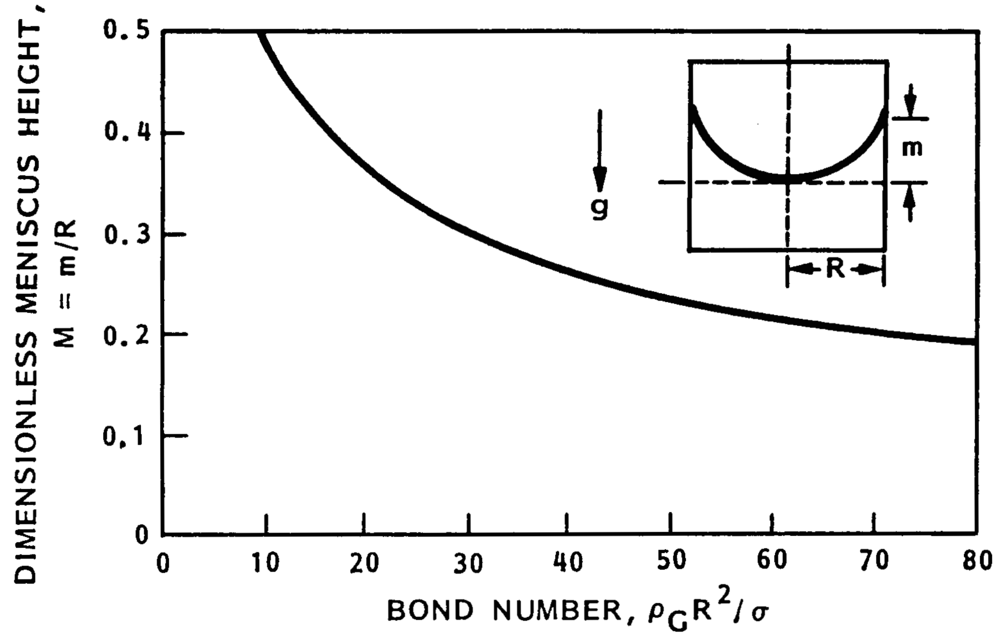

Fig. 6-1 Meniscus Rise Height for Cylindrical Container and Zero Contact Angle (Ref. 6-1)

acceleration field, the Bond number is 34, leading to a liquid-vapor interface that is primarily governed by acceleration but still curved. The meniscus height at the interception of the tank wall can be obtained from Fig. 6-1, which was determined by the exact solution of the differential equation for free-surface shape of liquid of zero contact angle in a cylindrical container (Ref. 6-1). This figure shows that the liquid will not sufficiently rise at the tank wall to keep the top of the tank, which holds the pump, wetted.

The maximum hydrostatic head that the management device will have to overcome is $9.3 \times 10^{-3} g_0$-cm ($36.6 \times 10^{-4} g_0$-in.) at depletion during an acceleration of 10^{-4} g_0. Reviewing the analysis for the open capillary devices shows that such systems would not meet the requirements and therefore an enclosed device would be preferred.

The depletion residual of the tank can be computed in the same manner as was done in section 4.4.2.3. The acceleration field is assumed to fully settle the liquid between two gallery channels. The liquid residual quantities for various numbers of gallery channels are shown in Table 6-1. The volume of the gallery channels per unit length is assumed to be the same as that shown in Fig. 4-1. The volumes shown in Table 6-1 are based on gallery channel lengths of 78.74 cm (31 in.).

Table 6-1 SHOOT LIQUID RESIDUALS

Number of Channels	Bulk Liquid Volume (L)	Channels Volume (L)	Total (L)
3	38.6	13.0	51.6
4	17.9	17.3	35.2
5	9.6	21.7	31.3
6	5.7	26.0	31.7

It can be seen that increasing the number of galleries by more than four does not reduce the residual unless depletion of the channels themselves takes place. In actuality the bulk liquid residual will be lower since the liquid-vapor interface will not be completely flat.

The choice of screen material should be based on the ones selected for the full-scale system analyzed in this report. The coarse plain Dutch screens were selected on the basis of their capillary retention only. NASA/Goddard is currently using 325 x 2300 mesh in ground testing the FEP. This fine screen is required for 1-g_0 tests in order to achieve a meaningful capillary rise. The results of these tests will be valuable in understanding the effect of pump heat dissipation on the screen, but caution must be taken when scaling to the full-scale gallery channel. Temperature gradients across the screens may be different.

Section 7

REFERENCES

1-1 D. Frank and D. Jaekle, Jr., "Cryogenic Fluid Management for Low-G Transfer," SPIE Proceedings, Vol. 619, 1986, p. 21

1-2 D. Petrosh, R. Nussle, and E. Otto, Effect of Contact Angle and Tank Geometry on the Configuration of the Liquid-Vapor Interface During Weightlessness, NASA-TN-D-2075, 1963

1-3 A. Stefan, and A. Armstead, Analytical and Experimental Investigation of Forces and Frequencies Resulting From Liquid Sloshing in a Spherical Tank, NASA-TN-D-1281, 1962

2-1 A.T. Van Urk, W. H. Keeson, H. Kamerlingh Onnes, Proc. Roy. Akad. (Amsterdam), Vol. 28, p. 58 (1925).

2-2 J.F. Allen and A.D. Misener, Proc. Cambridge Phil. Soc., Vol. 34, p. 299 (1938).

2-3 K. R. Atkins and Y. Narahara, Phys. Rev., Vol. 138, p. A437 (1965).

2-4 K. N. Zinoveva, Zh. Eksp. Teor. Fiz., Sov. Phys. - JETP, Vol. 2, No. 4, p. 774 (1956).

2-5 L. A. Girifalco and R. J. Good, J. Phys. Chem. Soc., Vol. 61, p. 904 (1957); Vol. 62, p. 1418 (1958); Vol. 64, p. 561 (1960).

2-6 M. Murakami et al., The Institute of Space and Astronautical Science, Report No. 604, June 1983.

2-7 P. Mason, F. Edeskuty, et al., The Behavior of Superfluid Helium in Zero Gravity, ICEC7, p. 99 (1978).

2-8 W. Reynolds, M. Saad, and H. Satterlee, *Capillary Hydrostatics and Hydrodynamics at Low-g*, LG-3 (1964).

4-1 Lockheed Missiles & Space Company, Inc., *P-95 Propellant Management System Engineering Analysis Report*, LMSC-A947283, 1969

4-2 Eugene P. Symons, *Wicking of Liquids in Screens*, NASA TN D-7657, May 1974

4-3 F. A. Staas, K. W. Taconis and W. M. Van Alphen, *Physica*, Vol. 27, p. 893 (1961).

4-4 J. C. Armour and J. N. Cannon, *AICHE Journal*, Vol. 14. No. 3, P415 (1968).

4-5 J. C. Fisher, *J. Appl. Phys.*, Vol. 19, p. 1062, (1948).

4-6 P. L. Marston, *J. Low Temp. Phys.*, Vol. 25, No. 3/4, p. 383, (1976).

4-7 J. W. Beams, *Phys. Rev.*, Vol. 104, No. 4, p. 880, (1956).

4-8 W. M. Fairbank, J. Leitner, M. M. Block and E. M. Harth, *Bull. Inst. Intern. Froid*, Annexe No. 1, p. 45, (1958).

4-9 M. L. Chu, Ph.D. Dissertation, University of Houston, Houston, Texas, (1967).

4-10 R. E. Apfel, *Acoustic Cavitation in Ultrasonics*, P. Edmonds, ed., Vol. 19 of series, *Methods of Experimental Physics*, ed. C. Marton, Academic Press, New York, (1981), 355.

4-11 P. D. Jarman and K. J. Taylor, *J. Low Temp. Phys.*, Vol. 2, No. 3/4, p. 389, (1970).

4-12 D. Lieberman, *Phys. Fluids*, Vol. 2, p. 466, (1959).

4-13 A. L. Hughes, *Proceedings of an International Conference on Instrumentation for High Energy Physics, Berkeley*, (Interscience Publishers, New York, 1961), p. 99.

4-14 D. Sette and F. Wanderlingh, *Phys. Rev.*, Vol. 125, p. 409, (1962).

4-15 D. Messino, D. Sette, and F. Wanderlingh, *J. Acoust. Soc. Am.*, Vol. 35, p. 926 and 1575, (1963).

4-16 B. Hahn and R. N. Peacock, *Nuovo Cimento*, p. 28, (1963).

4-17 J. R. Shadley and R. D. Finch, "Nucleation of Ultrasonic Cavitation by Alpha-Particle Irradiation of Liquid Helium," *Phys. Rev. A*, Vol. 3, No. 2, 780, (1971).

4-18 M. H. Edwards, R. M. Cleary and W. M. Fairbank, in *Quantum Fluids*, D. F. Brewer, ed. (North-Holland Publishing Co., Amsterdam, 1966), p. 140.

4-19 R. D. Finch, and M. L. Chu, "Production and Detection of Solitary Macroscopic Quantized Vortice in He II," *Phys. Rev.*, Vol. 161, No. 1, p. 202, (1967).

4-20 K. L. McCloud, Ph.D. dissertation, Ohio State University, (1968).

4-21 P. M. McConnell, M. L. Chu, Jr. and R. D. Finch, *Phys. Rev.* A1, 411, (1970).

4-22 V. A. Akulichev and V. A. Bulanov, "On the Tensile Strength of Quantum Liquids," Akust. Zh, (in Russian) Vol. 20, p. 817, (1974).

4-23 Dave Daney, National Bureau of Standards, Private Communication, May 1987.

4-24 W. M. Van Alphen, R. DeBruyn Ouboter, K. W. Taconis and W. DeHaas, Physica Vol. 40, p. 469, (1969).

4-25 J. B. Hendricks, and G. R. Karr, in the Proceedings of Advances in Cryogenic Engineering, Vol. 29, p. 697, (1983).

4-26 G. Krafft, J. Low Temp Phys. Vol. 31, p. 441, (1978).

4-27 L. J. Rybarcyk and J. T. Tough, J. Low Temp. Phys. Vol. 43, p. 197, (1981).

4-28 R. Cole, "Boiling Nucleation," in Advances in Heat Transfer, Vol. 10, p. 85, Academic Press, N.Y., (1974).

4-29 K. Nishigaki and U. Saji, Phys. Rev. B, Vol 33, No. 3, p. 1657, (1986).

4-30 T. H. K. Frederking et al., "He II Reservoir Heating to the Lambda Point Vicinity: Superheating Effects," to be presented in Low Temperature Physics Conference18, (1987).

5-1 S. W. K. Yuan, and T. C. Nast, "The Design of Fountain Effect Pumps," to be published in CEC, (1987).

5-2 Frederking, T. H. K., U.C.L.A, Private communication.

5-3 S. W. K. Yuan, Ph.D. Thesis, U.C.L.A., (1985).

5-4 U. Schotte, and H. D. Denner, Z. Phys. Vol. B41, p. 139, (1981).

5-5 S. W. K. Yuan, J. M. Lee, and T. H. K. Frederking, "Turbulent Transport of He II in Active and Passive Phase Separator Using Slit Devices and Porous Media," to be published in CEC, 1987.

5-6 A. Elsner, in Advances in Cryogenic Engineering, Vol. 18, p. 141, Plenum Press, NY, (1973).

5-7 H. D. Denner, G. Klipping, I. Klipping, and U. Schmidtchen, Cryogenics, Vol. 24, p. 403, (1984).

6-1 H. Satterlee and J. Chin, "Meniscus Shape Under Reduced-Gravity Conditions," Proceedings of Fluid Mechanics and Heat Transfer Under Low Gravity Symposium, 1965.

NASA
National Aeronautics and Space Administration

Report Documentation Page

1. Report No.
177463

2. Government Accession No.

3. Recipient's Catalog No.

4. Title and Subtitle
Study of Helium Transfer Technology for STICCR-Fluid Management

5. Report Date
July 1987

6. Performing Organization Code

7. Author(s)
D. Frank et al.

8. Performing Organization Report No.

10. Work Unit No.
159-41-06

9. Performing Organization Name and Address
Lockheed Missiles and Space Corporation
Palo Alto Research and Development
3251 Hanover Street
Palo Alto, CA 94304

11. Contract or Grant No.
NAS2-12051

13. Type of Report and Period Covered
Contractor Report

12. Sponsoring Agency Name and Address
National Aeronautics and Space Administration
Washington, D.C. 20546

14. Sponsoring Agency Code

15. Supplementary Notes

6 /

Point of Contact: NASA Ames Research Center
Attn: SR/Dr. Walter F. Brooks
Moffett Field, CA 94035

16. Abstract

The Space Infrared Telescope Facility (SIRTF) is a long-life cryogenically cooled space-based telescope for infrared astronomy from 2 um to 700 um currently under study by NASA-ARC (Reference AP), and planned for launch in approximately the mid 90's.

SIRTF will operate as a multi-user facility, initially carrying 3 instruments at the focal plane. It will be cooled to below 2K by superfluid liquid helium to achieve radiometric sensitivity limited only by the statistical fluctuations in the natural infrared background radiation over most of its spectral range. The lifetime of the mission will be limited by the lifetime of the liquid helium supply, and is currently baselined to be 2 years.

The purpose of this effort is to review candidates for a liquid management device to be used in the resupply of liquid helium, and to select an appropriate candidate.

17. Key Words (Suggested by Author(s))
Space Infrared Telescope Facility
Liquid Helium Transfer
Liquid Management Device
Zero-G
Cryogenics

18. Distribution Statement
Unclassified/Unlimited
Star Category 18

19. Security Classif. (of this report)
Unclassified

20. Security Classif. (of this page)
Unclassified

21. No. of pages
108

22. Price

NASA FORM 1626 OCT 86